



**T.C.
İSTANBUL UNIVERSITY
INSTITUTE OF GRADUATE STUDIES IN
SCIENCE AND ENGINEERING**



Ph.D. THESIS

**RAMAN AND AFM STUDY OF
GRAPHENEOXIDE PREPARED BY WET OXIDATION OF GRAPHENE**

Esra YAZICI

Department of Physics

Physics Programme

Ph. D. Student transferred from Fatih University which has been closed

SUPERVISOR

Assist. Prof. Dr. Mehmet Burak YILMAZ

June, 2015

İSTANBUL

**RAMAN AND AFM STUDY OF
GRAPHENE OXIDE PREPARED BY WET OXIDATION OF GRAPHENE**

by

Esra YAZICI

A thesis submitted to the Graduate School of Science and Engineering.

of

Fatih University

In partial fulfillment of the requirements for the degree of
Doctor of Philosophy

in

Physics

APPROVAL PAGE

This is to certify that I have read this thesis written by Esra YAZICI and that in my opinion it is fully adequate, in scope and quality, as a thesis for the degree of Doctor of Philosophy in Physics.



Assist. Prof. Mehmet Burak YILMAZ
Thesis Supervisor

I certify that this thesis satisfies all the requirements as a thesis for the degree of Doctor of Philosophy in Physics.

Prof. Mustafa KUMRU
Head of Department

Examining Committee Members

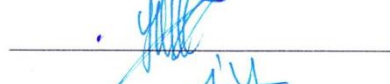
Assist. Prof. Mehmet Burak YILMAZ



Prof. Serkan ÇALIŞKAN



Assoc. Prof. Ramazan ÖZTÜRK



Prof. Yüksel KÖSEOĞLU



Assist. Prof. İbrahim YILMAZ



It is approved that this thesis has been written in compliance with the formatting rules laid down by the Graduate School of Sciences and Engineering.

Prof. Nurullah ARSLAN
Director

June 2015

RAMAN AND AFM STUDY OF GRAPHENE OXIDE PREPARED BY WET OXIDATION OF GRAPHENE

Esra YAZICI

Ph.D. Thesis – Physics

June 2015

Thesis Supervisor: Assist. Prof. Mehmet Burak YILMAZ

ABSTRACT

Graphene, a single layer of graphite, has attracted extensive interest due to its unique electronic, mechanical, and optical properties. Experimentally, it was first obtained in 2004 by Konstantin Novoselov and Andre Geim via mechanical exfoliation from graphite. Graphene enable a variety of applications such as field effect transistors (FETs), optical modulators, non-linear rectifiers, ultrafast lasers, large-area membranes and etc. Recently, there is an increasing interest in chemically modified graphene based materials. Through chemical modification and functionalization, it is possible to tune various properties of graphene. Graphene oxide (GO) is one such material which is unlike graphene is electrically insulating and may be used as an intermediate step for further functionalization of the sample. In this study, graphene samples prepared by micromechanical exfoliation of graphite were oxidized using wet chemistry. The samples are then investigated using Raman spectroscopy and Atomic Force Microscopy. Formation of nano-sized graphene oxide islands near the edges of the samples are observed for intermediate reaction durations. For longer oxidation durations it is possible to completely oxidize the sample surface. Single layer graphene was found to be more reactive than multilayer samples. We have demonstrated that using a few micrometer wide graphene it is possible to prepare completely graphene oxide nanodomains covered samples. Extensive experiments on many different graphene flakes indicate that local impurity doping of the graphene plays a central role in the formation of nanodomains. Although the domains are insulating, the rest of the sample remains to be conductive. Wet oxidation process were carried out for chemical vapor deposition (CVD) grown graphene.

Keywords: Atomic force microscopy, graphene, graphene oxide, Raman spectroscopy

GRAFENDEN ISLAK OKSİDASYONLA HAZIRLANAN GRAFENOKSİTİN RAMAN VE AFM İNCELEMESİ

Esra YAZICI

Doktora Tezi – Fizik

Haziran 2015

Tez Danışmanı: Yrd. Doç. Dr. Mehmet Burak YILMAZ

ÖZ

Grafen tek katman grafitte verilen isimdir. Eşsiz elektronik, mekanik ve optik özelliklerinden dolayı bilim dünyasında çok geniş bir ilgiye sahiptir. Deneysel olarak ilk defa Andre Geim tarafından 2004 yılında mekanik olarak katmanlarına ayırma yöntemiyle elde edilmiştir. Grafen çok geniş bir uygulama alanına sahiptir. Örneğin; alan etkili transistör, Optik modülatör, doğrultucular, ultra hızlı lazerler, geniş alanlı membranlar vb. Son zamanlarda kimyasal olarak değiştirilmiş grafen tabanlı malzemelere olan ilgi artmıştır. Kimyasal değişimle grafenin çeşitli özellikleri değişebilir. Grafen oksit (GO). GO grafenden farklı olarak yalıtkan özellik göstermektedir. Bu çalışmada kullanılan grafen örnekleri mekanik olarak katmanlarına ayırma yöntemiyle elde edilmiştir ve ıslak kimyasal yöntemle oksitlenmiştir. Daha sonra örnekler Raman spektroskopisi ve Atomik Kuvvet Mikroskobu kullanılarak incelenmiştir. Ortalama bir reaksiyon süresinde örnek kenarlarında nanoboyutlu grafen oksit adalarının oluştuğu gözlemlenmiştir. Uzun oksitlenme süresinde örneğin tamamı oksitlenebilir. Tek katmanlı grafenin çok katmanlı graphene göre daha reaktif olduğu görülmüştür. Birkaç mikrometre genişliğinde grafen kullanarak tamamı grafen oksit nano adalarla kaplı örnek elde edilebileceği gösterilmiştir. Farklı grafen örnekleri üzerinde yapılan detaylı çalışmalarda, grafen üzerinde bölgesel katkılanmanın nano adaların oluşumunda önemli rol oynadığı tespit edilmiştir. Nano adaların yalıtkan özellik göstermesine karşın, örneğin geri kalan kısmı iletken özellik göstermektedir. Oksitleme işlemi kimyasal buhar depolama (CVD) yöntemi ile büyütülmüş tek katmanlı grafen örnekleri için de gerçekleştirilmiştir.

Anahtar Kelimeler: Atomik kuvvet mikroskobu, grafen, grafen oksit, Raman spektroskopisi



To my parents

ACKNOWLEDGEMENT

First, I would like express my gratitude to my supervisor Assist Prof. Mehmet Burak YILMAZ for his helps, stimulation and valuable advice during this research.

I want to thank to Head of the Physics Department Prof. Mustafa KUMRU for his motivation and support in my thesis.

I am also grateful to my colleague Serhat YANIK for his valuable support in the studies.

Also I want to thank my friends Tayyibe, Zeynep and Merve to their motivations and I have to knowledge all my colleagues in research room A-104. I would also express appreciation my brother Harun, my sisters Sema and Eda especially my father Rahmi YAZICI and my mother Ayşe YAZICI to existence in my life.

I would like to convey thanks to Fatih University, Bio Nano Technology R&D Center for providing laboratory facilities.

This work supported by TUBITAK “The Scientific and Technical Research Council of Turkey” under grant number 110T801.

TABLE OF CONTENTS

ABSTRACT.....	iv
ÖZ	v
DEDICATION.....	vi
ACKNOWLEDGMENT	vii
TABLE OF CONTENTS.....	viii
LIST OF FIGURES	x
LIST OF SYMBOLS AND ABBREVIATIONS	xv
CHAPTER 1 INTRODUCTION	1
1.1 Motivation.....	1
CHAPTER 2 BACKGROUND.....	3
2.1 Allotropes of carbon.....	3
2.2 Graphene	6
2.2.1 Introduction	6
2.2.2 Band Structre of Graphene	8
2.2.3 Electronic Properties	10
2.2.4 Mechanical and Optical Properties	13
2.3 Graphene oxide	14
CHAPTER 3 METHODS.....	18
3.1 Graphene Production Methods.....	18
3.1.1 Mechanical Exfoliation Method.....	18
3.1.2 Other Graphene Production Methods.....	20

3.2 Characterization Methods	21
3.2.1 Raman Spectroscopy	21
3.2.2 Atomic Force Microscopy	27
3.3 Wet Oxidation Method.....	31
CHAPTER 4 RESULT AND DISCUSSIONS.....	33
4.1 Introduction	33
4.2 Determination of Graphene Thickness.....	34
4.3 Sulfuric Acid Intercalation During Oxidation with Hummers Method	37
4.4 Oxidation of Single Layer Graphene by Wet Chemistry	43
4.4.1 Edge Oxidation.....	45
4.4.2 The Effect of Charge Puddles on Oxidation	51
4.5 Oxidation of CVD Grown Graphene	57
CHAPTER 5 CONCLUSIONS	66
REFERENCES	68
CURRICULUM VITAE.....	79

LIST OF FIGURES

FIGURE

1.1	Structure of graphene	1
2.1	a), b) Diamond and its crystal structure, (c), (d) graphite and its crystal structure..	4
2.2	Crystal structure of a) fullerene and b) carbon nanotube	5
2.3	Graphene as the building block of graphitic forms of carbon	7
2.4	The band structure of sp^2 hybridized ethylene	8
2.5	Electronic band structure of graphene	9
2.6	Crystal structure of graphene	10
2.7	a) π - π^* band structure of graphene, b) Brillion zone	11
2.8	Ambipolar electric field effect in single layer graphene. The insets show the changes in the position of the Fermi energy E_F with changing gate voltage V_G ...	12
2.9	Quantum Hall effect in single layer graphene	12
2.10	a) Scanning electron microscopy (SEM) image of graphene flake with circular holes (scale bar, 3 μ m), b) Schematic illustration of suspended graphene	13
2.11	Optical image of partially covered with single and bilayer suspended graphene	14
2.12	Schematic illustration of a graphene oxide sheet. sp^2 and sp^3 -hybridized carbons include hydroxyl and epoxide functional groups in its basal plane, but the edges are decorated by carboxyl and carbonyl groups	16

3.1	The steps of preparation of graphene samples by exfoliation method.....	19
3.2	Energy level diagram to explain Raman scattering.....	22
3.3	Schematic representation of Stokes and anti-Stokes lines	22
3.4	Rayleigh and Raman signals	24
3.5	Instrumentation for modern Raman spectroscopy consists of four components: a laser source, collection optic, wavelength analyzer and detector	25
3.6	a) The G mode of graphite lies at around 1581 cm^{-1} has E_{2g} symmetry. b) The D peak at nearly 1350 cm^{-1} is a breathing mode of A_{1g} symmetry	26
3.7	Raman spectrum of single layer graphene (top) and graphite (bottom).....	27
3.8	Dependence of the potential energy vs the distance between tip and the sample during their interaction.....	28
3.9	Block diagram of AFM	29
3.10	AFM modes; a) contact, b) non-contact and c) tapping and d) lateral force.....	30
3.11	AFM image of single layer graphene obtained in our studies.....	31
4.1	a) optical image of graphene which has different layer on SiO_2/Si substrate, b) The shape of G and 2D peak from monolayer to eight layer	35
4.2	The shape of 2D from monolayer to eight layers.....	36
4.3	Schematic of Intercalation. Graphene layers and intercalant layer are shown as solid line and solid circle, respectively	37
4.4	a) Electrochemical reaction of graphite with H_2SO_4 , b) Ammonium persulfate/sulfuric acid graphite intercalation	38
4.5	a) Optic image of sample before oxidation, b) optic image of sample after oxidation without cleaning, c) and d) Raman spectra obtained from part 1 and 2, respectively.....	39

4.6	a) optic image of a few layer graphene, c),d) G and D' peak before (red) and after (blue) oxidation at different point, 1 and 2 respectively, on the graphene surface	40
4.7	a), b), c), Raman maps of G peak position, FWHM, and intensity, respectively.....	41
4.8	a),b),c) Raman map of D' peak position, FWHM, and intensity, respectively.....	42
4.9	a) optic image of graphene sample, b) AFM image of graphene before oxidation, c) AFM image of graphene after oxidation, d) Raman spectra before and after oxidation, f) Effect of oxidation on the thickness of a few layer graphene sample is illustrated using AFM contact mode.....	43
4.10	a), b) Optical image of graphene sample prior and after oxidation respectively, c) G peak position prior and after oxidation process	44
4.11	a) Optic image of graphene sample prior and after oxidation process, b) Raman spectra of graphene before and after oxidation.....	45
4.12	Schematic of Intercalation. Graphene layers and intercalant layer are shown as solid line and solid circle, respectively a) Optical image of a pristine graphene prior to oxidation. b) Raman map of D peak intensity, c) AFM topography, and d) LFM images after oxidation of the same sample for 10 min. via wet chemistry. Images indicate that the oxidation starts from the edges of the sample	46
4.13	a) Lateral force images of single layer graphene samples for different oxidation durations. All images are at the same scale. Bright regions are unoxidized and dark regions are oxidized graphene (graphene oxide). The width of oxidized parts is increasing with oxidation duration. b) The plot of oxide width versus oxidation duration yields an oxidation rate of approximately 0.2 $\mu\text{m}/\text{min}$ for the solution used in this study.....	47
4.14	Raman spectra of pristine graphene (red), partially oxidized graphene (green) and graphene oxide (blue). The presence of both a broad and a sharp peak at around 1580 cm^{-1} in the partially oxidized graphene indicates the coexistence of both graphene and graphene oxide within the laser beam spot.....	48

4.15	Optical images of graphene samples after oxidation.....	49
4.16	Optical image of single layer graphene before a) and after b) 10 min oxidation..	50
4.17	a) Topography and b) Lateral Force images of a 4 min-oxidized graphene flake. c) The full view of the same flake demonstrating that the flake is completely covered with GONDS	51
4.18	Raman spectra of graphene as a function of gate voltage	52
4.19	a) Optical image of a single layer graphene prior to oxidation, (b) LFM image of graphene shown in a) after oxidation. (c) and (d) Topographic and LFM images of partially oxidized part of graphene shown in (b). (e) Raman D peak intensity map from the same flake after oxidation	54
4.20	Raman maps of single layer graphene before oxidation; a) G peak position, (b) G peak FWHM, c) 2D peak position and d) 2D/G Peak intensity	55
4.21	Raman maps of single layer graphene after oxidation; a) G peak position, b) G peak FWHM, c) D peak position and d) D Peak FWHM	56
4.22	a) G FWHM versus G peak position, b) 2D peak position versus G peak position, c) 2d Peak position I_{2D}/I_G ratio versus G peak position, d) 2D peak FWHM versus the. The dashed lines are added as a guide to indicate general trends with charge doping	58
4.23	Raman spectra of CVD grown graphene (blue) and exfoliated graphene (red)....	59
4.24	Optical images of CVD grown graphene	60
4.25	Optical image of CVD grown single layer graphene after oxidation.....	60
4.26	a) Lateral force and, b) topographic images of CVD grown graphene after oxidation.....	61
4.27	Magnified a) lateral force and b) topographic images indicated in 4.25.....	62
4.28	AFM images, a) lateral force and b) topographic images indicated in 4.26	62
4.29	Raman spectrum of non-oxidized region of CVD grown graphene (blue), single layer a), double layer b) and triple layer graphene	63

4.30 Raman maps of CVD grown graphene.....	64
4.31 a) Optical image and (b-e) Raman maps of non-oxidized region on the CVD grown graphene	65



LIST OF SYMBOLS AND ABBREVIATIONS**SYMBOL**

V_G Gate voltage

E_F Fermi energy

P Dipole moment

α Molecular polarizability

ν Frequency

λ Wavelength

k Spring constant

ABBREVIATION

AFM	Atomic Force Microscopy
BLG	Bi Layer Graphene
CCD	Charge Coupled Device
CNT	Carbon Nanotube
CVD	Chemical Vapor Deposition
DI	Diluted Water
FET	Field Effect Transistor
FWHM	Full Width at Half Maximum
GO	Graphite oxide
GOND	Grapheneoxide Nano Island
I-AFM	Current Atomic Force Microscopy
LFM	Lateral Force Microscopy
PSPD	Position Sensitive Photodetector
RGO	Reduced Graphene Oxide
SEM	Scanning Electron Microscopy
SLG	Single Layer Graphene
STM	Scanning Tunneling Microscopy
QHE	Quantum Hall Effect

CHAPTER 1

INTRODUCTION

1.1 MOTIVATION

Graphene is the single layer of graphite. It can be viewed as the building block of fullerene, carbon nanotubes, and the graphite. All of these structures are composed entirely of sp^2 hybridized carbon atoms. It has been known as theoretical model for decades but experimentally obtained by Konstantin Novoselov, Andre Geim and their collaborators in October 2004.

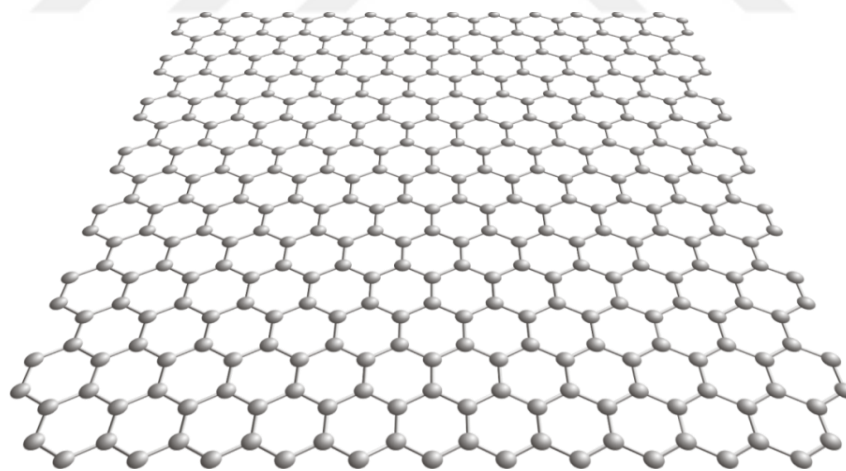


Figure 1.1 Structure of graphene

Graphene has been the subject of widespread interest over the last decade due to its unique electronic, mechanical and optical properties which have many applications including electronic devices, biosensors and composite materials [1-3]. However its superior electrical transport qualities [4] are offset by the lack of an electronic band gap

[5]. As a result, rather than working with pristine graphene, many researchers are concentrating their efforts on novel graphene derived materials which might allow for devices with tunable electronic properties. Chemical modification and functionalization of graphene is of great interest to alter its intrinsic properties. Among various methods, wet chemical oxidation is widely used for obtaining large quantities of graphene oxide (GO) or reduced GO. It is also often used as an intermediary step for further functionalization of the graphene.

Atomic force microscopy (AFM), scanning electron microscopy (SEM), four-probe and Hall effect measurements are widely used as characterization techniques for graphene studies. Raman spectroscopy provides quick and accurate information about the number of graphene layers and their crystalline quality and impurity doping of the sample. It is also a non-invasive technique. Surface topographical and mechanical properties can be investigated in detail with AFM. In the “current AFM” mode (I-AFM) it also provides information on the local conductive properties of the sample.

In this study we have researched graphene/graphite and graphene oxide by Raman spectroscopy and AFM. Graphene and graphite samples were prepared by micromechanical exfoliation of graphite onto 300 nm SiO₂/Si wafers and they were oxidized with wet chemistry. Raman microscopy and AFM were used prior and after oxidation in order to determine the effect of oxidation process on the samples. The results were compared with previous studies in literature. Raman spectra obtained from graphite samples after oxidation give strong evidence about sulfuric acid intercalation between the graphene layers and oxidation. Also AFM, lateral force and I-AFM images verify the Raman results. In our study we also have investigated the effect of wet oxidation on Chemical vapor deposition (CVD) grown graphene. Indications of oxidation are clearly seen in the Raman and AFM results after the reaction. Raman map, AFM and lateral force images revealed that some regions on the CVD grown graphene were not oxidized.

CHAPTER 2

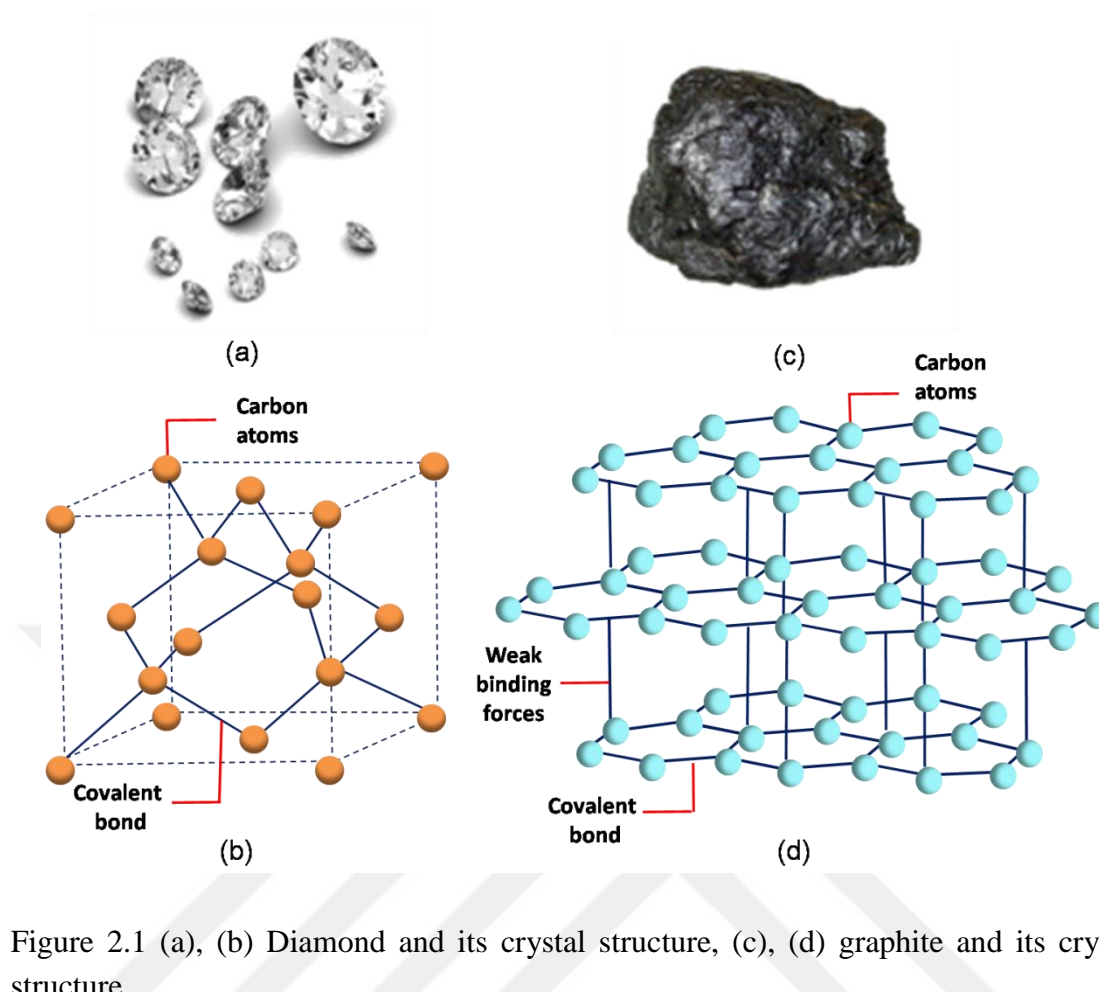
BACKGROUND

2.1 ALLOTROPES OF CARBON

Carbon is the vital element for life because all living things on earth contain carbon. It is one of the elements of group IV of the periodic table. It has four available electrons in its outermost orbit. These electrons form covalent chemical bonds. It has unique chemical properties. Carbon atoms can combine with other carbon atoms to form long chains. It has several allotropes and the most common known are diamond and graphite like structures (fullerenes and carbon nanotubes).

In ancient Greek, diamond was named *αδάμας (adámas)*. It was derived from “proper”, “unalterable”, unbreakable”, “untamed”. It is believed that diamond was first mined and recognized in India. It has been known in India for probably 3000 years [6]. It was first used as jewelry in XIth century as an ornament on Hungarian queen’s crown and since then it has been used as the most precious jewelry.

Diamond is an allotrope of carbon where carbon atoms are bonded with sp^3 hybridization in tetrahedral crystal structure. Each carbon atom bonds to four other carbon atoms separated by 0.154 nm. The bond angle between the C-C-C is 109.5 degrees. Four valence electrons of each carbon come together to form very strong covalent bonds. It is difficult to break atoms apart or move them in relation to one another and as a result presents great resistance to compression. Diamond is known to be the hardest material and can be cut only by another diamond. It is electrically insulating but has excellent heat and phononic conductivity. It is optically transparent from deep ultraviolet to far infrared and it disperses light [7-9].



Graphite was first discovered by villagers from Gray Knotts in England in 1500s. They assumed that this strange and black rock was lead. They used it to mark their sheep. During the reign of Elizabeth (1533-1603), government used the graphite as a refractory material to make moulds for making cannonballs. The modern pencil was discovered in 1795 when Napoleon Cont baked a mixture of clay and powdered graphite. It was called black lead or plumbago at first. It was also called molybdaena, but was later shown that molybdaena refer to two different types of materials, molybdenite and graphite. It was named by Abraham Gottlieb Werner in 1789 after the word “graphein” which means “to write” in Greek.

Graphite shows sp^2 hybridization where carbon atoms arranged as regular hexagons with a 120-degree C-C-C bond angle. Carbon atoms generate sheets of six sided rings with p-orbitals perpendicular to the plane of the ring. Three of the four valence electrons of each carbon atom is shared by the three nearest neighbor atoms. The

remaining electron in the out of plane p-orbital is delocalized. P-orbitals allow for weak Van der Waals forces that hold the sheets together. Since the forces holding the sheets together are weak, they can be easily separated from each. The distance between the graphite layers is 0.334 nm. Graphite is an anisotropic material and it has different properties in different directions. It has good electrical and thermal conductivity due to covalent and metallic bond within a carbon layer. On the other hand it shows poor electric and thermal conductivity perpendicular to the carbon layers. It absorbs light and appears black in color.

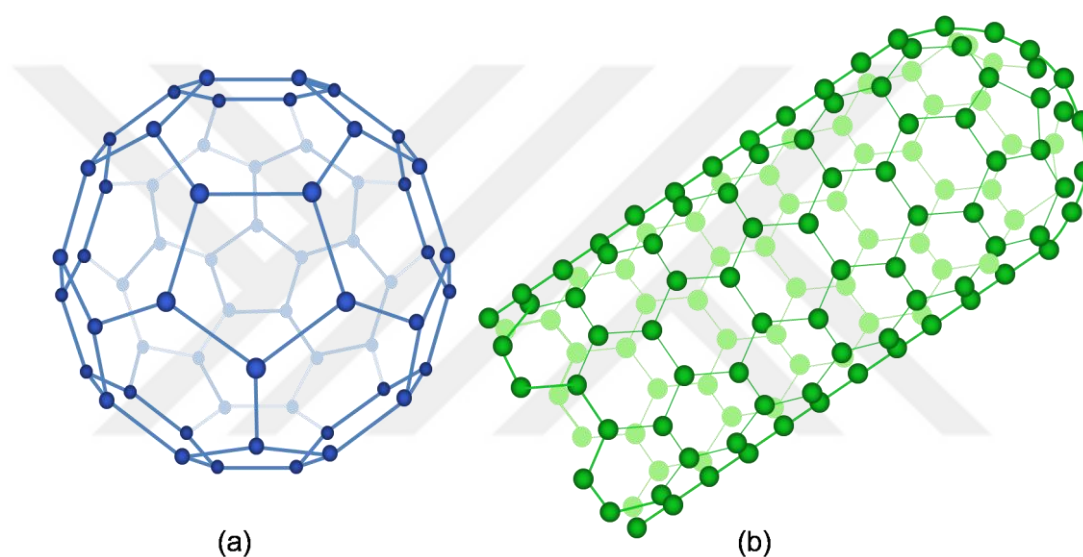


Figure 2.2 Crystal structure of (a) fullerene and (b) carbon nanotube.

Fullerenes are molecules of pure carbon atoms. The molecular sphere form of fullerene was first identified in 1985 by Kroto [10] but its structure remained unclear because of the lack-of large scale and improved synthesis methods. Kratschmer and his collaborators achieved the synthesis of C₆₀ in 1990 [11]. The discovery of fullerenes was awarded the Nobel Prize in 1996. It can be found as hollow sphere, ellipsoid, tube and many other shapes. The most popular known fullerene is C₆₀ and it is also called as buckyballs. The structure of fullerenes has similarities with graphite, which consists of stacked graphene sheets in hexagonal structure but it can be also found in pentagonal structure. It is physically extremely strong and it can resist to high pressure. Recently it

has been one of the subjects of popular researches, such as material science and electronics.

The cylindrical structure of fullerene is named as carbon nanotubes (CNT). They were first observed by Sumio Iijima in 1991 and then he synthesized single-wall carbon nanotube [12]. Their diameters range from 0.4 to 2-3 nm but can be nearly a micrometer to millimeters in length. It has a closed structure but the ends can be opened as well [13]. They can be either metallic or semiconducting depending on the chirality of the tube. CNT are strong, flexible and stiff material and also have very high current capacity [14]. They are very good thermal conductor along the length of the tube. These extraordinary properties make them useful in many applications such as electronics, optics and other field of material science

In summary, graphite, fullerenes, and CNTs are formed by carbon atoms bonded in sp^2 hybridization forming a hexagonal lattice structure. These carbon allotropes opened a new era in nanotechnology due to their unique properties. The two dimensional, infinitely wide single layer structure formed by the sp^2 hybridized hexagonal rings can be viewed as the building block for all of these carbon allotropes. This 2D structure which is studied in more detail in later parts is graphene.

2.2 GRAPHENE

2.2.1 Introduction

Graphene is the monolayer of packed carbon atoms with hexagonal rings. It Graphene has extremely good electrical, optical mechanical and thermal properties [1-3]. These properties make graphene extraordinarily intriguing for both fundamental science and technological application.

Graphene has been studied theoretically since 1940s at which time P.R. Wallace calculated the band structure of graphene [15]. He researched the electronic structure of graphene and he showed that energy momentum dispersion of electronic state near the Fermi level is linear. Peierls and Landau asserted that 2D crystals were thermodynamically unstable in the 1930s [16, 17]. According to this view, experimentally producing and transferring 2D planar graphene to another substrate

could not be achieved. This opinion was later extended by Mermin [18]. In 2004 Konstantin Novoselov and Andre Geim performed an experiment at the University of Manchester and they demonstrated that it was possible to isolate “free state” graphene sheets. This finding proved that despite the graphene is monoatomically thin it can exist as thermodynamically stable either on a supporting substrate or in the suspended form. It also exhibited high crystalline quality in 2D form and charge carriers can travel thousand of interatomic distance without scattering [1, 19-21]. This superb discovery brought them a Nobel Prize in 2010 [2, 3].

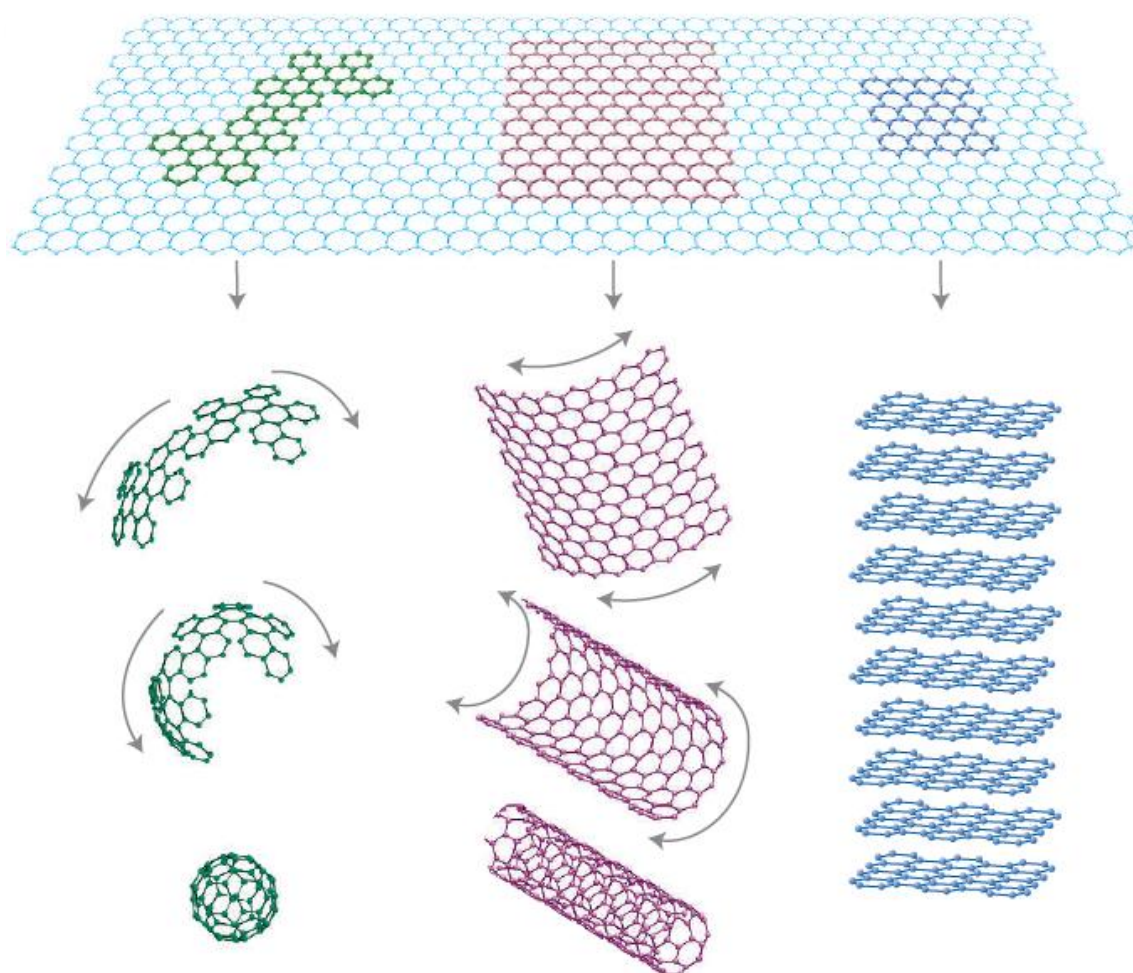


Figure 2.3 Graphene as the building block of graphitic forms of carbon.

2.2.2 Band Structure of Graphene

As we mentioned, graphene is the single layer of graphite in sp^2 hybridization which includes π and σ states. The sp^2 hybridization of carbon atoms in graphene is illustrated in the Figure 2.4. The electron configuration of carbon is $1s^2 2s^2 2p^2$. $2s$, $2p_x$ and $2p_y$ electrons form σ bond in the planar sp^2 orbitals. This bond provides strong covalent bond with nearest carbon atoms. Each carbon atoms is bonded with three other carbons through the sp^2 hybridization in the graphene layer. On the other hand p_z electron forms π orbitals perpendicular to the graphene layer. It remains unbonded and it overlaps with π bond of its nearest neighbor carbon atom forming weak van der Waals interaction between the graphene layers.

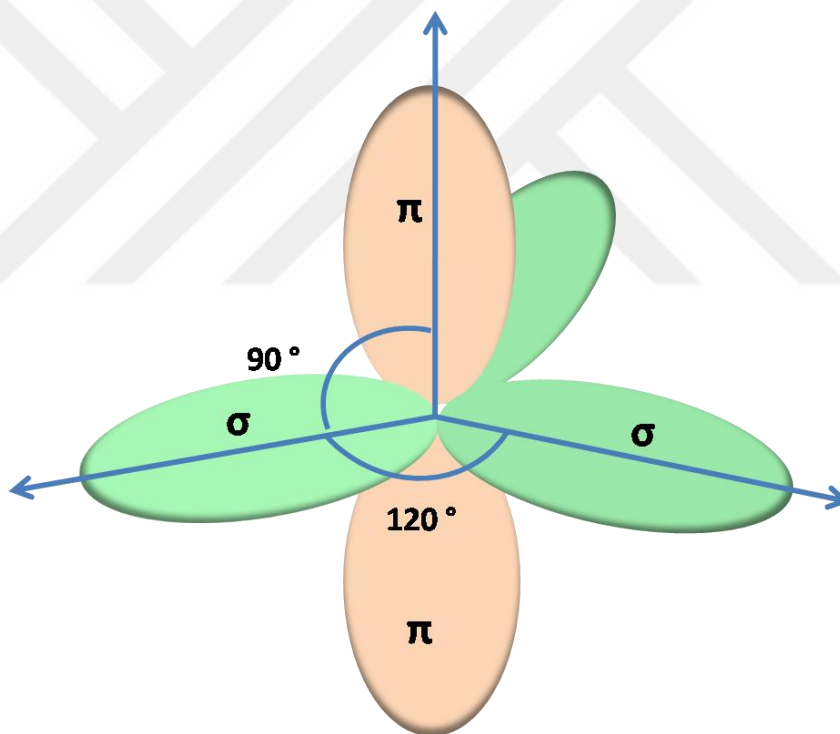


Figure 2.4 The band structure of sp^2 hybridized ethylene.

Figure 2.5 shows the electronic band structure of graphene. It was calculated by Wallace using nearest-neighbor, tight-binding approximation in 1947 [15]. It shows that valence and conduction band, consisting of the bonding and antibonding π and π^* (blue lines) orbitals. The π and π^* groups are decoupled from σ and σ^* (red lines) because of

the reversal symmetry and they are nearer to the Fermi level since they contribute less in the chemical bonding. Fermi level is set as zero for simplicity and it separates occupied and empty states. The π bands present the largest separation at the Γ point but they touch at K point (green circle) of the Brillouin zone. There is no overlap or gap between the π and π^* at that point. Because of this graphene is called as a zero band gap semiconductor or as a semi-metal. The π band take a significant role for electronic conductivity in the graphene [22].

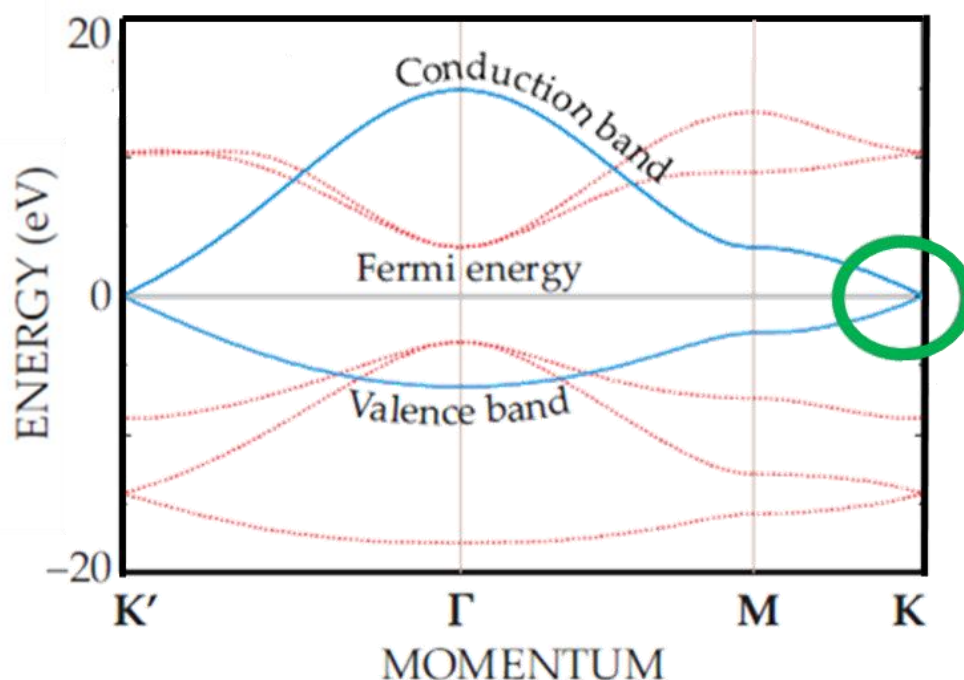


Figure 2.5 Electronic band structure of graphene [22].

The honeycomb structure of graphene consists of two interpenetrated triangular sub-lattice arranged with σ bond. Just a single π orbital exists for every carbon atom in the crystal lattice. This orbital adds to delocalized arrangement of electrons [23]. Figure 2.6 shows these two nested triangular sub-lattices in a honeycomb graphene lattice. One of the triangular is A plotted by dashed blue line and the other one red dashed triangular is B. The unit cell includes two carbon atoms. The carbon-carbon inter atomic length is 1.42 \AA in the lattice. Each atom includes one s orbital and two in-plane p orbitals. Hybridization of p orbital which is perpendicular to the plane structure has effect to

form π^* (conduction) and π (valance) bands. The π -electrons are effective for the electronic properties of graphene.

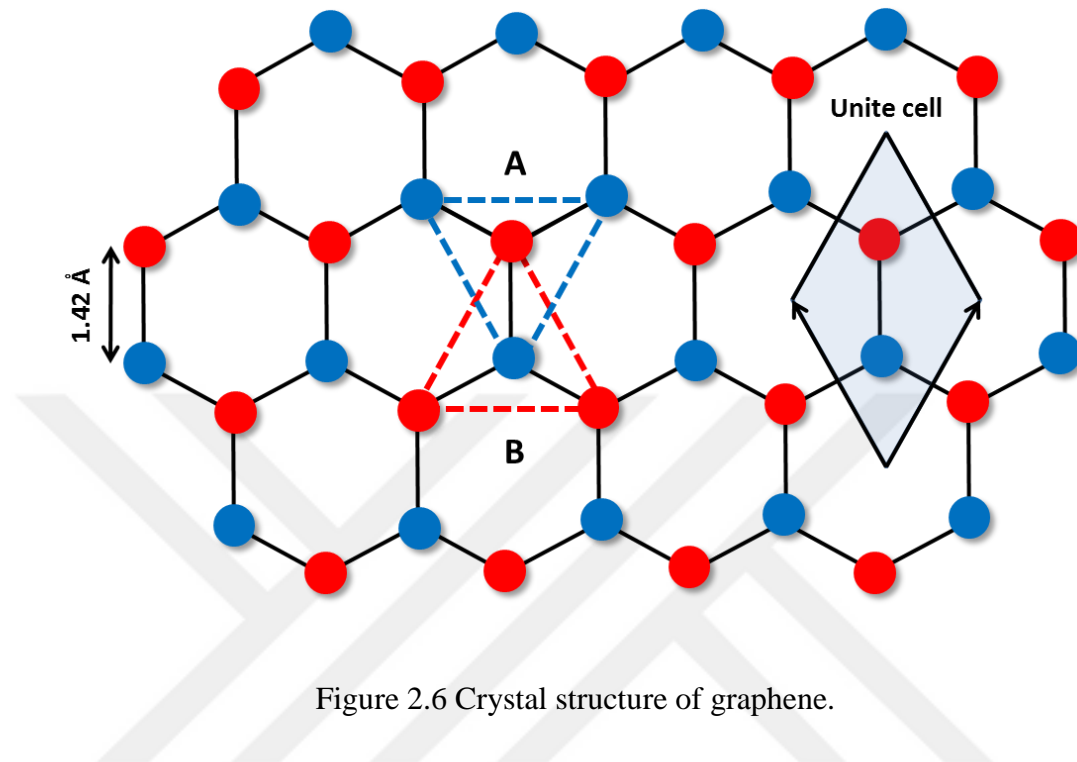


Figure 2.6 Crystal structure of graphene.

2.2.3 Electronic Properties

The Fermi surface of graphene is represented by six double cones (see Figure 2.7a). Red and blue cones indicate the valance and conduction band, respectively. These cones touch at discrete points (K and K') in the Brillion zone. In the case of intrinsic graphene the Fermi level locates at the connection points of these double cones. Density of state is zero at that point so that the intrinsic graphene exhibits low electrical conductivity. Energy-momentum dispersion near the Fermi level is linear both for the electrons and the holes. This linear relationship is similar to energy-momentum relationship of photons and the excitation equation can be described by the Dirac equation for massless fermions which travel at a constant speed. Due to this similarity the charge carriers in graphene are labeled as massless Dirac fermions and the point where the conduction and valance bands meet is called the Dirac point [24].

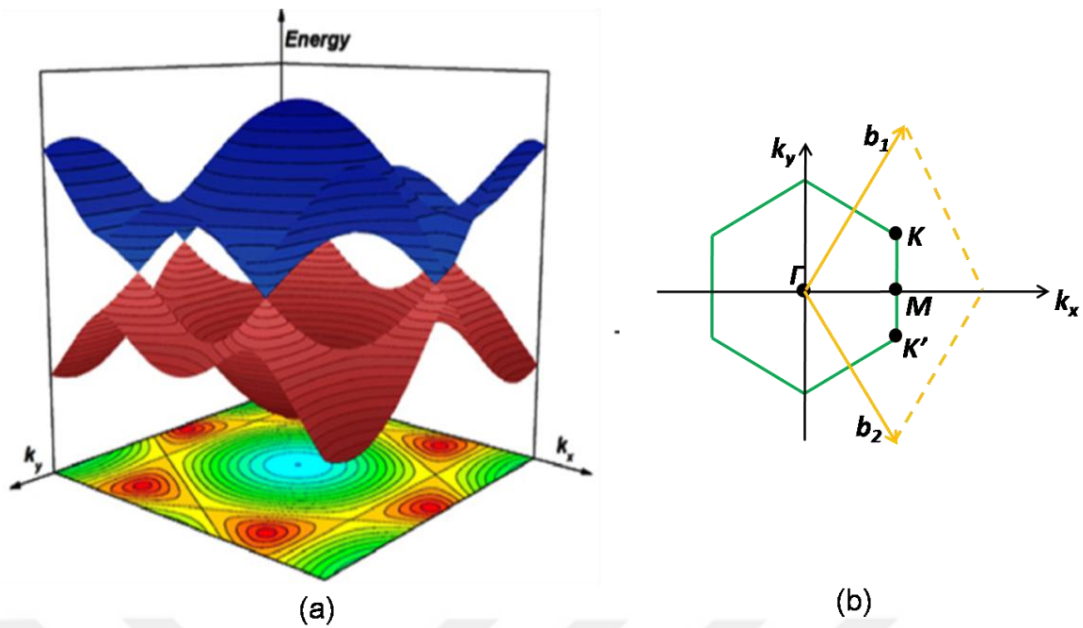


Figure 2.7(a) π - π^* band structure of graphene [25], (b) Brillouin zone

The early theoretical studies predicted extremely high mobility and ambipolar field-effect in graphene [15, 26]. High quality 2D crystal lattice of graphene causes extraordinary high electrical properties [27-29]. This high quality provides an unusually low density of defect which generates scattering that obstructs the charge transport. The extraordinary high value of charge carrier mobility, over $200,000 \text{ cm}^2 \text{ V}^{-1} \text{ s}^{-1}$, was obtained in suspended single layer graphene diminishing the impurity scattering by Kim's group at Columbia University [4]. Graphene exhibit an ambipolar field effect that is charge carriers can be symmetrically tuned between the electrons and the holes by changing the direction of applied electric field. Temperature has weak effect on electron mobility in graphene and mobility is very high even at room temperature [28]. In the case of both electrically and chemically doped devices, electron mobility in graphene can remain high even at high carrier density [30]. There is also evidence of ballistic transport on close to micrometer scale [31].

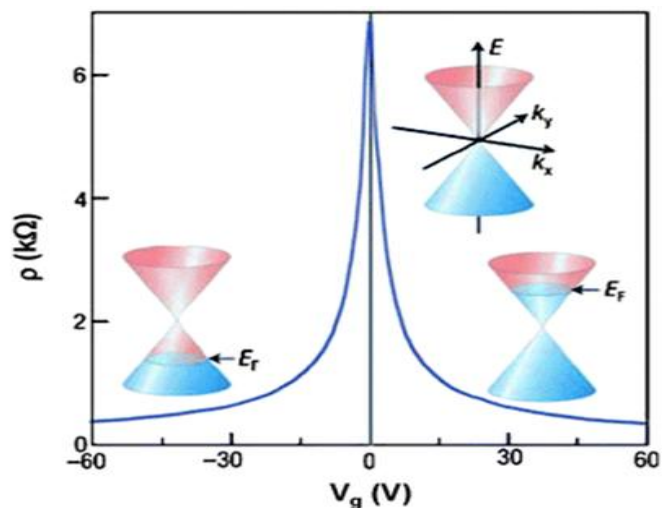


Figure 2.8 Ambipolar electric field effect in single layer graphene. [32].

Single layer graphene shows quantum hall effect (QHE) for both electrons and holes at low temperature and high magnetic field due to its anomalous mobility. But it is different from the conventional QHE. The plateaus arise at half integers of $4e^2/h$ whereas typical arise at $4e^2/h$ (see Figure 2.9) [20, 21].

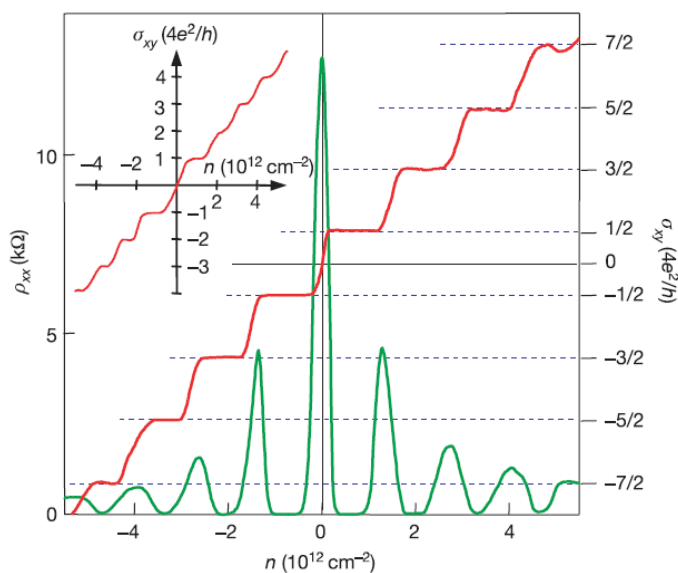


Figure 2.9 Quantum Hall effect in single layer graphene [20].

2.2.4 Mechanical and Optical Properties

The mechanical properties of graphene including Young's modulus and fracture strength have been examined using numerical simulation [33, 34]. The Young's modulus was investigated with force-displacement measurements by using AFM for suspended graphene [35]. Circular membrane of few layer graphene were also probed by force-volume measurements by AFM [36]. The elastic properties and intrinsic breaking strength of suspended single layer graphene were investigated by AFM (Figure 2.10a and b) [37]. The Young's modulus and fracture strength of graphene were determined to be 1.0 TPa and 130 GPa respectively [38]. Paper like materials obtained from individual graphene oxide layers were studied [39]. It is reported that the average elastic modulus and the highest fracture strength of this oxide layer were nearly 32 GPa and 120 MPa, respectively.

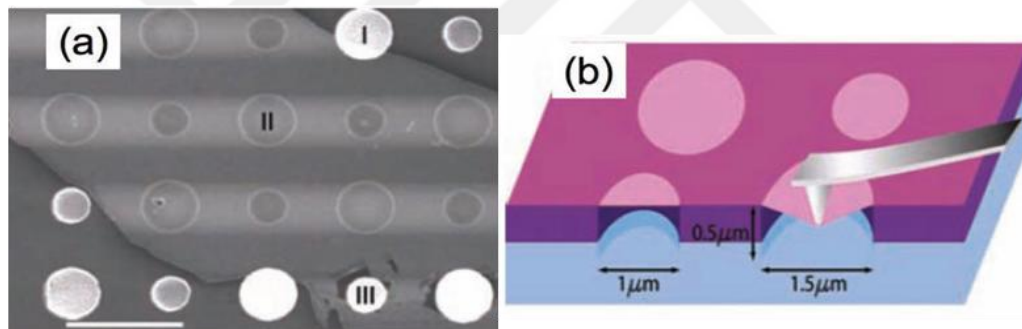


Figure 2.10 a) Scanning electron microscopy (SEM) image of graphene flake with circular holes (scale bar, 3 μm), b) Schematic illustration of suspended graphene [37]

In addition to its unique electrical and mechanical properties graphene also presents interesting optical properties. It is optically transparent and it absorbs only 2.3% of white light. The transmittance of graphene linearly diminishes with the number of layers [40].

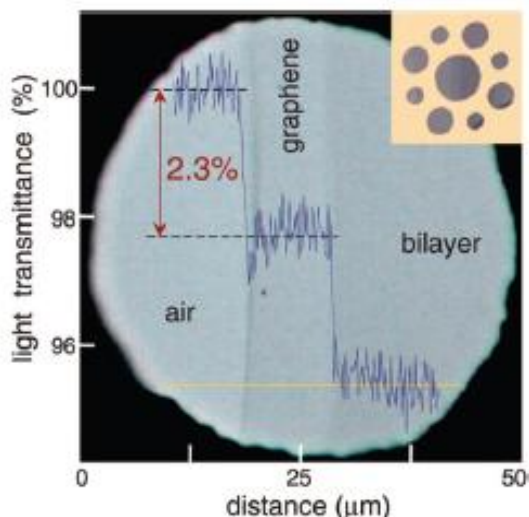


Figure 2.11 Optical image of partially covered with single and bilayer suspended graphene [40].

2.3 GRAPHENE OXIDE

Although it's the extraordinary electrical, thermal, mechanical and optical properties of graphene [4] are unfortunately offsetted by the lack of an electronic band gap [5]. As a result, rather than working with pristine graphene, many researchers are concentrating their efforts on novel graphene derived materials which might allow for devices with tunable electronic properties. A few nanometer wide graphene ribbons, for example, have a bandgap opening that can be controlled by changing the width of the ribbon, [41-43] whereas, hydrogenated graphene (that is graphane), [44, 45] fluorinated graphene (fluorographene) [46, 47] and graphene oxide [48, 49] are insulators. Functionalization with diazonium salts is becoming popular as another route for controlling the electronic structure of graphene [50-54]. In addition to being a simple method for producing large amounts of graphene oxide, Hummers method [55] or its modified versions [56, 57] are also useful as an intermediary step for further functionalization of graphene [58].

Graphene oxide is usually obtained by exfoliation of graphite oxide through sonication in a solvent [59]. There are, however, examples of direct oxidation of graphene, as well. For example, several groups used Atomic Force Microscope (AFM) lithography to induce local anodic oxidation on single and multi-layer graphene flakes

[45, 60-62]. More recently, Wang *et al.* showed that the single layer graphene (SLG) flakes may be oxidized in a controlled fashion using wet chemistry [63].

Graphene oxide includes a range of reactive oxygen functional groups (carboxyl, hydroxyl or epoxy) which randomly attach to the graphene lattice. C-C π - and σ - bonds are broken and it causes breakdown of conductivity. The attachment of functional groups give the opportunity to use GO for some applications, such as in polymer composites, energy related materials, sensors, paper-like materials, field-effect transistor (FET) and biomedical applications [64].

The oxidation of graphite into graphite oxide is one of the important techniques to produce large scale graphene [58]. It was first synthesized by Brodie when he was researching the structure of graphite [65]. After Brodie's discovery, Staudenmaier [66], Hummers and Offeman [55] improved Brodie's mixture. Brodie and Staudenmaier used a mixture of potassium chlorate (KClO_3) with nitric acid (HNO_3) whereas Hummers and Offeman used potassium permanganate (KMnO_4) and sulfuric acid (H_2SO_4) in the reaction. The most graphene oxide is produced by Staudenmaier method but it can take several days. Both Brodie and the Staudenmaier's methods produce highly toxic ClO_2 gas during the reaction [67]. On the other hand, Hummers method has relatively shorter reaction time and it does not produce the hazardous ClO_2 gas which makes it a popular choice in the graphene oxide production. Today this method is being widely used with some modifications.

During the oxidation of graphite, sp^2 -hybridized structure within some layers breaks up and defects are formed [68]. The intercalation of functional groups (epoxy and hydroxyl) between the graphite layers lead to an increased distance between the adjacent sheets from 3.4 \AA to nearly 6.8 \AA [69]. The single layer GO layers can be easily obtained from graphite oxide by sonication in water with same structural defects. [67].

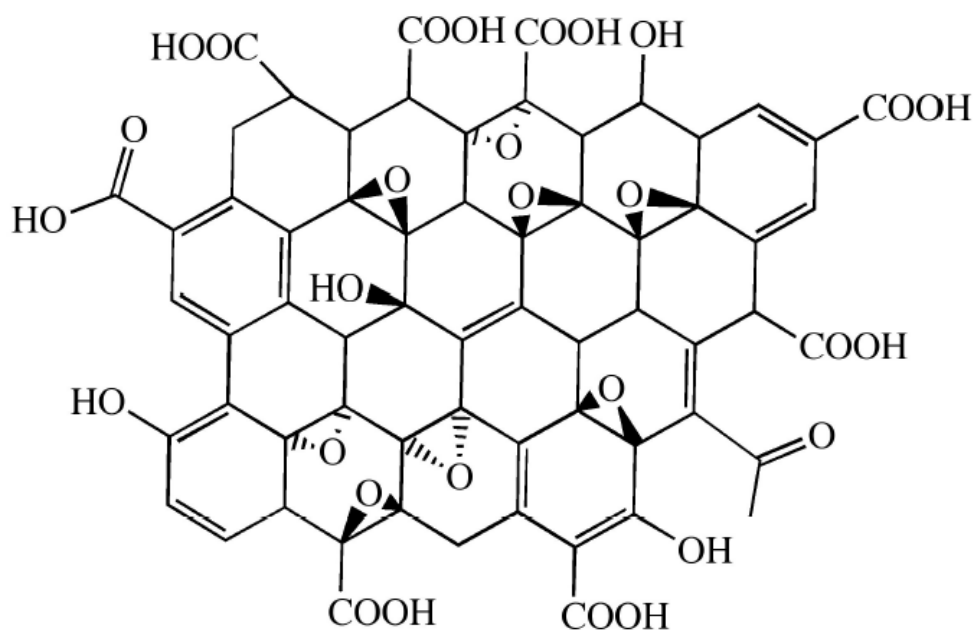


Figure 2.12 Schematic illustration of a graphene oxide sheet. sp^2 and sp^3 -hybridized carbons include hydroxyl and epoxide functional groups in its basal plane, but the edges are decorated by carboxyl and carbonyl groups.

Beside oxidation mechanism, the chemical structure of GO has been debated over the years. Several methods have been presented to explain chemical structure of GO, such as Hofmann [70], Ruess [71], Scholz-Boehm [72], Nakajima-Matsuo [73] and Lerf-Klinowski (LK) [74]. Among these methods LK appears to be the best model. This model reveals that GO involve two different randomly disturbed domains having sp^2 and sp^3 hybridized carbon atoms. Epoxy and hydroxyl functional groups exist on its basal plane on the GO regions. But the edges of GO layer are decorated with carboxyl and carbonyl groups (see Figure 2.12) [75, 76]. These functional group make graphene oxide sheets strongly hydrophilic, so it is easy to disperse the graphene layer in water [77].

Even though graphene is electrically a good conductor, graphite oxide and GO are electrically insulating materials due to the disturbed sp^2 bonding. The electrical conductivity can be recovered by restoring the π -network through chemical reduction of the GO sheets. There are several methods for this treatment but the most commonly used are chemical, thermal and electrochemical. The new material obtained after

reduction is called reduced graphene oxide (RGO). After the reduction, atomic C:O ratio increases, band gap of RGO becomes smaller and RGO becomes conductive again [78]. GO sheets become more hydrophobic (nonpolar) as a result of reduction and this hydrophobicity adversely affect the dispersion properties. RGO sheets contain structural defects and residual oxygenated functional groups induced during the process [79]. Generally hydrazine, hydroquinone, sodium borohydride (NaBH_4), or ascorbic acid are used as reduction agents [80].



CHAPTER 3

METHODS

3.1 GRAPHENE PRODUCTION METHODS

In the graphene technology there are two important obstacles for applications. One of them is mass-production and other one is reproducibility of graphene based device performances. Researchers have widely studied to overcome these problems [8-9]. The most easy, fast and cheap production technique is mechanical exfoliation method. It also provides high crystalline quality samples. But in order to use graphene in any application, large scale graphene production is necessary. Mechanical exfoliation method presents simple, fast and cheap production and produced graphene demonstrates extraordinary electrical and optical properties but the sample size and quantity is small for applications. Researchers have studied other graphene synthesis methods such as epitaxial growth, chemical vapor deposition (CVD), chemical exfoliation, and etc. In our study graphene samples were prepared from natural graphite flakes by mechanical exfoliation.

3.1.1 Mechanical Exfoliation Method

As the most common production method of graphene, mechanical exfoliation has been used since the discovery of pencil. Graphene sheets are simply produced by pushing the pencil on the paper but you can not control the thickness. The remarkable experimental studies in the scientific field in order to create single layer graphene have started in the 1990s.

Ruoff and his friends showed one approach utilizing AFM tip and attempted to control the little columns designed into the HOPG by plasma etching. The watched

most slabs were more than 200 nm thick and it comprised of right around 600 layers. Enoki's group changed over the nanodomains into the nanometer measured locales of graphene on HOPG in 2001. Later Kim's gathering at Columbia College changed Ruoff's technique and they exchanged the columns to a tipless cantilever and they effectively put the sections on the SiO₂ substrate. By this technique they got 10 nm sheets or almost 30 layers [82]. All these process were complicate and also they had yet to obtain single layer graphene. On the other hand, in 2004, A. Geim and his group at Manchester were successful to obtain single layer graphene using a much more simple approach. This approach does not enable large size graphene layers but it produces high quality samples which are useful for fundamental laboratory research. Its main principal is based on peeling of layers from graphite sheets by an adhesive tape. The quality of the obtained single layer graphene is influenced from adhesive tape and graphite flakes used during the graphene production. If substrate have more tape residue derived from adhesive high quality graphene can not be produced.



Figure 3.1 The steps of preparation of graphene samples by exfolation method.

The steps of the mechanical exfoliation are shown in Figure 3.1. Initially, (SiSiO₂/Si) substrate is cleaned with piranha solution which is H₂SO₄:H₂O₂ (3:1). This solution removes metals and organic contamination due to its highly oxidative feature. After cutting the substrate into 2x2 cm pieces, they are placed in the piranha solution

and kept in an ultrasonic bath for 45 minutes. After sonication, substrates are rinsed by DI water and dried by N_2 .

A few graphite flakes are placed onto a scotch tape. The tape is folded and peeled many times until various thin graphene and graphite layers cleave and cover the surface of the scotch tape. Subsequently, tape is attached to the SiO_2/Si wafer (oxide layer of 300nm). It is pressed softly on the wafer in order to form good contact between the flakes on the tape and the substrate. The tape is, then, slowly pulled out of the surface. Many graphene flakes which have different size, shape, and thicknesses ranging from a single layer up to hundreds of layers remain back on the surface. The samples are scanned under an optical microscope in order to identify the location and size of single layer graphene flakes among hundreds of graphite flakes. Due to the finite transmission of graphene and an interference effect, graphene layers can be detected under the optical microscope when it is placed on the 300 nm SiO_2 coated substrate[81]. Raman Spectroscopy and AFM are also used to confirm the number of layers within the identified flakes.

3.1.2 Other Graphene Production Methods

Although mechanical exfoliation method is widely used due to the high quality of the flakes and low cost of production, other methods are also used to produce graphene, such as chemical exfoliation (oxidation of graphite), epitaxial growth and CVD method. Chemical oxidation method can produce large amounts of graphene but the product is usually low crystalline quality due to the difficulty of removing the oxygen groups attached to the basal plane of the flakes. This procedure is briefly described in Section 2.3. Silicon carbide (SiC) is used as substrate for epitaxial growth. When SiC is heated to high temperatures for controlled durations, it is possible to form a single layer graphene flake on the surface of the crystal [82] This technique can be suitable for future industrial applications because it produces large scale graphene layers. However the prepared graphene has more defects in its crystal structure when compared to exfoliated graphene.

Among graphene production methods, CVD is being widely used for growing large scale graphene sheets for future technological applications. For example, Bae et al. managed to obtain a 30 inch monolayer predominated graphene using roll-to-roll production method [83]. In this method, graphene is grown on copper foils by

dissolving carbon atoms from organic molecules such as methane or acetone at high temperature. The resulting product consists of grains (domains) and hence the flakes are not single crystal. The grain act as a line defect and increases the carrier scattering which decreases the carrier mobility [84].

3.2 CHARECTERIZATION METHODS

A key step for carbon research and application after production of graphene is detection and characterization of graphene at both laboratory research and mass production. Characterization method must be nondestructive during process and fast. It must provide maximum information about structure and electronic features at high resolution. It also must give sufficient structural and electronic information. Raman spectroscopy and atomic force microscopy (AFM) can present all these mentioned above.

3.2.1 Raman Spectroscopy

Raman spectroscopy is a light scattering spectroscopy and it gives information about the vibrational and rotational modes of molecules in different states. It was discovered by Krishna and Raman in 1928 and they were awarded Nobel Prize in physics in 1930. Two possible scattering can occur in spectroscopic technique; elastic and inelastic scattering after incident photons interact with the atoms or molecules. In the elastic scattering the incident frequency does not change and it is equal to the scattered frequency. Raman spectroscopy is based on inelastic scattering of light. In the case of inelastic scattering, there is energy difference between the scattered and incident photon. The photons are first absorbed by the sample and then reemitted. The original value of frequency of reemitted light is not conserved and it is shifted up or down. Vibrational and rotational information about molecules can be obtained based on the amount of this shift.

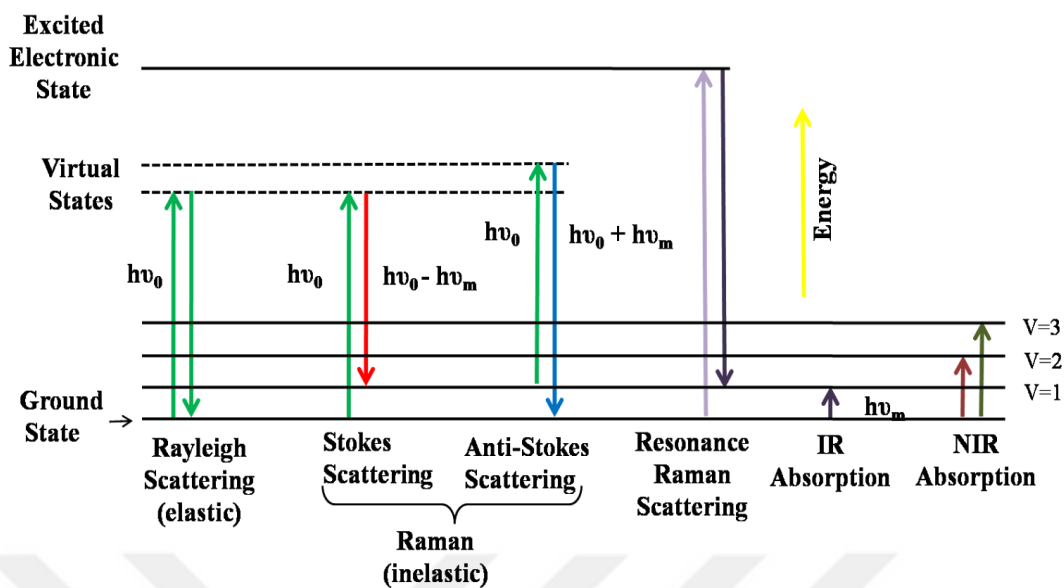


Figure 3.2 Energy level diagram to explain Raman scattering.

Molecular polarizability α create an electric field E and it causes a deformation in the molecular structure. The Raman effect is based on this deformation. Laser beam induces an electrical dipole moment $P = \alpha E$ and this dipole moment deforms the molecule which initiates vibrations at the specific frequency ν_m of the molecule.

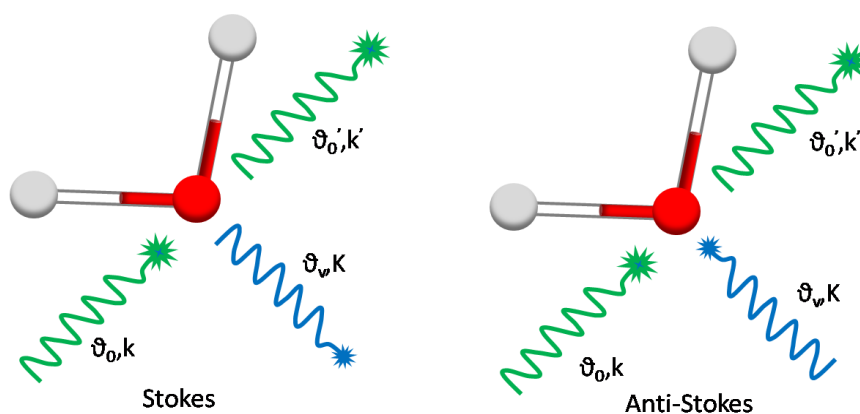


Figure 3.3 Schematic representation of Stokes and anti-Stokes lines.

After excitation of molecules with the incident beam (monochromatic laser light) light can be emitted at three different frequencies. First, a molecule is excited by absorbing a photon with ν_0 frequency and then molecule wants to turn back to its initial state. During this transition molecule emits a photon with the same frequency ν_0 . This is an elastic scattering and also called Rayleigh scattering. A molecule in its basic vibrational state absorbs a photon with ν_0 frequency by a Raman active mode. During the reemission, a photon with a smaller energy is emitted. The difference with corresponding frequency ν_m is used to initiate a Raman-active vibrational mode of the molecule. After reemission, scattered light frequency will be $\nu_0 - \nu_m$ which is called Stokes frequency. In a third type of scattering a molecule already excited to a Raman-active vibrational mode absorbs a photon. Then the molecule decays back to a lower energy vibrational state, resulting in higher energy photon emission of frequency $\nu_0 + \nu_m$. This type of Raman frequency is called Anti-stokes frequency. The energy difference between the incident and scattered beam is represented by Raman shift in wave number (cm^{-1}).

$$\nu = \frac{1}{\lambda_{\text{incident}}} - \frac{1}{\lambda_{\text{scattering}}}$$

λ is wavelength (unit is cm). If a filter is not used scattered light has a strong peak at around 0 cm^{-1} . Nearly 99.9999 % of all incident photons are scattered as elastic Rayleigh. These photons are not useful for practical studies of molecular characterization. The rest of the incident photons are scattered as either Stokes or anti-Stokes inelastic Raman signal with frequencies $\nu_m \pm \nu_0$. The positions of stokes and anti-stokes bands exist as symmetric on each side of 0 cm^{-1} .

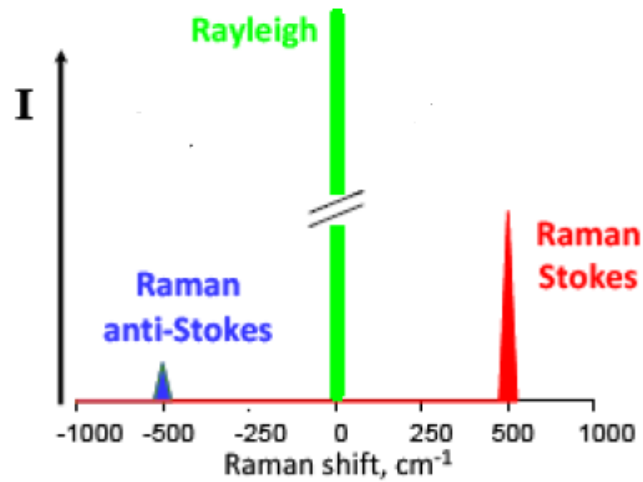


Figure 3.4 Rayleigh and Raman signals.

Raman spectrometers consist of four components: light source, collection optics (sample illumination system), wavelength analyzer and detector. Lasers are used as light source and its spectral region can be in the ultraviolet, visible or infrared. Generally argon and krypton laser are used. The light from the laser source first focused on the sample. After interaction with the sample, scattered light is collected with a lens and passed through an interference filter. As mentioned earlier 99% of all scattered light is Rayleigh scattering which has the same frequency as the incident beam. Less than 1 % of the scattered light is due to Raman scattering with a different wavelength. The laser rejection filter is used to remove the Rayleigh scattered light allowing only the Raman scattered light to go through. Then a grating diffracts the light for wavelength analysis. Charge coupled device (CCD) generates an electrical signal in response to the intensity of light. These electrical signals are sent to the computer for analysis.

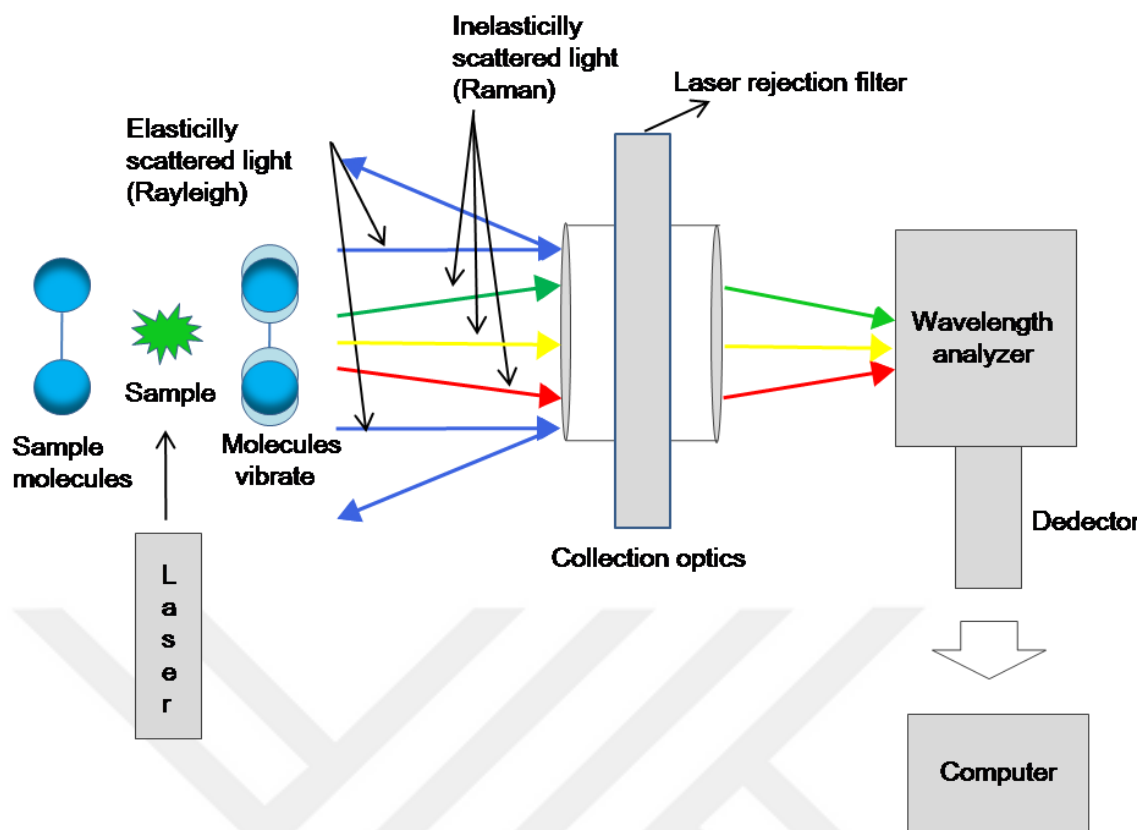


Figure 3.5 Instrumentation for modern Raman spectroscopy consists of four components: a laser source, collection optic, wavelength analyzer and detector.

Raman spectroscopy offers a versatile tool for identification and analysis of carbon based research. Therefore it is one of the most popular techniques for spectroscopic analysis. It can be used to determine number of layers of few layer graphene [85-87], impurity doping level [88-90], edge type [91], strain [92], concentration of defects [93-95], and etc. and therefore is one keystone for graphene research.

Raman scattering from carbon materials present similar features in the range of $200\text{-}8000\text{ cm}^{-1}$ (see Figure 3.7). Carbon based materials like graphite and graphene have two distinct Raman peaks labelled as G and D peaks which lies at around 1580 cm^{-1} and 1350 cm^{-1} , respectively.

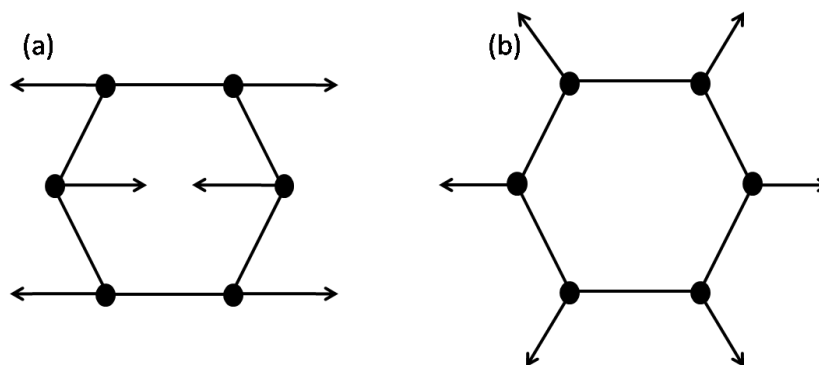


Figure 3.6 a) The G mode of graphite lies at around 1581 cm^{-1} has E_{2g} symmetry. b) The D peak at nearly 1350 cm^{-1} is a breathing mode of A_{1g} symmetry.

G peak has E_{2g} symmetry at the centre of the Brillion zone. This E_{2g} mode has a bond-stretching motion. It can, also, be explained by linear opening and closing of the carbon sp^2 pairs. G band is sensitive to charge transfer and it can be an indicator of doping or impurity. The D peak corresponds to the in plane breathing mode of A_{1g} symmetry at around K zone boundary. This peak is Raman inactive in graphene and graphite and does not appear in absence of defects in crystal structure. Therefore, D peak is an important indicator to reveal any defects or impurities within the crystal structure. Graphene also has a second order peak at around 2700 cm^{-1} called the 2D peak. it's the shape, position and intensity of this peak changes with the number of layers in a graphene flake, allowing one to identify the number of layers of the sample under study [96].

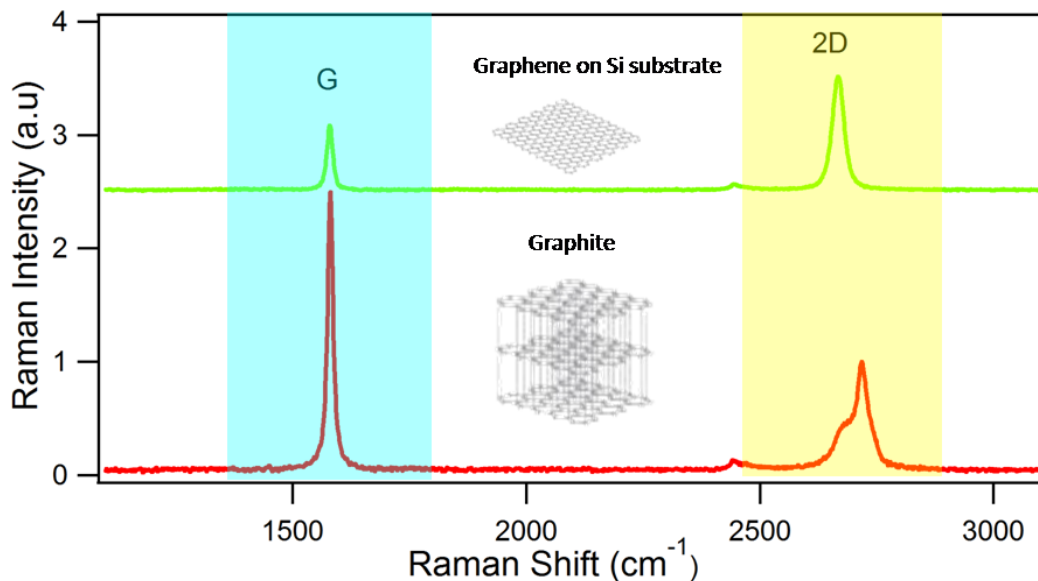


Figure 3.7 Raman spectrum of single layer graphene (top) and graphite (bottom)

We used a dispersive Raman microscope (Thermo, DXR Raman) for Raman measurements. During the measurements we used a 532 nm wavelength laser and the laser power was set to 1 mW.

3.2.2 Atomic Force Microscopy

A scanning tunneling microscope (STM) can be used to study conductive materials but not the non-conductive materials. Binnig and Quate who developed the (STM) demonstrated first ideas of AFM in 1986 to scan non-conductive surface and they used an ultra-small probe. AFM is used for surface science to obtain images of surfaces in atomic resolution and it does not require any vacuum condition. It provides a 3D profile of the surface on a nanoscale. Beside its advantages it has some disadvantages. Scanning size is limited to micrometers and also the height profile is limited to a few microns. The tip should be long and thin, and otherwise it might start sensing some step edges.

AFM measures the forces between a sharp tip and the sample. A cantilever with the sharp tip mounted on its end is scanned over the surface of the sample as the tip interacts with the surface. The interaction between the tip and the surface results in attractive or repulsive force which bends the cantilever up or down. These conditions

appear in different modes which are chosen according to the characteristic features of the sample. Cantilevers are generally made from silicon or silicon nitride. The radius of the tips is of the order of nanometers. The dependence of the van der Waals forces which is the most basic interaction between the tip and the surface as a function of the distance between the tip and the sample is shown in Fig 3.8.

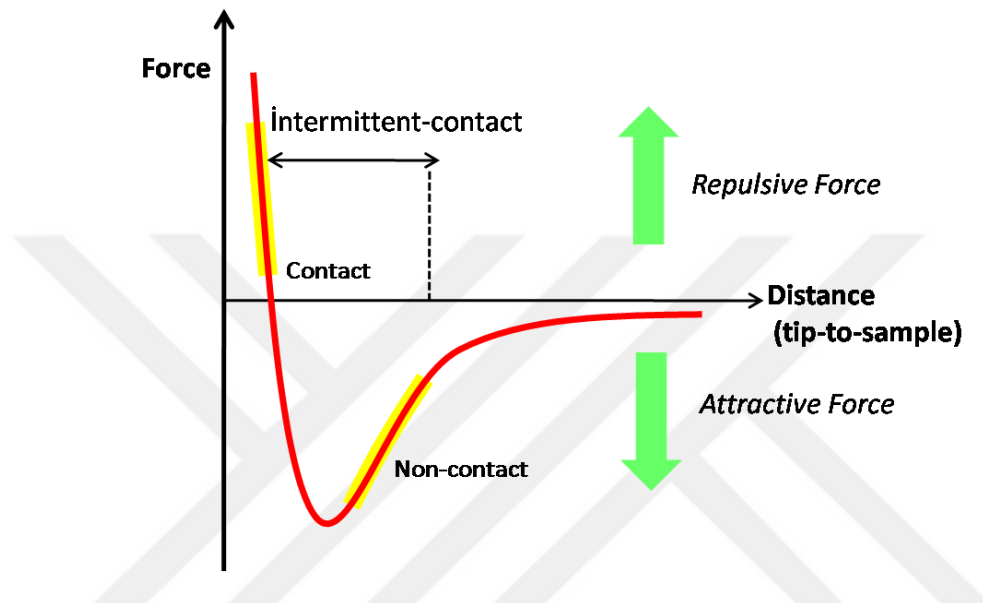


Figure 3.8 Dependence of the potential energy vs the distance between tip and the sample during their interaction.

A focussed laser beam is reflected off the cantilever and the reflection is tracked with a position sensitive photodetector (PSPD). Highly accurate position control of the cantilever and the sample is achieved with the help of piezo crystals. AFMs are most commonly operated in three different modes: contact, non-contact and tapping mode.

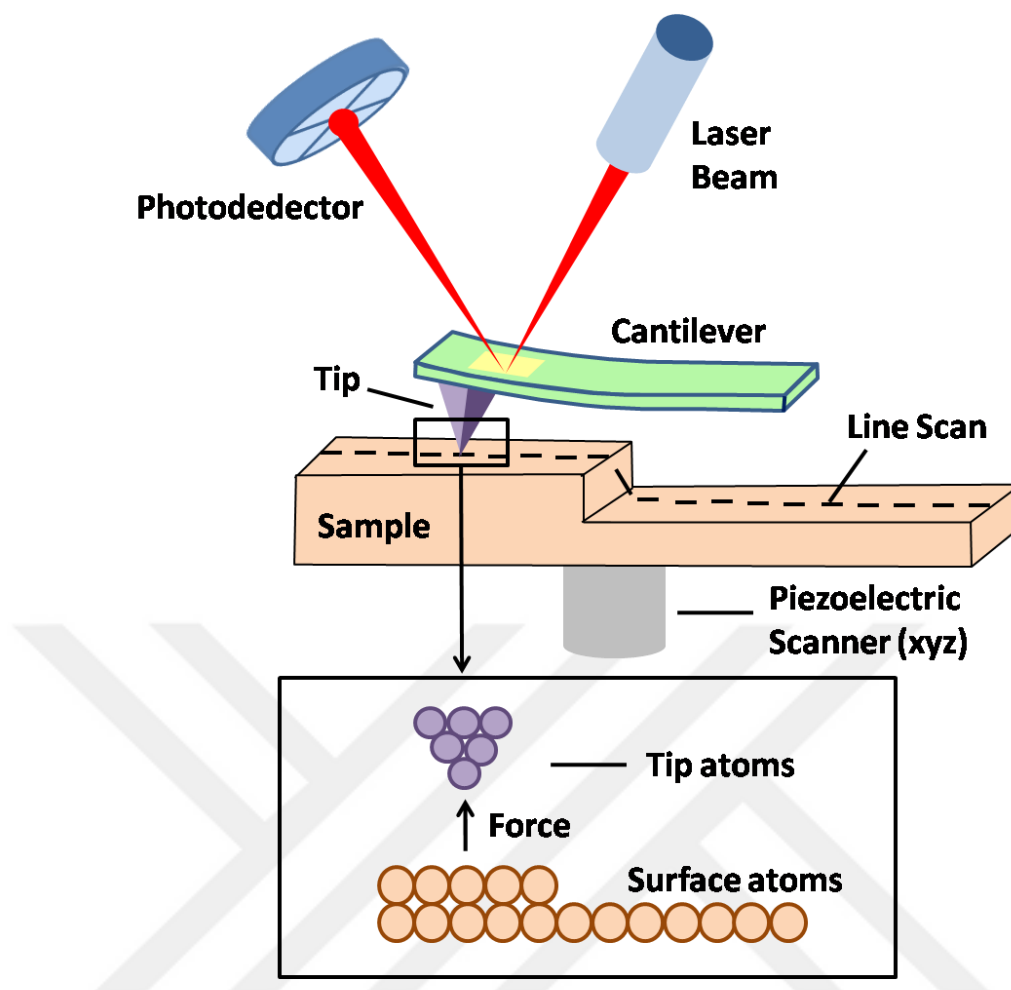


Figure 3.9 Block diagram of AFM

In the contact mode, the tip is in physical contact with the sample surface and the resulting interatomic force is repulsive. Surface topography can be imaged in two ways: First, the height of the cantilever can be kept constant and the variation of its deflection can be used as an indication of surface topography. This mode is generally used for atomically flat surfaces to obtain an atomically resolved image. In such cases, variation of the applied force will be small and hence cantilever deflection will be small as well. Second method is to keep the repulsive force constant force by moving the cantilever up or down such that its deflection remains the same. Then the topography image is formed based on this vertical motion of the cantilever. In contact mode, data acquisition is fast, resolution is high and frictional information between the sample and the AFM tip can be collected as an additional benefit. The frictional interaction causes the cantilever to twist during the scanning of the surface which can be monitored by the PSPD. This

twisting motion can be then used to form Lateral Force (frictional force) Microscopy images of the sample under study. The major downside of contact mode is that, sensitive samples can be easily damaged by the AFM tip.

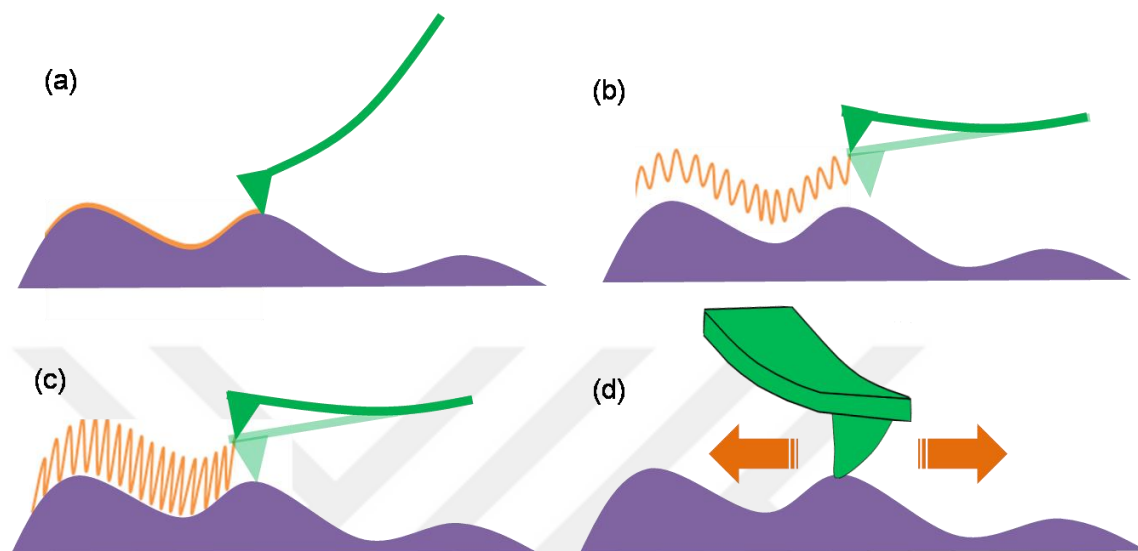


Figure 3.10 AFM modes; a) contact, b) non-contact and c) tapping and d) lateral force

In non-contact mode, the tip does not contact the sample surface. Interaction force is attractive. The cantilever is instead oscillated near at its resonance frequency. The interaction force between the tip and the cantilever changes the vibrational resonance frequency of the cantilever which results in a change in the amplitude of the cantilever oscillations. The oscillation amplitude varies from a few nanometers (<math><10\text{ nm}</math>) to a few picometers. This amplitude is used as a feedback to monitor sample cantilever interaction. By adjusting vertical piezo scanner to keep the oscillation amplitude constant, a height image is recorded. Changes in the phase of oscillations relative to the vibrational driver can also be used to analyse mechanical properties of the sample under study.

In the tapping mode, AFM is operated in a mixture of contact and non-contact modes. The cantilever is allowed to oscillate up and down at a very close distance to the surface such that the tip can come into physical contact with the surface during the

oscillation. This close proximity increases the local interaction between the tip and the sample allowing higher resolution and sensitivity. In addition, it eliminates the frictional force which is likely to damage sensitive samples.

AFM is one of the characterization methods for researching graphene. It gives a chance to observe graphene flake edges, flakes corrugation, interplanar distance. The thinnest graphene flake was first optically monitored by AFM. As it is known thickness of single layer graphene is 0.34 nm but it is measured as nearly 1 nm due to the airspace between the single layer graphene and substrate (see Figure 3.11).

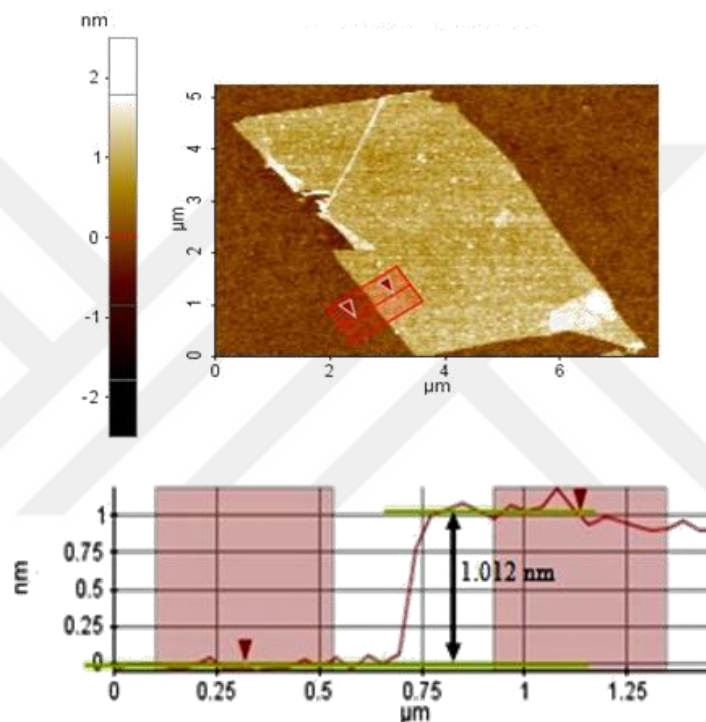


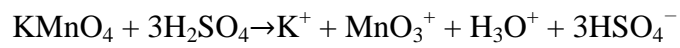
Figure 3.11 AFM image of single layer graphene obtained in our studies.

3.4 WET OXIDATION METHODS

We used two different solutions for oxidation process. One of them is 0.4 M KMnO_4 in 50% H_2SO_4 and other is 0.015 M KMnO_4 in 50% H_2SO_4 (1:1 volume ratio) which was used by Wang *et al.* [63]. Then the substrates containing graphene samples are immersed in these solutions for various durations. Immediately afterwards, substrates were rinsed with plenty of DI water. Often it is observed that the substrate surface is largely contaminated with chemical residues (presumably MnO_2 crystallites)

after this procedure. These contaminants are effectively removed by immersing samples in 3% H₂O₂ for 10 minute. AFM images before and after H₂O₂ treatment show no signs of structural changes to oxidized samples but the image quality improves upon the removal of the residues.

In these solutions the strong oxidative agent arises due to chemical reaction of the H₂SO₄ and KMnO₄. It's named as dimanganeseheptoxide (Mn₂O₇). The chemical is formed as a result of the following reactions:



CHAPTER 4

RESULTS AND DISCUSSIONS

4.1 INTRODUCTION

Graphene samples were prepared by mechanical exfoliation method on SiO₂/Si substrates using natural graphene flakes. CVD grown single layer graphene was obtained commercially. Appropriate SLG are located under optical microscope and the number of layers is confirmed using a dispersive Raman microscope (Thermo Scientific, DXR Raman). Measurements were made using a 532 nm laser beam with a power ranging between 1 and 3 mW and 100X objective with estimated beam spot diameter of 0.6 μm. Despite having varying impurity doping levels, all samples used in this study had high crystalline quality with no D peak in the Raman spectra of the as prepared samples. The variations in the impurity doping levels within each sample were determined by recording Raman maps. In the Raman maps, image resolution was set either to 0.5x0.5 μm² or 1x1 μm². During the mapping, Raman data is collected for 3s at each location on the sample. In the analysis of Raman spectra, graphene D, G and 2D peaks were fitted to Lorentzian peaks to identify parameters such as peak position, intensity and width before and after oxidation of the samples. Topographic and lateral force microscopy image of single layer graphene before and after chemical treatments were obtained by AFM (Park System, XE-series) in contact mode (AFM tip: APP Nano, SHOCONA-10). The AFM tip force was set to 4.9 nN.

For the oxidation of the samples we followed the recipe suggested by Wang *et al*[63]. We prepared solutions of 0.015 M KMnO₄ in 50% H₂SO₄ (1:1 volume ratio) and then the substrates containing graphene samples are immersed in these solutions for various durations. Immediately afterwards, substrates were rinsed with plenty of DI water. Often it is observed that the substrate surface is largely contaminated with

chemical residues (presumably MnO_2 crystallites) after this procedure. These contaminants are effectively removed by immersing samples in 3% H_2O_2 for 10 minute. AFM images before and after H_2O_2 treatment show no signs of structural changes to oxidized samples but the image quality improves upon the removal of the residues.

4.2 DETERMINATION OF GRAPHENE THICKNESS

As we mentioned in Chapter 1, our purpose is oxidation of exfoliated single layer graphene. For this reason, a lot of SiO_2/Si substrates which include a lot of graphene and graphite layers were prepared. The exfoliation method enables us to obtain many graphene flakes but only a few of them are single or bi-layer thick. We know that single layer graphene is very thin and its thickness is only 3.4 nm and therefore it is very difficult to observe single layer graphene. But silicon wafer with 300 nm thick SiO_2 layer on top of it make graphene visible under optical microscope [81]. Silicon wafers were scanned under optical microscope and locations of suitable sample were determined.

Figure 4.1a shows the optical image of a sample. The sample consists of many different thicknesses; single, double, triple etc. It is clearly noticed that sample contrast changes with thickness of the graphene. Single layer is light colored and it becomes darker as the sample thickness increases. Even though optical image shows changes in the thicknesses of the flakes it does not tell us how many layers there are within a flake.

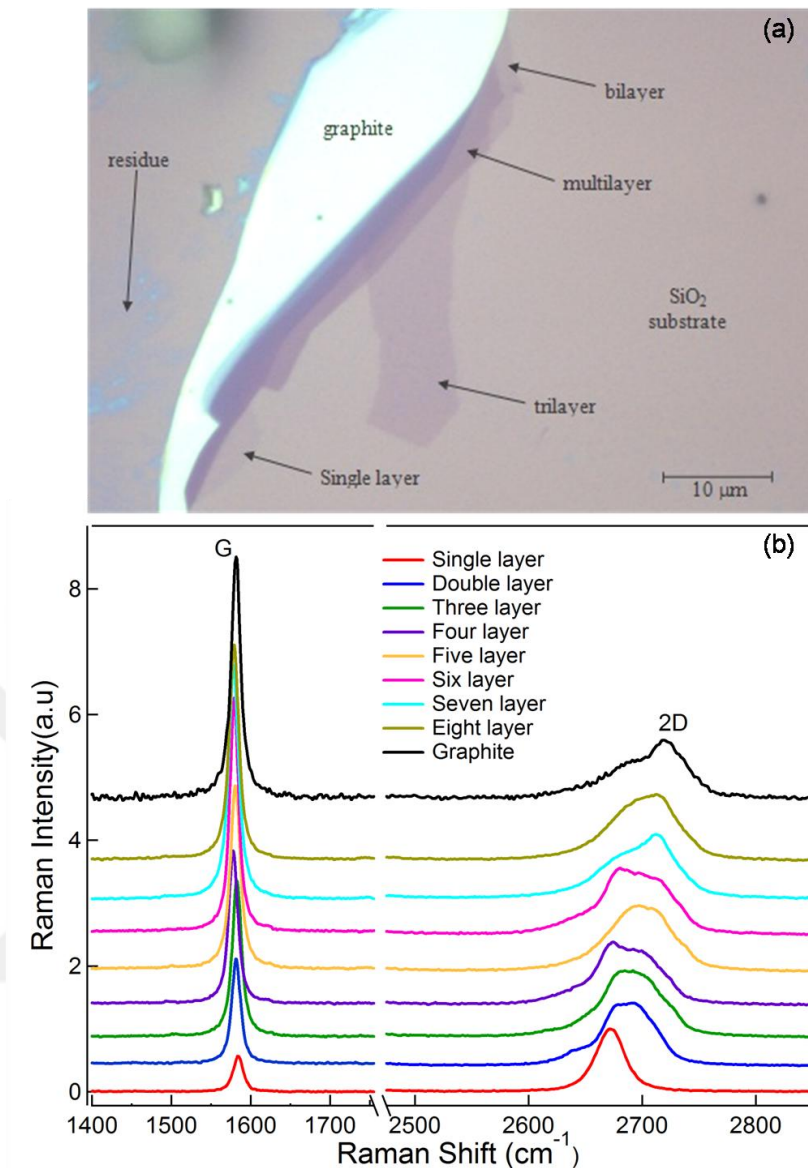


Figure 4.1 a) optical image of graphene which has different layer on SiO₂/Si substrate, b) The shape of G and 2D peak from monolayer to eight layer.

Raman spectra of samples from single layer to eight layers are plotted in the Figure 4.1b. Each layer has different 2D peak shape. As it is known the shape of 2D peak is unique and different for each thickness and it is a fingerprint feature for identifying the number of layers in few layer samples. The Raman spectrum of single layer graphene is distinctly different when compared to others. 2D peak is highly symmetrical and its intensity is higher than the G peak intensity. In the case of double, triple, fourth or multilayer graphene G peak intensity is higher than 2D peak intensity.

2D peak shape does not represent a distinguishing feature after 10 layers and identifying the number of layer using 2D peak shape is almost impossible. During our study, we collected many Raman spectra from many different flakes. Comparing optical image contrasts and Raman 2D peak shapes, we were able to prepare a 2D peak shape library for graphene flakes up to eight layers thick as shown in Fig. 4.2.

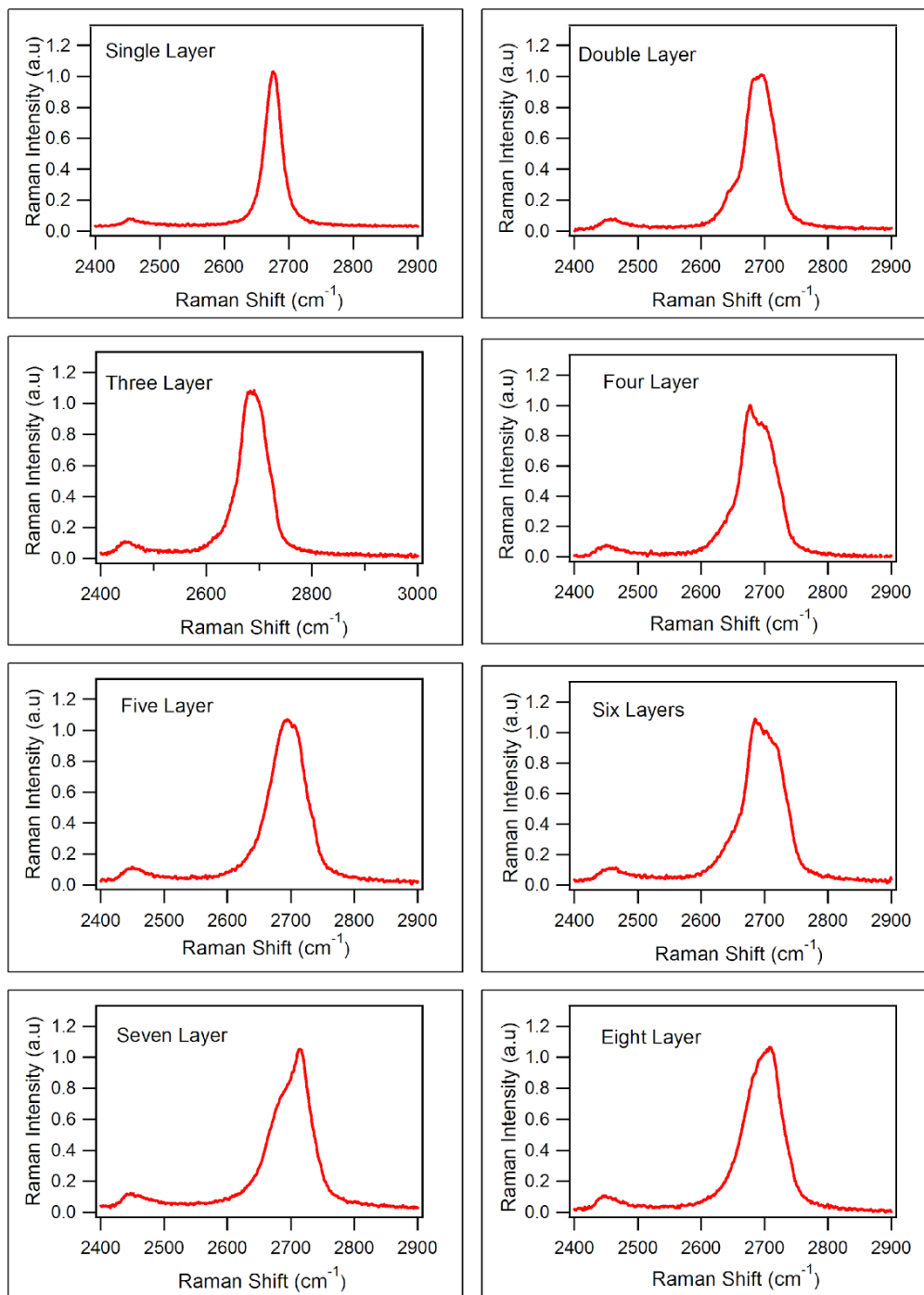


Figure 4.2 The shape of 2D from monolayer to eight layers.

4.3 SULFURIC ACID INTERCALATION DURING OXIDATION WITH HUMMERS METHOD

During our experiments, we identified a critical role of the sulfuric acid as an intercalant during the oxidation of graphite using Hummers method and its modified versions. Sulfuric acid, normally, does not intercalate between the graphite layers due to the positive Gibbs free energy of the process. Therefore, either electrochemical lowering of this energy or an additional oxidizing chemical is used along with sulfuric acid. In general, intercalation phenomena is described in terms of staging.

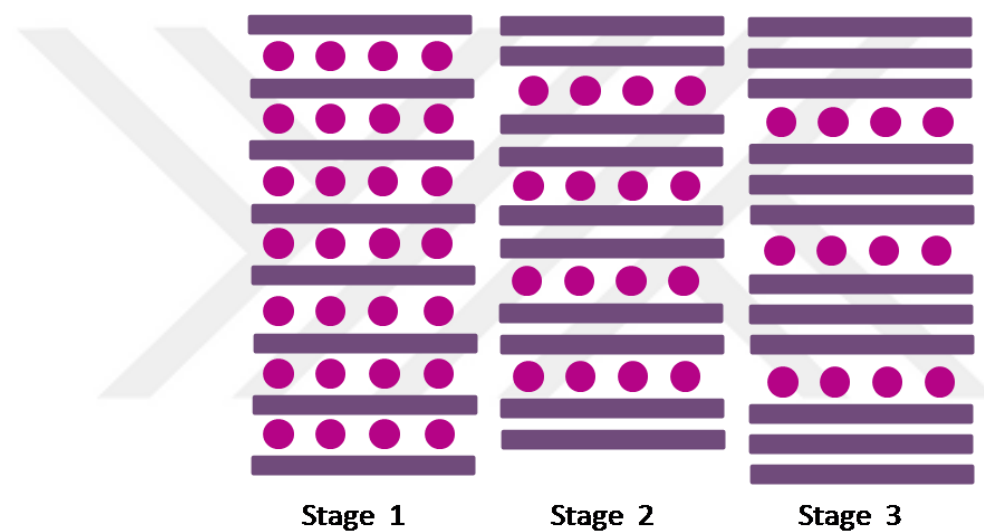


Figure 4.3 Schematic of Intercalation. Graphene layers and intercalant layer are shown as solid line and solid circle, respectively.

As it is shown in Figure 4.3, the numbers of graphene layers in between adjacent intercalant layers determine the stage of the graphite intercalation compound. For example, in stage 1 there is a graphene layer and in Stage 2 there are two graphene layers between the intercalant layers. The stage of the graphite can be monitored using Raman spectroscopy. In 1986, P.C. Eklund *et al.* carried out an electrochemical intercalation experiment (see Figure 4.4a). The Raman spectrum of graphite just has a single G peak in the 1580 cm^{-1} region. But once sulfuric acid starts to intercalate into graphite we see the formation of a secondary peak at around 1605 cm^{-1} . As more

sulfuric acid is intercalated, G peak completely disappears at Stage 2 and a sudden blue shift occurs at the start of stage 1. In a more recent experiment (Figure 4.4 b) similar results are obtained using ammonium persulfate/sulfuric acid mixture by A. M. Dimiev et al. in 2013[97].

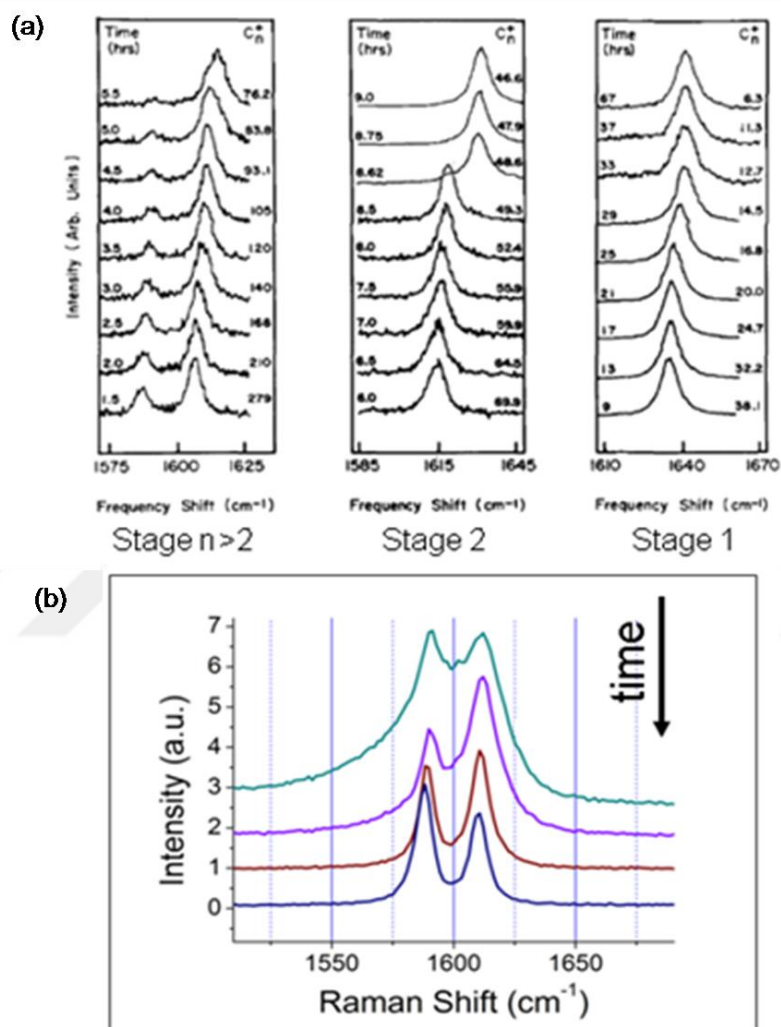


Figure 4.4 a) Electrochemical reaction of graphite with H₂SO₄, b) Ammonium persulfate/sulfuric acid graphite intercalation.

In an experiment, we studied a flake which consists of both bilayer graphene (BLG) and a relatively thick graphite region. We immersed the sample into the oxidation solution for 1 minute and without rinsing with DI water studied the sample under optical and Raman microscopes. In figure 4.5a and b, the optical images of the sample

before and after oxidation are shown. The regions labeled as 1 and 2 are the bilayer layer and graphite portions of the flake respectively. In the Raman spectrum of the bilayer region, G peak has completely disappeared and a secondary peak D' peak is observed at around 1610 cm^{-1} after the oxidation (see Figure 4.5c). In light of the former studies, the formation of D' peak can be explained by sulfuric acid intercalation. In the case of graphite layers the results are different. Upon oxidation both G and D' peaks are observed (see Figure 4.5d) in the same Raman spectrum. The intensity of the D' is higher than G peak. Similar spectra are previously observed for stage $n > 2$ intercalation in graphite.

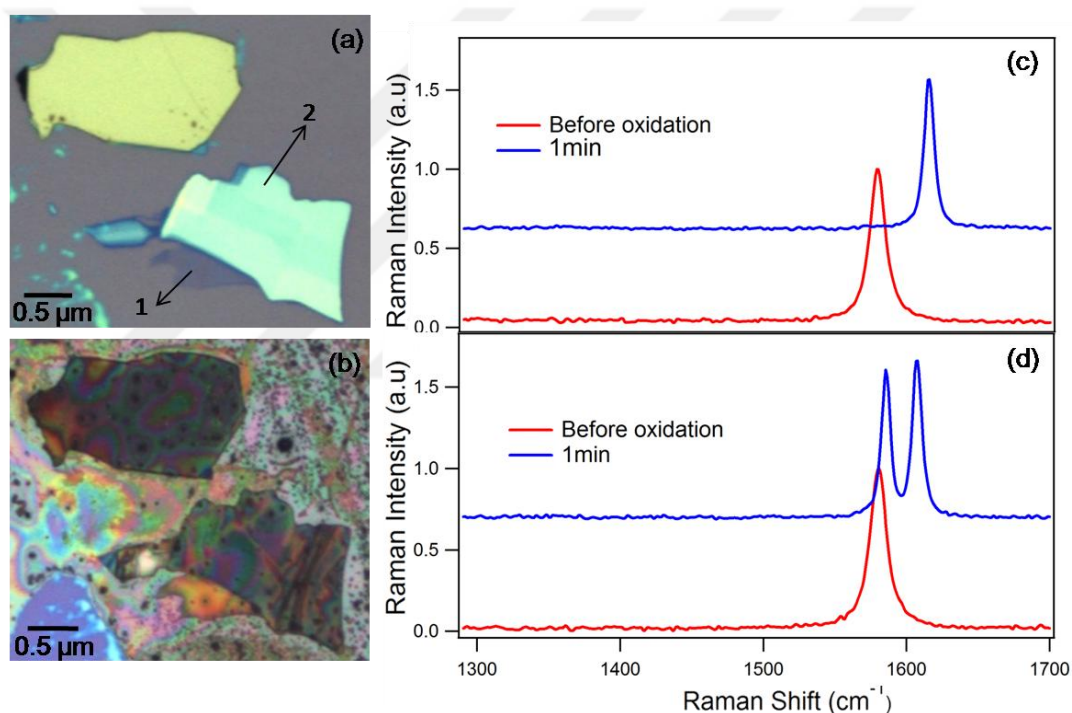


Figure 4.5 a) optic image of sample before oxidation, b) optic image of sample after oxidation without cleaning, c) and d) Raman spectra obtained from part 1 and 2, respectively.

A second sample containing four layer graphene was immersed into the same solution for 1 minute. After oxidation, substrate was rinsed with DI water. It was also dipped in the 3% H_2O_2 for 10 minutes to remove residuals deposited onto the substrate from the solution. Figure 4.6a shows optical image of graphene. Looking at the 2D peak shape we determined that this is a four layer thick sample. It is noted that, the upper left

corner of the sample is thicker, probably the flake is folded onto itself. So, the thicker part is 8 layers thick. After immersing into the oxidative solution, the Raman spectra at different positions (1 and 2) are shown in Figure 4.6.b and c.

At position 2, there is no change in Raman spectrum (see Figure 4.6c) whereas, a D' peak appears at around 1610 cm^{-1} at position 1 (see Figure 4.6b). In this particular sample we can see a slight shift the G peak position as well. Note that at both positions, the spectra do not contain a D peak. Therefore, we can conclude that there are no structural defects in the sample at this stage.

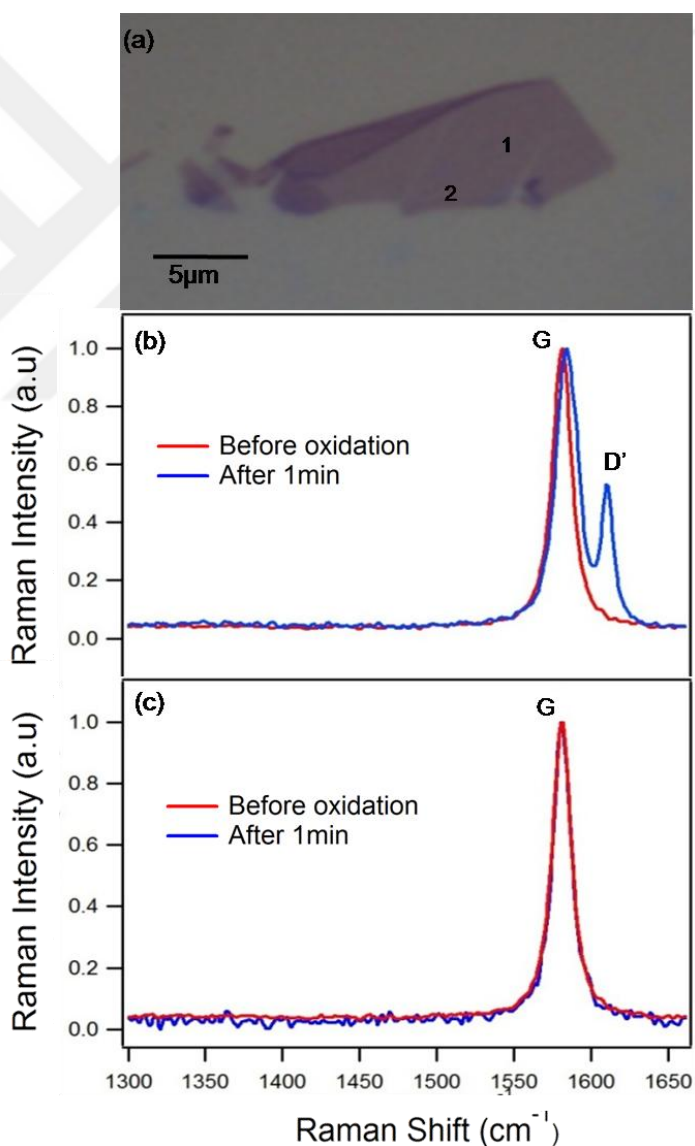


Figure 4.6 a) optic image of a few layer graphene, c),d) G and D' peak before (red) and after (blue) oxidation at different point, 1 and 2 respectively, on the graphene surface.

In order to see how the Raman peaks differ on the sample we have collected Raman spectra as a function of position on the sample and obtained the so called Raman Maps. The image resolution was $1 \times 1 \mu\text{m}^2$ with a 3s data collection time. Figure 4.7a-c show that the peak position, the peak width and the peak intensity of the G peak as a function of position, respectively. The data is obtained by applying Lorentzian fit to G peak of Raman spectrum from each location. In figure 4.7b it is shown that G peak intensity is nearly uniform on the four layer parts however as is expected, it is stronger on the folded part and is weaker at the edges. The G peak position is quite different at different positions on the sample. For example red square corresponds to 1585 cm^{-1} and purple is 1579 cm^{-1} . Such shifts in the G peak position can be attributed to the adsorbate or intercalant doping of the sample. We also see a broadening of the peak width. There is a slight increase of the G peak width in the charge doped region and it is consistent with the shift of the peak position.

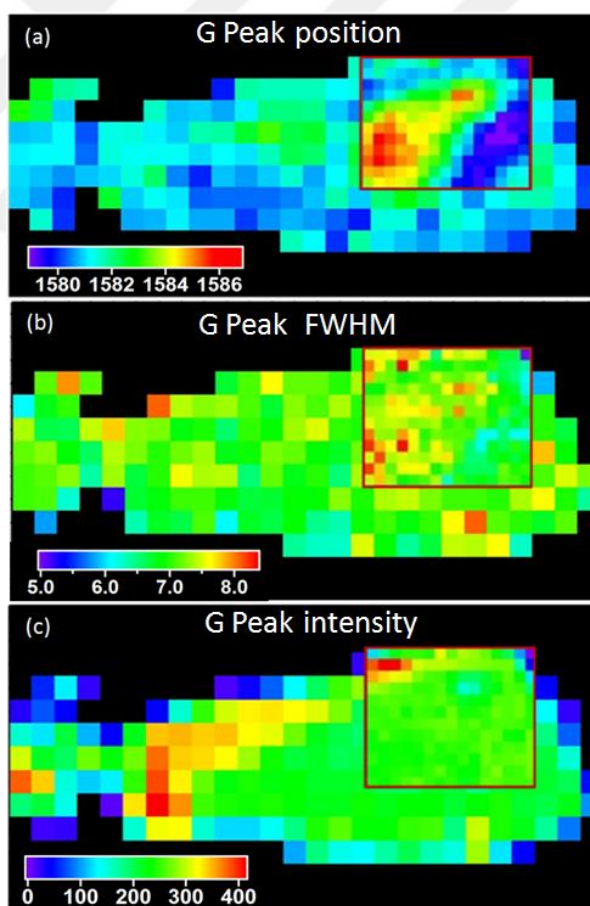
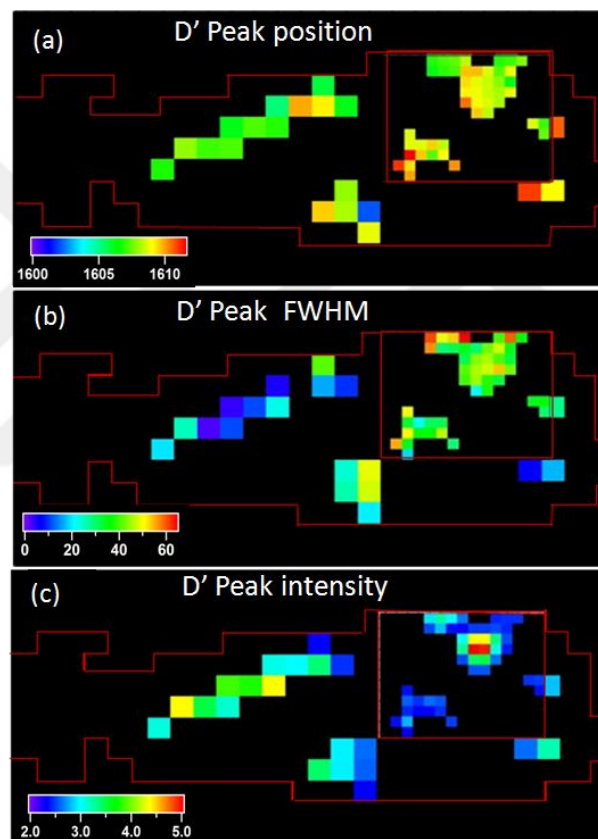


Figure 4.7 a), b), c), Raman maps of G peak position, FWHM, and intensity respectively.

The D' peak appears only at certain spots (see Figure 4.8a and b) (image resolution is $1 \times 1 \mu\text{m}^2$). The sample edges are indicated by red line and there is no D' peak at the black points. The peak intensity is not uniform and can be interpreted as nonuniform sulfuric acid intercalation. The variations of the peak position are mostly due to the inaccurate fitting for weak D' intensities at certain locations. It is interesting to note that there is good correlation between existences of D' peak and the shift in the G peak position. In light of previous experimental work, we conclude that the D' feature observed at this early stage of oxidation is due to the intercalation.



Şekil 4.8 a),b),c) Raman map of D' peak position, FWHM, and intensity, respectively.

In a third experiment, studying sulfuric acid intercalation, we have collected AFM images in contact mode after subjecting the samples to oxidative solution. Figure 4.9a shows the optical image of a graphene sample. The AFM topographic images of the graphene before and after oxidation are shown in Figure 4.9b and c, respectively. The sample was dipped in 3% H_2O_2 for 15 minutes to remove residues from the substrate

surface. Figure 4.9e demonstrates the differences between the two topographic scans. The thickness of the sample is nearly 3 nm higher after the oxidation process. When combined with the raman spectrum in Fig. 4.9d showing the D' peak after oxidation, the increase in height can be attributed to the intercalation of the sulfuric acid in between the layers of the flake.

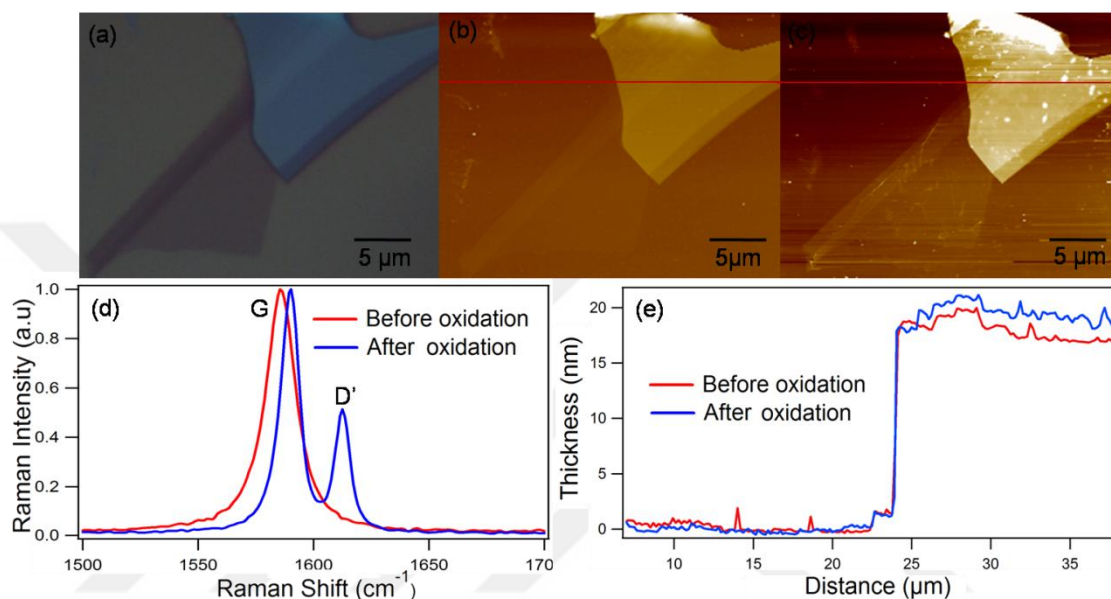


Figure 4.9 a) optic image of graphene sample, b) AFM image of graphene before oxidation, c) AFM image of graphene after oxidation, d) Raman spectra before and after oxidation, f) Effect of oxidation on the thickness of a few layer graphene sample is illustrated using AFM contact mode.

4.4 OXIDATION OF SINGLE LAYER GRAPHENE BY WET CHEMISTRY

In our previous studies, we used first oxidation includes 5 g potassium permanganate with 40 ml sulfuric acid and DI water. We observed that this solution has a lot of particles. In the subsequent experiments we used the solution utilized by Wang and his collaborators [63]. This solution consists of 0.015 M KMnO_4 in 50% H_2SO_4 (1:1 volume ratio). We immersed the graphene flakes supported by SiO_2/Si substrates into this solution for different durations ranging from 1 to 15 minutes. Raman and AFM measurements were carried out prior to and after the oxidation process.

Figure 4.10a and b show the optical image of such a sample before and after oxidation. Raman spectra from single layer graphene obtained after various oxidation durations are shown in Figure 4.10c. Despite an upshift in the position of the G peak, there were no signs of oxidation in the first 3 minutes of exposure to the solution. But after 5 min of oxidation a strong defect peak at around $\sim 1350\text{ cm}^{-1}$ is observed. A sharp but weak G peak mixed with the broad graphene oxide peak features is still visible in the spectrum obtain after 5 min of oxidation. This is indicative of the coexistence of both graphene and graphene oxide on the flake. The G peak completely disappears after 10 min of oxidation.

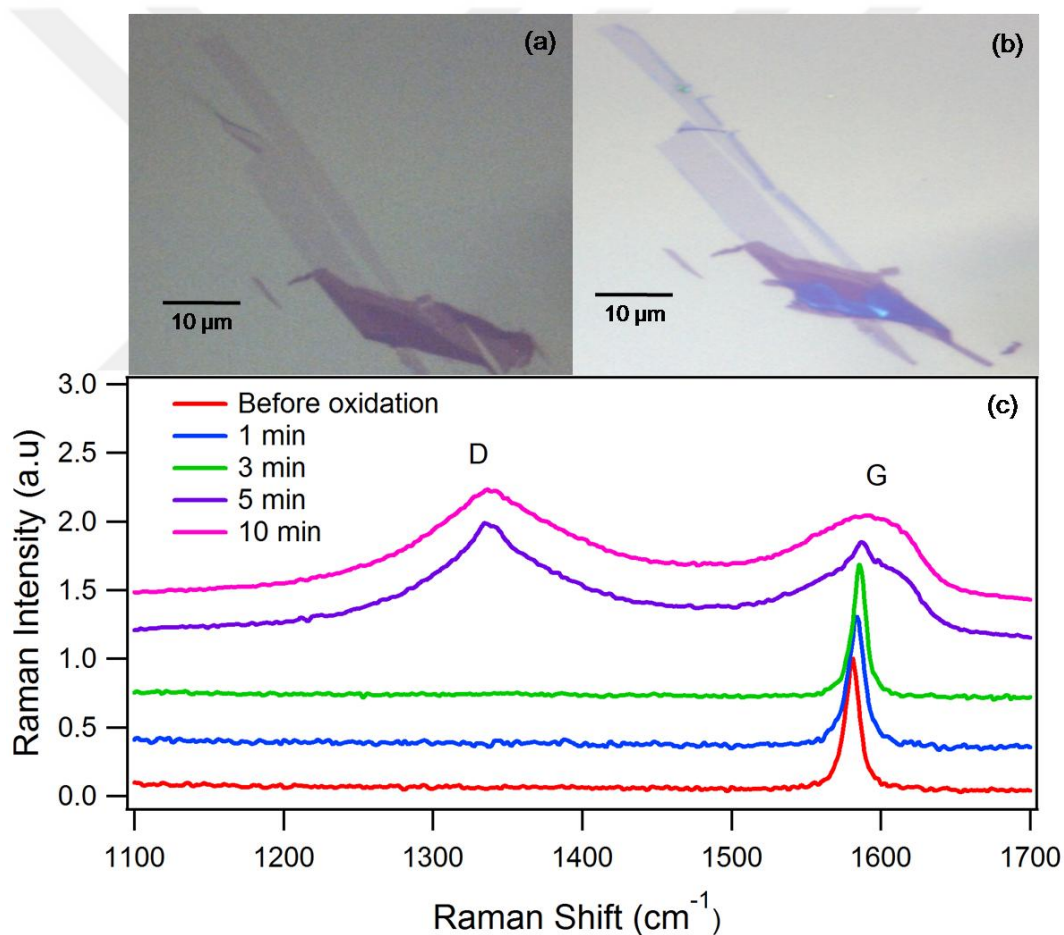


Figure 4.10 a), b) Optical image of graphene sample prior and after oxidation respectively, c) G peak position prior and after oxidation process.

During experiments the reactivity of few layer graphene flakes was also monitored as well. For the oxidation durations investigated in this study (up to 15 min.); two or

more layer graphene flakes did not show any sign of oxidation. This result is consistent with previous studies where SLG is found to be more reactive than multilayer flakes [98, 99]. Figure 4.11 presents the optical image and Raman spectra from two bilayer samples (Raman data is from the upper flake) subjected to oxidative solution for 15 min. The sample was repeatedly immersed into the solution, rinsed with DI water, and the Raman spectra were collected at the end of each oxidation step. There is no sign of D peak at 1350 cm^{-1} in all spectra. However, 2D peak shape is observed to alter and peak position to shift possibly due to impurity doping.

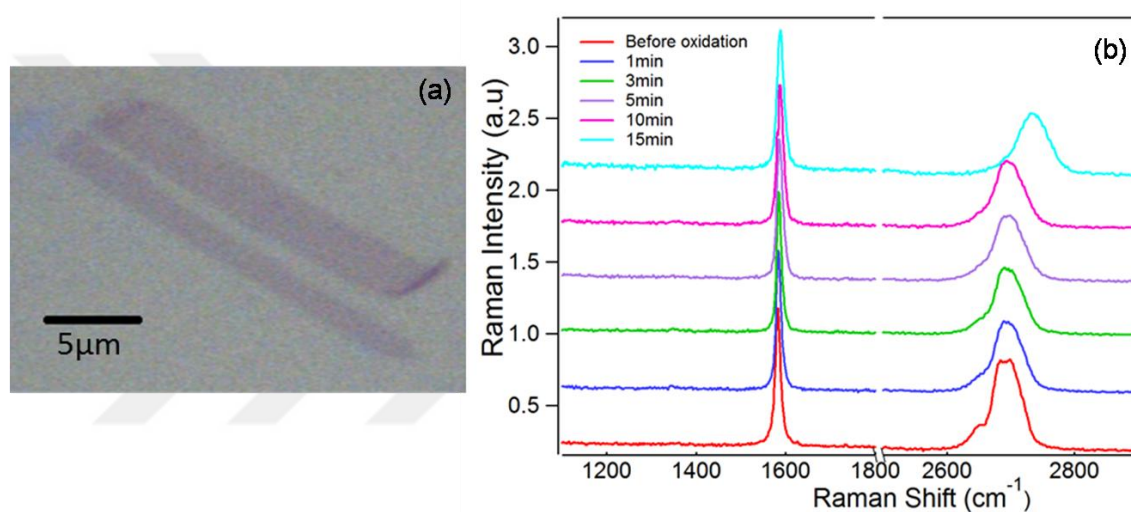


Figure 4.11 a) Optic image of graphene sample prior and after oxidation process, (b) Raman spectra of graphene before and after oxidation.

4.4.1 Edge Oxidation

Figure 4.12 displays Raman D peak intensity map and contact mode topography and lateral force microscopy (LFM) images of a SLG flake oxidized via wet chemistry for 10 min. as outlined in the experimental section along with its optical image prior to oxidation. The optical microscopy image (Figure 4.12a) shows a typical contrast of graphene region relative to the substrate. Figure 4.12b shows the D peak intensity as a function of position in the same region as the optical image (image resolution is $0.5 \times 0.5\ \mu\text{m}^2$) after the reaction. The oxidized regions present a strong D peak. It is, however,

observed only in a region near the edges with the center of the sample remained unoxidized. The topography image in Figure 4.12c is consistent with these observations. In this image, the edges of the sample are 0.6 nm higher than the central part which in turn is about 0.8 nm thick relative to the substrate (see inset). The increased height at the edges of the sample is an indication of the oxide in this region. The images in LFM mode can be used as a high contrast imaging visualization tool to observe different regions on the sample. In the image shown in Figure 4.12d, brighter pixels correspond to lower frictional force. Comparing with the Raman map and the topography image, we conclude that pristine graphene have reduced frictional interaction with the AFM tip relative to SiO₂ substrate and the graphene oxide at the edges. Overall, these images confirm that the oxidation process initiates at the edges of the sample almost uniformly. This behavior is expected as the defects at the edge of the graphene are preferred sites for attachment of foreign atoms or functional groups.

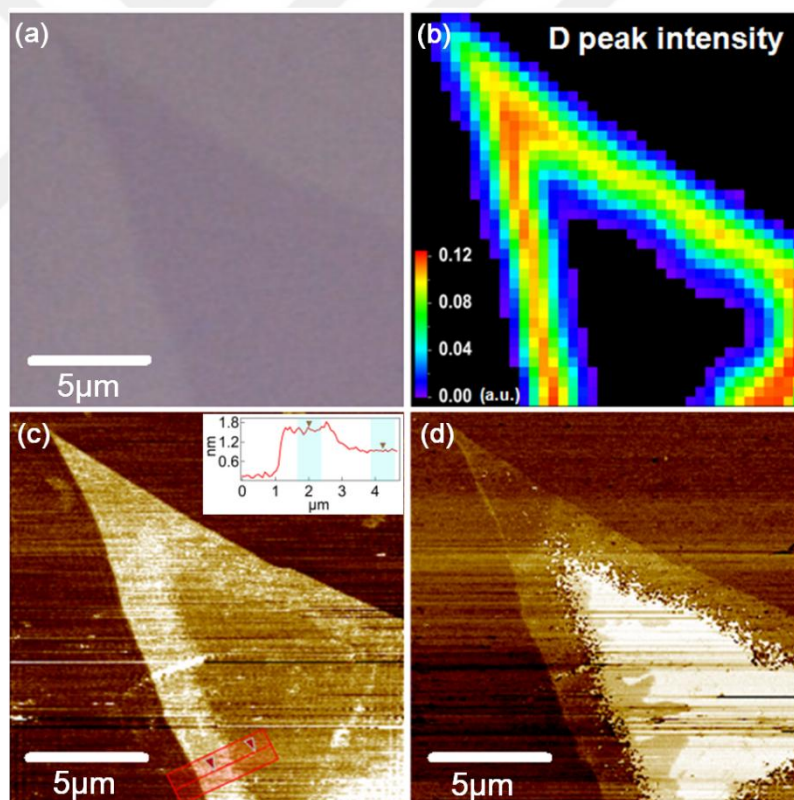


Figure 4.12 a) Optical image of a pristine graphene prior to oxidation. b) Raman map of D peak intensity, c) AFM topography, and d) LFM images after oxidation of the same sample for 10 min. via wet chemistry. Images indicate that the oxidation starts from the edges of the sample.

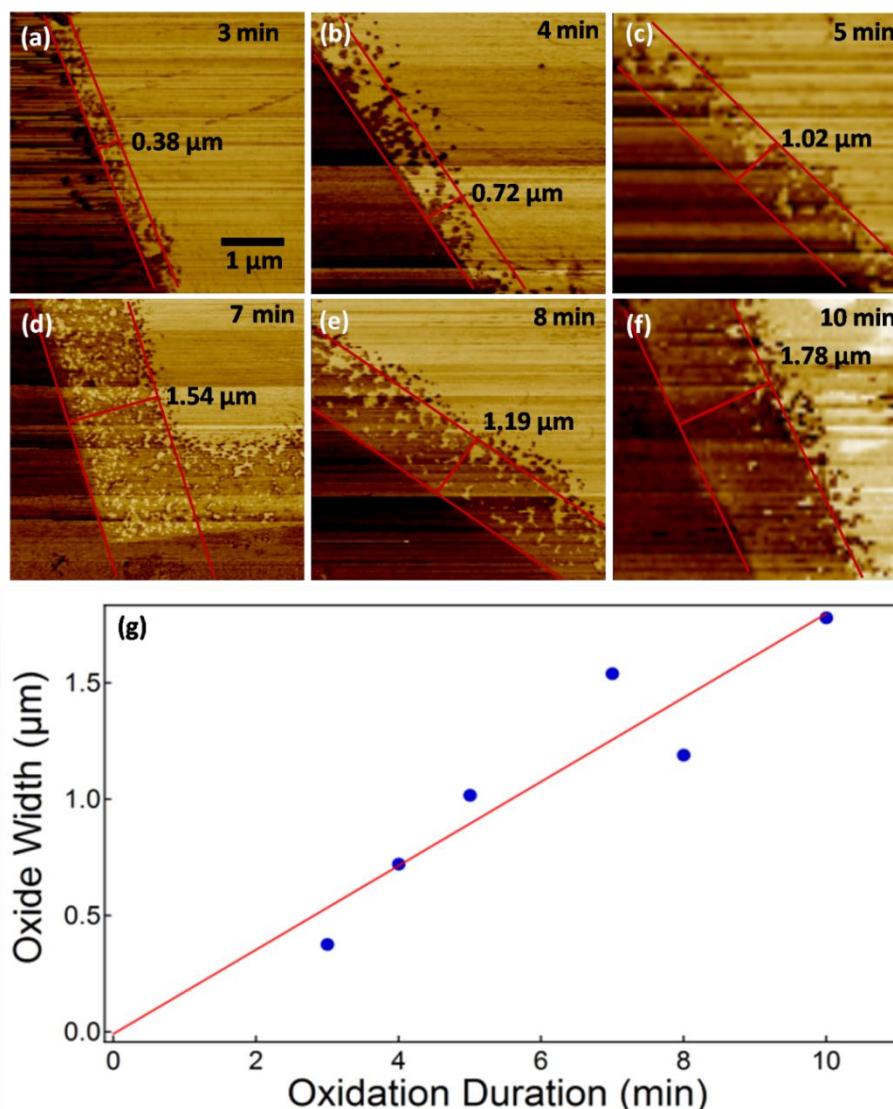


Figure 4.13 a) Lateral force images of single layer graphene samples for different oxidation durations. All images are at the same scale. Bright regions are unoxidized and dark regions are oxidized graphene (graphene oxide). The width of oxidized parts is increasing with oxidation duration. b) The plot of oxide width versus oxidation duration yields an oxidation rate of approximately $0.2\mu\text{m}/\text{min}$ for the solution used in this study.

LFM images of graphene samples oxidized for durations ranging from 3 to 10 minutes are presented in Figure 4.13. The images reveal two phenomena about the oxidation mechanism. First, the oxidation initiates at the edges on all samples and progresses inwards as a function of oxidation duration. From a linear fit of oxide width vs. oxidation duration (Figure 4.13g), the rate of oxidation is determined to be approximately $0.2\mu\text{m}/\text{min}$. Second, the interface between graphene and graphene oxide regions is not abrupt but rather covered with many nano-sized graphene oxide domains. For short durations (3 and 4 minutes) the oxide domains dominate the edges but at

longer durations (10 minutes and more) the edges become completely oxidized with graphene oxide nano islands (GONDs) scattered near the graphene/GO interface.

As we mentioned in Chapter 3, the first order scattering of A_{1g} (the D peak) is at around 1350 cm^{-1} and is symmetry forbidden in ideal graphene. The absence of the D peak in pristine graphene is an indication of the high crystalline quality of the samples used in this study. Upon oxidation, some structural changes in the graphene lattice due to the formation of various oxygenated functional groups on the basal plane and at the edges are expected [57]. Formation of sp^3 hybridization by covalent chemistry and other structural defects result in the appearance of a strong D peak and a broader G peak [57] as seen in the Raman spectrum from the completely oxidized graphene (blue curve) in Figure 4.14. The 2D peak in the same spectrum is much weaker and accompanied by other higher order peaks such as D+G. In some of our Raman spectra we came across a mixed phase, where (GO) features are observed in the same spectrum (green curve in Figure 4.14). We also observed this phase in Figure 4.10. Similar features can also be seen in the work of Wang *et al.* but they do not discuss the reasons for such features [63]. We will explain the microscopic origin of such spectra further below.

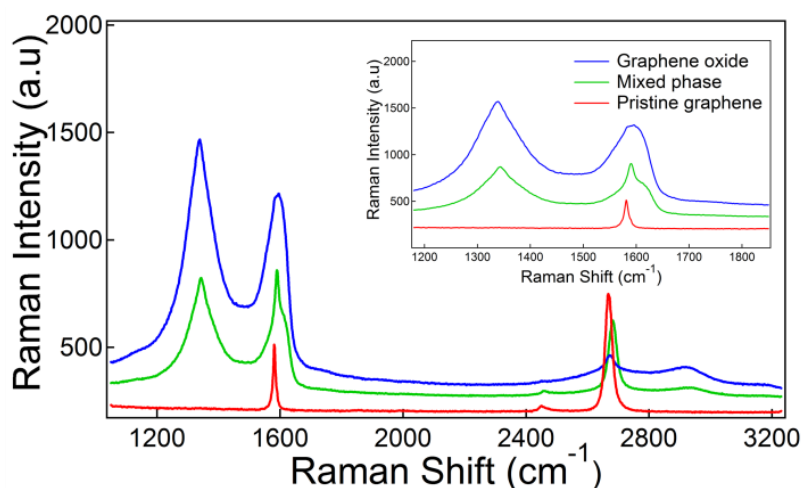


Figure 4.14 Raman spectra of pristine graphene (red), partially oxidized graphene (green) and graphene oxide (blue). The presence of both a broad and a sharp peak at around 1580 cm^{-1} in the partially oxidized graphene indicates the coexistence of both graphene and graphene oxide within the laser beam spot.

The contrast difference between the regions that are oxidized and non-oxidized can be clearly seen in optical images. We earlier mentioned that oxidation starts from the edges. Looking at the images, it is obvious that the colour of the edges, namely the oxidized parts are lighter while the parts that are non-oxidized are darker. The samples in figure 4.15 have been exposed to oxidation for 7 and 8 minutes. Therefore, whole sample was not oxidized. The images before and after the oxidation of another sample that has been oxidized for a longer duration (10 minutes) are presented in figure 4.16. After the longer reaction time, the sample has been completely oxidized and the contrast of the whole sample has changed. This change in contrast of graphene oxide relative to the contrast of graphene is due to the formation of a band gap from 1 to nearly 3 eV in graphene oxide which results in higher transmission of the visible light compared to graphene.

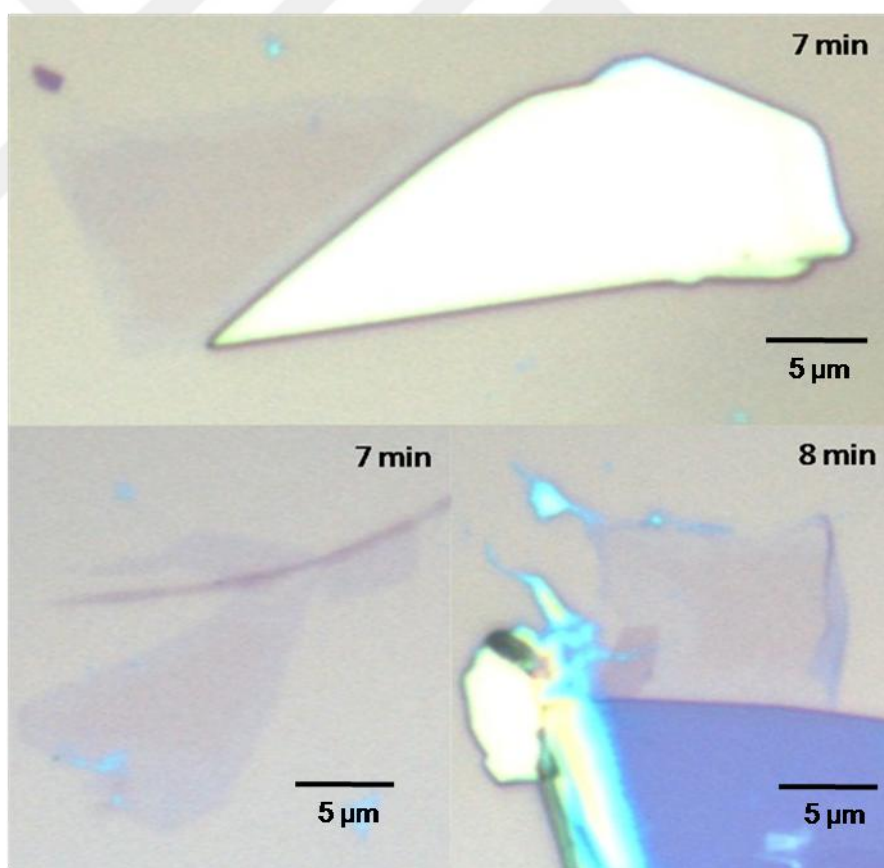


Figure 4.15 Optical images of graphene samples after oxidation

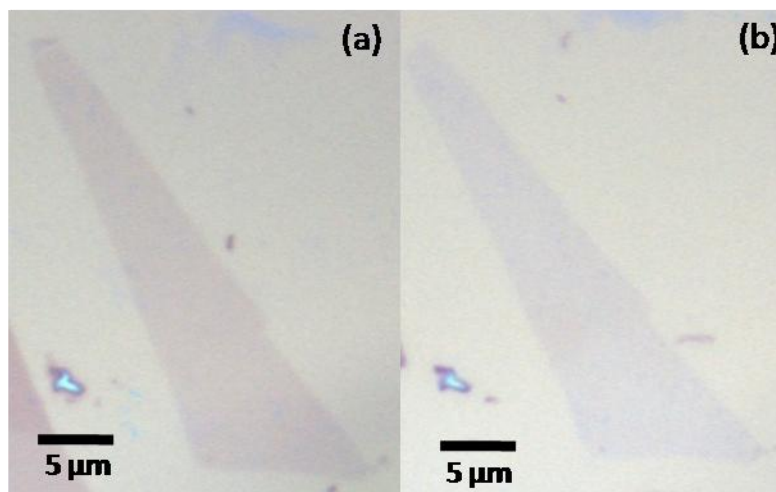


Figure 4.16 Optical image of single layer graphene before (a) and after (b) 10 min oxidation.

Figure 4.17a and b present close-up images of the nano-domains from a 4 minute-oxidized sample. The topography and the LFM images are consistent in that the highest regions on the topography image (that is graphene oxide) present a higher frictional interaction with the AFM tip relative to graphene covered regions. A thin (~ 70 nm) uniformly oxidized area is visible at the edge of the sample. GONDs are of the order of several tens of nanometers. Different sized domains with several big ones coalesced together are visible in the image indicating that either smaller domains formed later into the reaction or that different domains grow at different rates. Both of these possibilities point to nonuniform reactivity within the graphene sample. In large flakes (>10 micrometers), for modest oxidation times (up to 10 min), nano-domains are seen only in regions near the graphene/graphene oxide interface with no sign of oxidation at the central portion of the samples as demonstrated in Figures 4.12 and 4.13. The domains are not connected to the edges of the samples and therefore their increased reactivity cannot be attributed to the reduced coordination of atoms at the edge. On the other hand, the observation of the islands exclusively near the graphene/GO interface means that the effect is somehow related to these regions being near the edge of the sample.

If the sample under study is a few microns wide, it is possible to obtain completely GOND covered flakes (Figure 4.17c). Such samples provide a conductive 2D graphene medium with GONDs scattered within the sample. As a result, they provide a large graphene/graphene oxide interface and may be probed through electrical

measurements. Further, such samples may be useful for device applications with additional functionalization of the domains and fast electrical probing of these regions through the conductive graphene medium. Raman measurements from completely GOND covered samples similar to the one in Figure 4.17c present spectra containing peaks typical of both graphene and graphene oxide at the same time as shown in Figure 4.14 (green curve) explaining the origin of the mixed phase Raman spectrum.

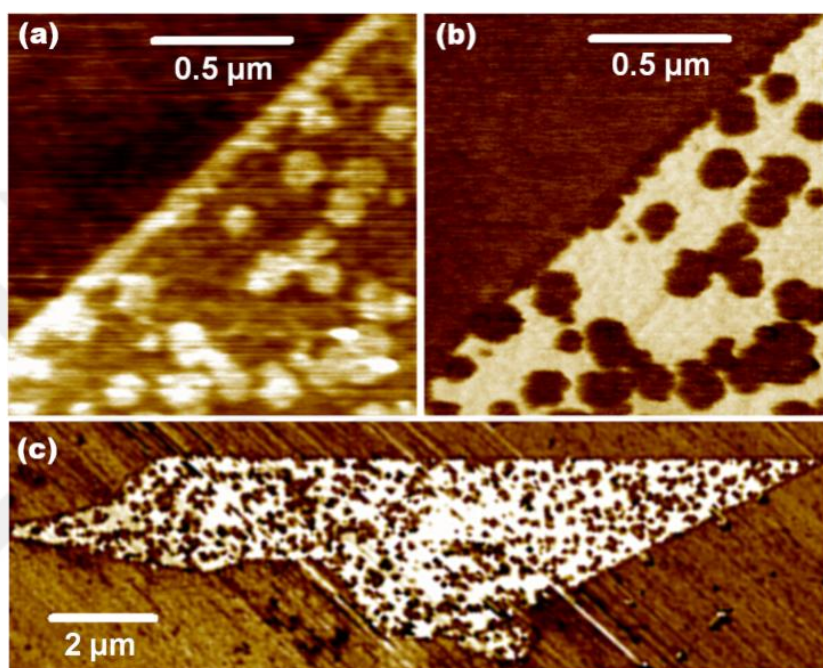


Figure 4.17 a) Topography and b) Lateral Force images of a 4 min-oxidized graphene flake. c) The full view of the same flake demonstrating that the flake is completely covered with GONDs.

4.4.2 The Effect of Charge Puddles on Oxidation

One of the reasons that affect the chemical reactivity of graphene may be impurity induced charge doping. SiO_2 covered silicon is very useful for device fabrication but its surface is not smooth and it can contain charge impurities. Thus exfoliated graphene is strongly influenced from the substrate. These charge impurities form electron-hole charge fluctuations (or puddles) which can cause scattering and effect the electronic performance of graphene devices. Raman spectroscopy is the most useful technique to

investigate the carrier doping level, defects, etc. Electron and hole doping cause a change in G peak position. G peak upshifts and downshifts for p type doping and n type doping, respectively. However, G peak position only upshifts in the case of lower level doping (below $\sim 3 \times 10^{13} \text{ cm}^{-2}$) for both n type and p type due to the phonon dispersion modification near the Kohn anomaly [100].

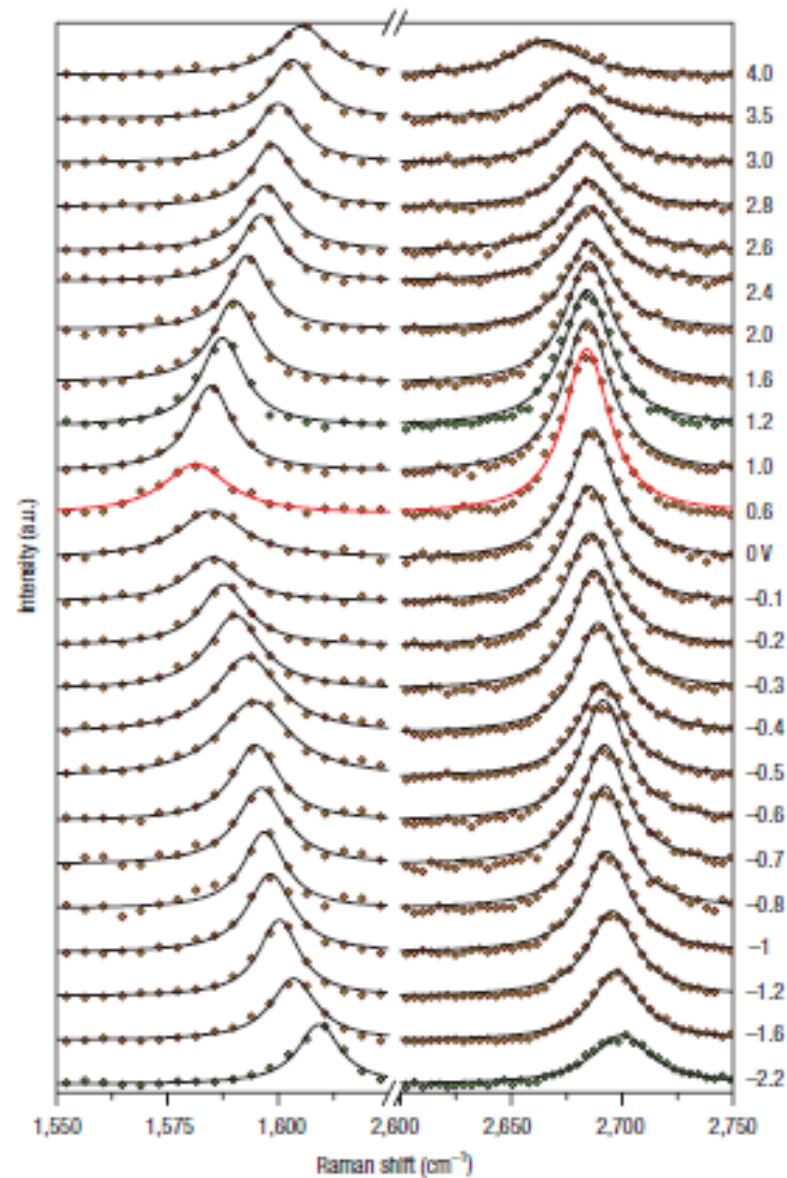


Figure 4.18 Raman spectra of graphene as a function of gate voltage.

Das *et al.* [101] investigated the dependence of G and 2D peaks on the doping level of graphene (Figure 4.18). Raman spectra of G (left) and 2D (right) peaks of single layer graphene at different values of top-gate voltages are monitored. G peak has its smallest value as $\sim 1583.1 \text{ cm}^{-1}$ at 0.6 V and it upshifts for both electron and hole doping. The FWHM of G peak decreases for both electron and hole doping. 2D peak dependence to gate voltage is different. Its position does not change ($< 1 \text{ cm}^{-1}$) until a gate voltage of 3 V (corresponding to a charge concentration of $3.2 \times 10^{13} \text{ cm}^{-2}$). At higher gate voltages, the position of 2D peak increases for p doping.

The effect of charge puddles and ripples on the overall chemical reactivity of SLG was previously pointed out for the case of covalent bonding with diazonium salts [102] and oxidative etching of graphene [98, 103, 104]. In the study of Yamamoto *et al.* such nonuniform reactivity is attributed to charge inhomogeneity within the samples due to doping from the substrate and other impurities. Wang *et al.* demonstrated that control over the local reactivity is possible by patterning the substrate and hence changing local doping within graphene [105]. Our results obtained in a few flakes displaying different reactive patterns also show the role of impurity doping in the formation of GONDS. For example, in Figure 4.19, we present a narrow flake which is oxidized for 7 minutes. This particular sample is completely oxidized except for a small region on the lower right corner containing GONDS as evidenced by the AFM images in 4.19 b-d. The Raman D peak intensity map given in Figure 4.19e presents a reduced D peak intensity from the same region. This result is curious as the partially oxidized region is very near the edge of the sample and expected to be completely oxidized as the rest of the flake.

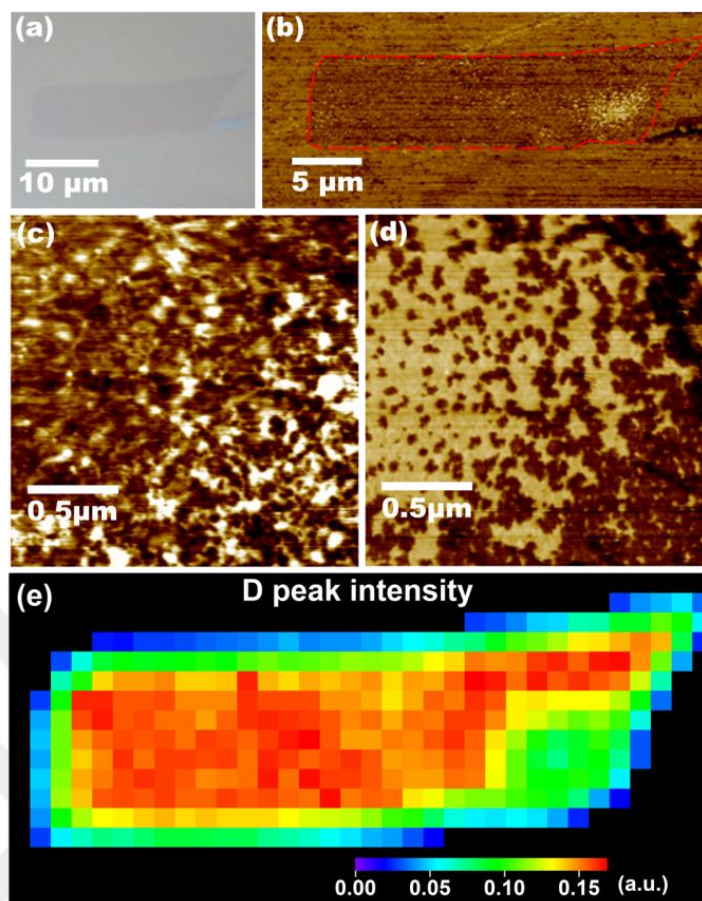


Figure 4.19 a) Optical image of a single layer graphene prior to oxidation, (b) LFM image of graphene shown in a) after oxidation. (c) and (d) Topographic and LFM images of partially oxidized part of graphene shown in (b). (e) Raman D peak intensity map from the same flake after oxidation.

Raman map data from the flake presented in Figure 4.19 prior to its oxidation is shown in Figure 4.20. The four images show how the G peak position, G peak full width at half maximum (FWHM), 2D peak position, and the intensity ratios of 2D peak to G peak change at different locations on the flake, respectively. Such data may be used to study the local impurity doping state of the graphene samples [106, 107]. The stiffening of the G-mode phonons along with a reduction in its FWHM is associated with increased hole or electron doping of the flake. Even though the 2D peak upshifts in position for modest doping of either kind, it moves in opposite directions for high carrier concentrations [101]. In agreement with previous work, the map data shows that the edges of the samples have higher shifts in peak positions and are therefore have increased impurity doping [106]. However, the lower right part of the sample (including

the inner portions) is significantly less doped from the rest of the sample. This is the same region which was not fully oxidized in Figure 4.19.

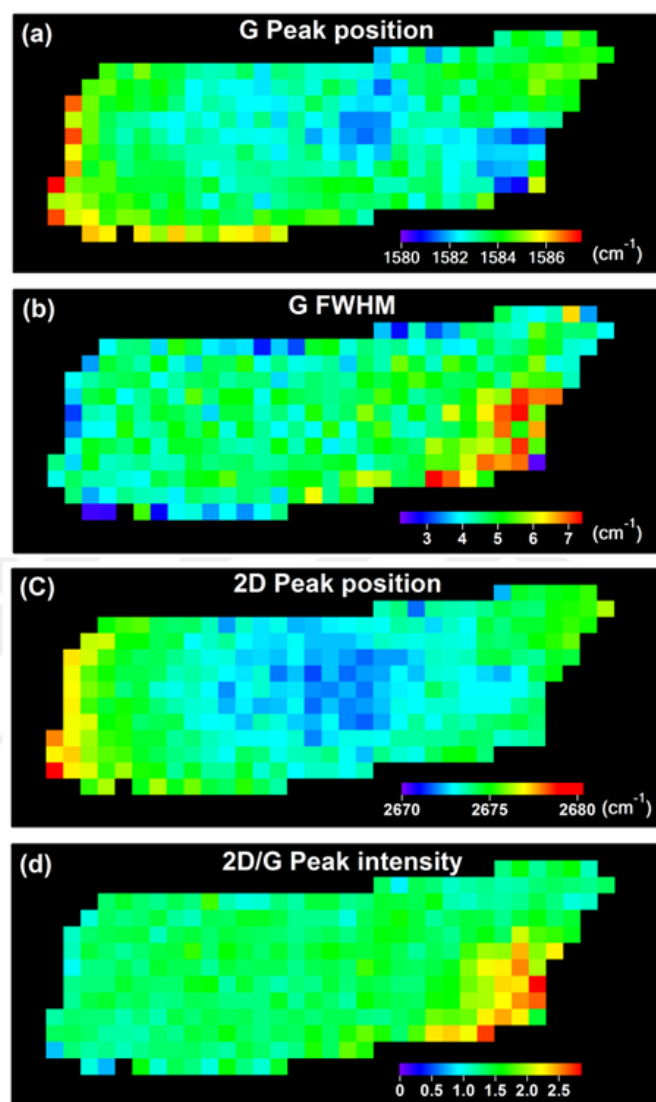


Figure 4.20 Raman maps of single layer graphene before oxidation; a) G peak position, b) G peak FWHM, c) 2D peak position and d) 2D/G Peak intensity.

The behavior of G and D peak after oxidation are shown in Figure 4.21. G peak position (Fig 4.21a) downshifts at the right corner below and it is uniform at the rest of sample. FWHM presents the uniformity at the whole sample in Figure 4.21b. The D peak position downshifts and FWHM reduces at the same region. This is expected

because nano islands are formed in this region. D peak position downshifts and FWHM are uniform at the rest of the sample. The results of G peak and D peak are consistent with each other.

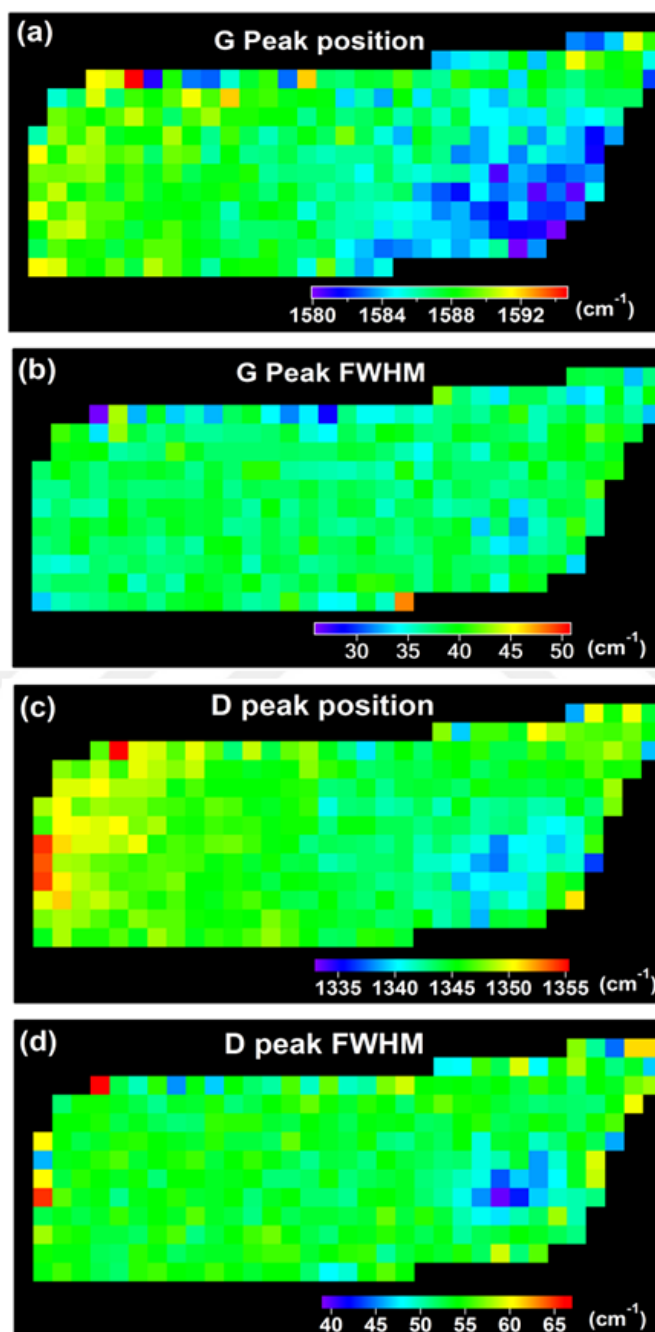


Figure 4.21 Raman maps of single layer graphene after oxidation; a) G peak position, b) G peak FWHM, c) D peak position and d) D Peak FWHM.

Various G and 2D peak parameters from the same flake prior to its oxidation are plotted in Figure 4.22 a-d and the corresponding Raman image maps are provided in 4.21. Such data may be used to study the local impurity doping state of graphene [90, 108]. The stiffening of the G-mode phonons along with a reduction in its FWHM is associated with increased hole or electron doping of the flake [96, 101, 105, 109, 110]. Even though the 2D peak upshifts in position for modest doping of either kind, it moves in opposite directions for high carrier concentrations [101]. According to the data in Figure 4.22 s-d, Raman data from the partially oxidized region of the flake (blue diamonds) had smaller impurity doping when compared to the rest of the sample prior to the reaction. Therefore, in agreement with Yamamoto *et al.*, the wet oxidative reactivity of the graphene, too, is affected by the local doping state of the flakes. The resolution of Raman microscopy is of the order of 1 micrometer in diameter and therefore we cannot map out smaller sized variations in the impurity state of the sample. However, graphene is known to have local charge variations at a smaller scale [89]. Accordingly, we attribute the formation of the GONDs near the edge of the sample to these nanoscale variations in the doping level. As evidenced by the data in Figure 4.12 and Figure 4.13, for larger flakes, the nano-domains appear at the interface of the uniformly oxidized area at the edge and the unoxidized central region. The impurity doping near the edge of the SLG flakes is stronger than inner regions [108]. Thus, along with the uniform oxidation at the edge, the nano-domain formation is first observed close to the edge. As the reaction progresses, either due to extended exposure to the oxidative solution or due to a redistribution of the charge within the graphene resulting from the reaction at the edge causes formation of new GONDs farther away from the edge. In the case of small flakes (less than 5 μm in width), the whole surface is close enough to the edge and have favorable conditions for nano-domains formation throughout the sample resulting in flakes similar to the one shown in Fig. 4.23c. The FWHM of 2D peak is plotted against the 2D peak position (see Figure 4.22d)

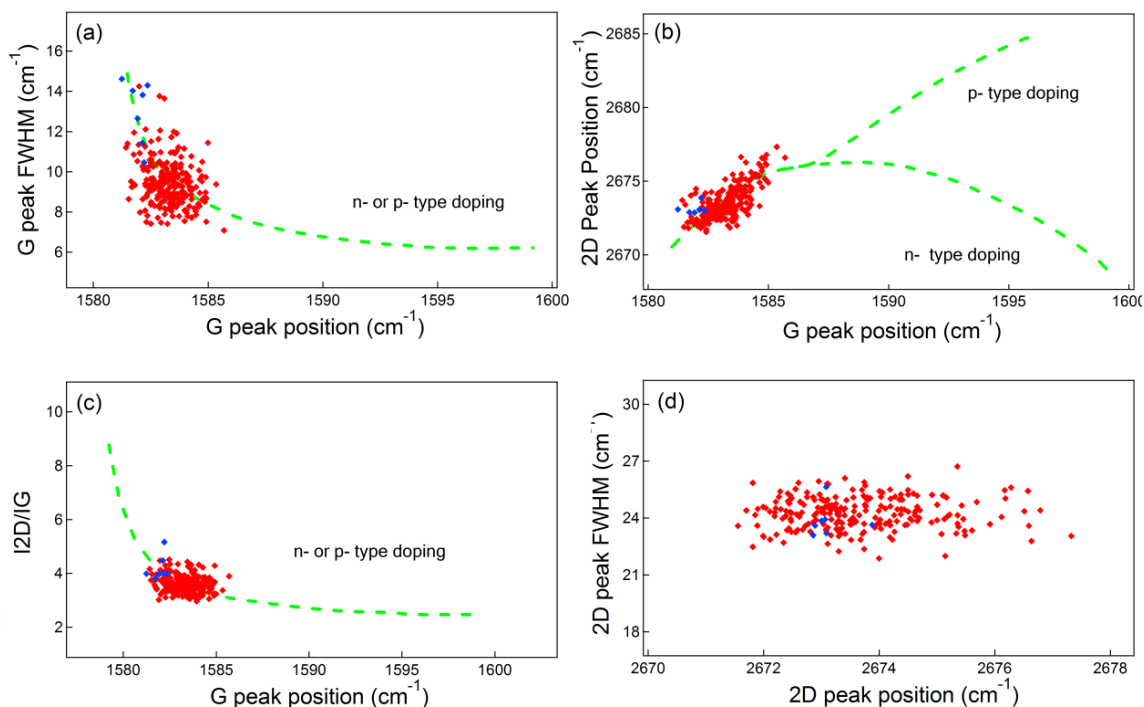


Figure 4.22 a) G FWHM versus G peak position, b) 2D peak position versus G peak position, c) 2d Peak position I_{2D}/I_G ratio versus G peak position, d) 2D peak FWHM versus the. The dashed lines are added as a guide to indicate general trends with charge doping.

4.5 OXIDATION OF CVD GROWN GRAPHENE

CVD grown graphene can have different reactive properties when compared with exfoliated graphene. To investigate the differences, we performed similar experiments using CVD grown graphene which is transferred onto SiO_2/Si . During the experiments we first scanned the sample under optical microscope. Then we carried out characterization of the sample using Raman spectroscopy and AFM. The Raman spectra were compared with that from the exfoliated graphene. Then, wet oxidation process was carried out and Raman map and AFM measurements were performed to determine the state of the graphene after the oxidation.

Figure 4.23 shows the Raman spectra of CVD grown single layer graphene and exfoliated single layer graphene. Exfoliated graphene has high crystalline quality so that its Raman spectrum does not contain a D peak feature. As we mentioned previously CVD grown graphene has low crystalline quality which can be confirmed by the Raman

spectrum displaying the D peak at 1350 cm^{-1} . The positions of the D, G and 2D peaks of exfoliated graphene lie at around 1350 cm^{-1} , 1580 cm^{-1} and 2700 cm^{-1} respectively. But these peaks upshift in CVD graphene. In addition, the relative intensities of G and 2D peaks are different in the case of CVD graphene and exfoliated graphene.

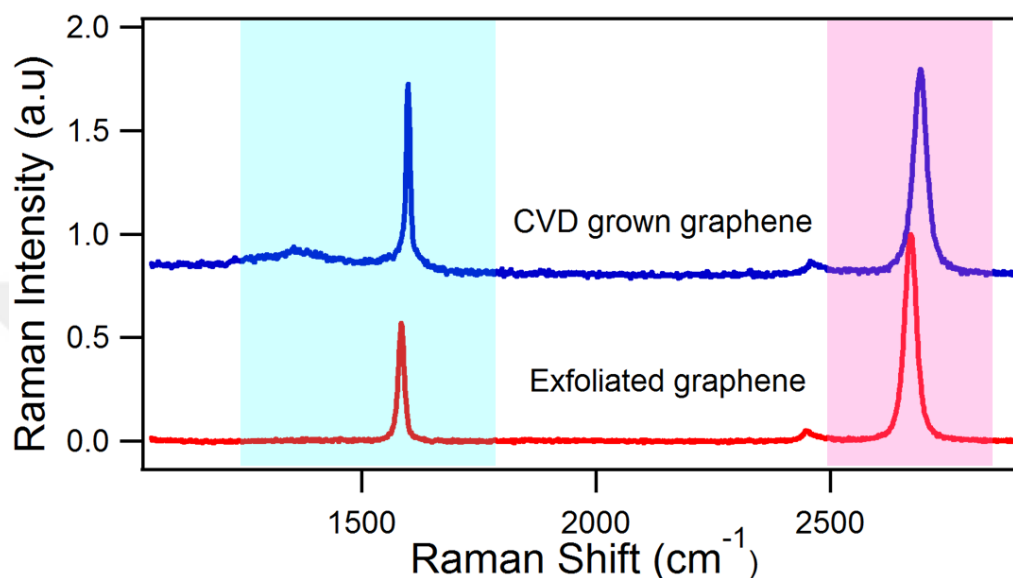


Figure 4.23 Raman spectra of CVD grown graphene (blue) and exfoliated graphene (red).

Figure 4.24 shows the optical images taken from different points on CVD graphene. The surface of the flake is clearly not uniform. In Figure 4.24a a dark line is seen in the middle of the image. AFM studies indicate that this line is thicker relative to the rest of the flake indicating a wrinkle formed in the sheet possibly during the transfer onto the SiO_2/Si substrate. The transfer of the sheet is fairly tricky and such folds and tears can easily occur on the sheet (see Figure 4.24b). PMMA is used during the transfer of graphene onto substrate and often some residues remain on the flake after its removal. For example, the blue stain in Figure 4.24c is attributed to such a contamination on the flake. The grain boundaries can be observed in the images as very thin lines. These boundaries include many defects so that strong oxidation can occur at these regions. There are little dark regions on the sample but some of them are bigger (see Figure 4.24d). These regions may be double or triple layer or single layer with

different crystal structure. In order to investigate these point some analysis were done using Raman spectroscopy.

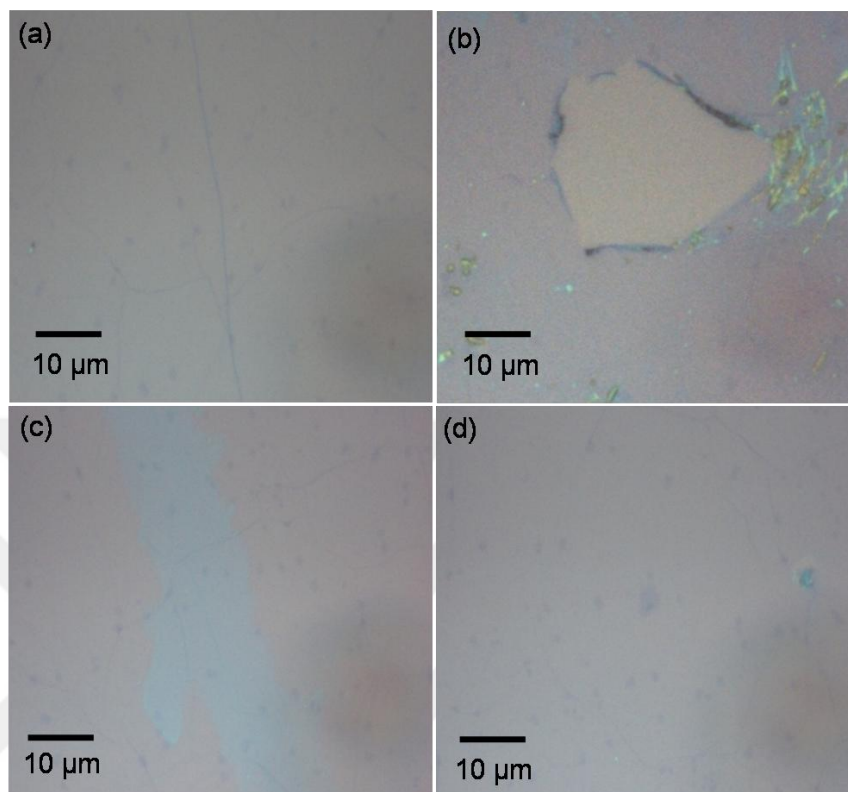
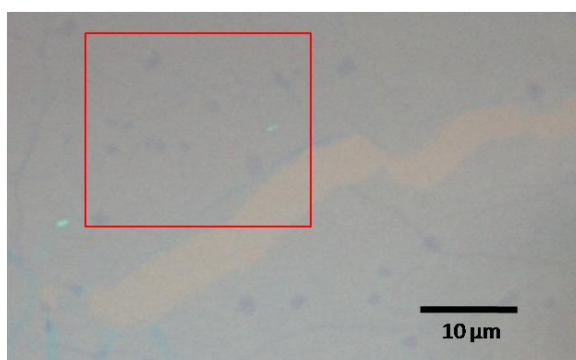


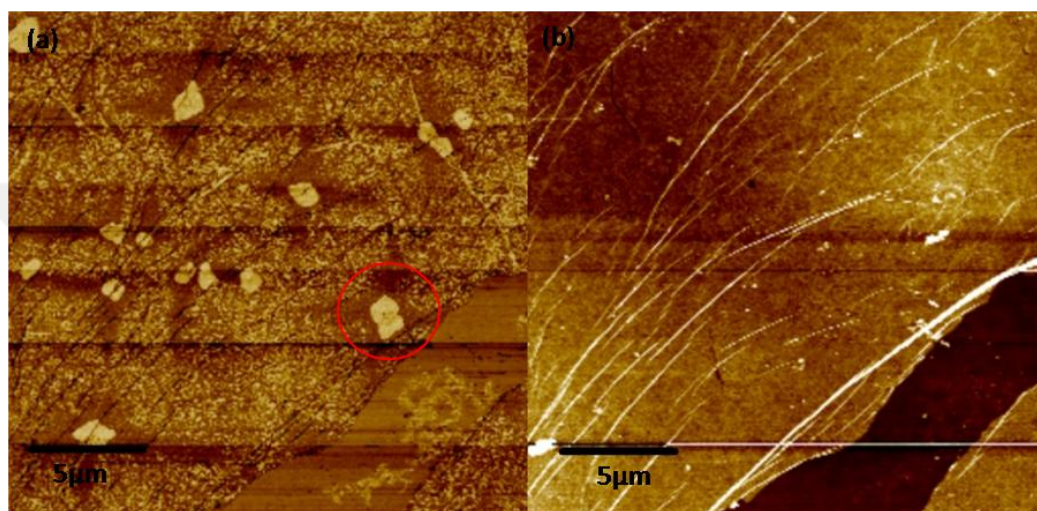
Figure 4.24 Optical images of CVD grown graphene.

After scanning and characterization steps, sample was oxidized for 7 minutes. AFM and Raman map analysis were done for the region displayed in Figure 4.24.



4.25 Optical image of CVD grown single layer graphene after oxidation.

Post-oxidation lateral force and topographic images of the sample are shown in Figure 4.26. There are three distinct features observed in these images: First, certain regions on the flakes are not oxidized at all. Second, each one of these unoxidized regions are at the center of a cross shaped completely oxidized region. Third, the rest of the sample is covered with GONDs. These features are not apparent in the topography image due to the height scale of the image.



4.26 a) Lateral force and, b) Topographic images of CVD grown graphene after oxidation.

A magnified view of the area around one of the non-oxidized regions (see Figure 4.27a) is shown in Figure 4.26. The non-oxidized part is better resolved in lateral force image, but can not be easily differentiated in the topographic image. The domain edge can be barely identified near the tip of the red arrow mark in Figure 4.27b.

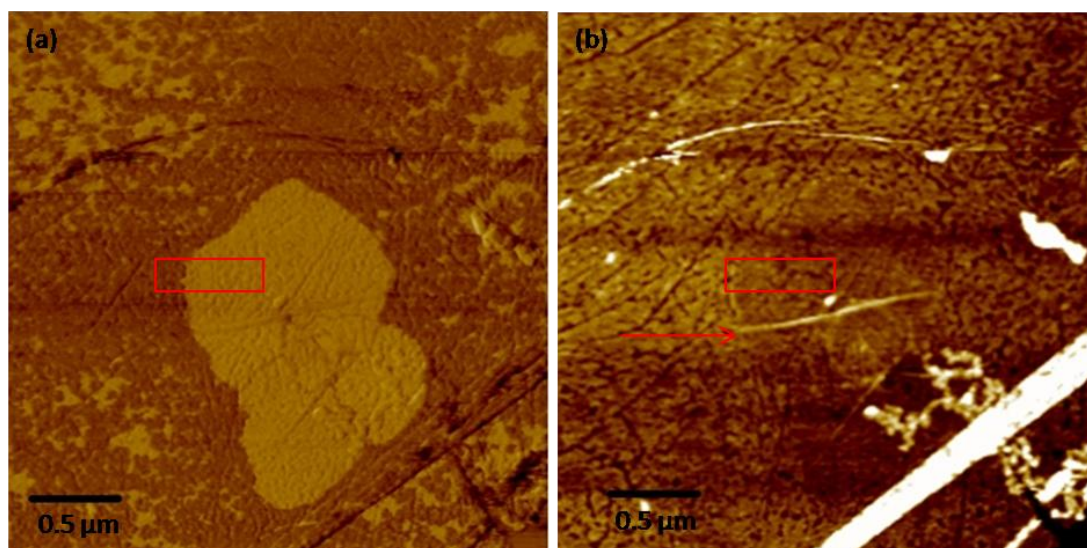


Figure 4.27 Magnified a) lateral force and b) topographic images indicated in 4.25.

To confirm that the oxidized region is in fact thicker than the non-oxidized region the area inside the red rectangle in Figure 4.27 is displayed in Figure 4.28. In the topography image (Figure 4.28b), the left side (oxidized part) appears brighter than the non-oxidized right side. This confirms that oxidized part is in fact thicker than the non-oxidized part.

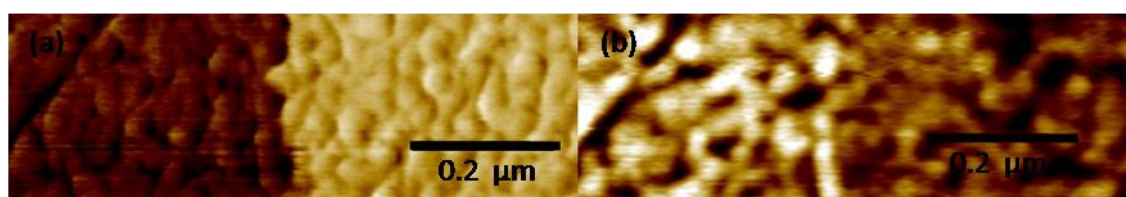


Figure 4.28 AFM images, a) lateral force and b) topographic image indicated in 4.26

The question is why certain regions of the graphene sheet are not oxidized at all? One possible explanation is that these regions are multilayer domains. Since, multilayer graphene is less reactive it is reasonable that they are not oxidized. However, the comparison of the 2D Raman peak shape from these regions to our library shown in Figure 4.29 indicate that the peak shape best matches that of the single layer. Therefore,

we attribute these differing reactive patterns on the CVD graphene to changes in the graphene sheet structure during the growth of the films.

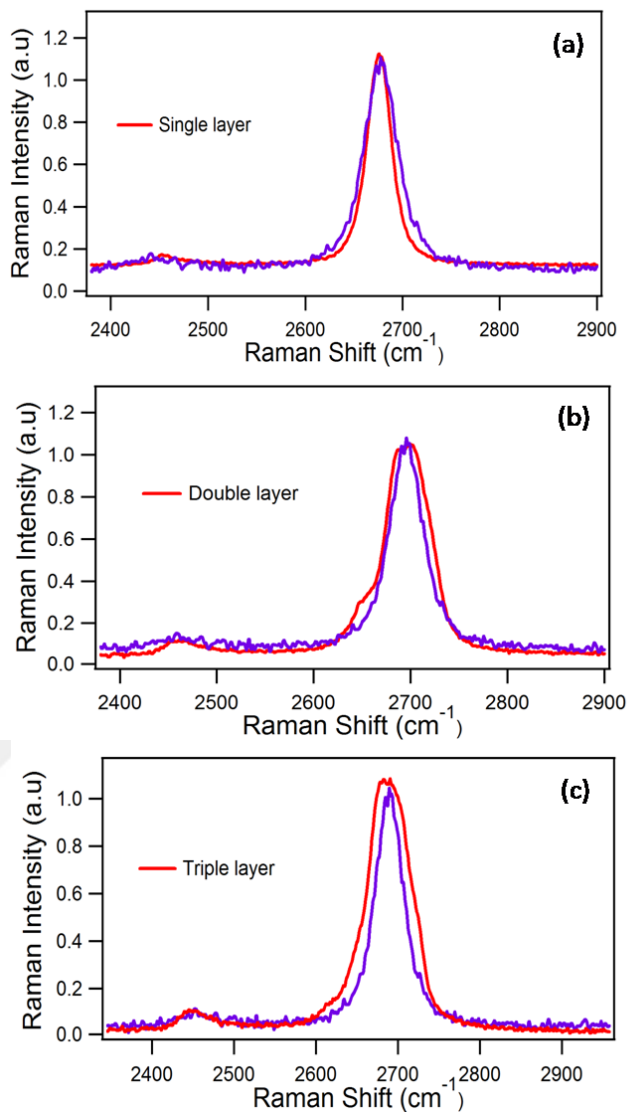


Figure 4.29 Raman spectrum of non-oxidized region of CVD grown graphene (blue), single layer a), double layer b) and triple layer graphene.

Raman maps of the oxidized CVD graphene is presented in Figure 4.30 and is consistent with AFM results. According to our results from the exfoliated graphene, we can say that most of the CVD graphene is more reactive and charge inhomogeneity is effecting the reactivity not only at the edges of the flake but throughout the whole sheet.

In the oxidized regions, the G peak is upshifted in position in comparison to less oxidized or non-oxidized regions (see Figure 4.30a).

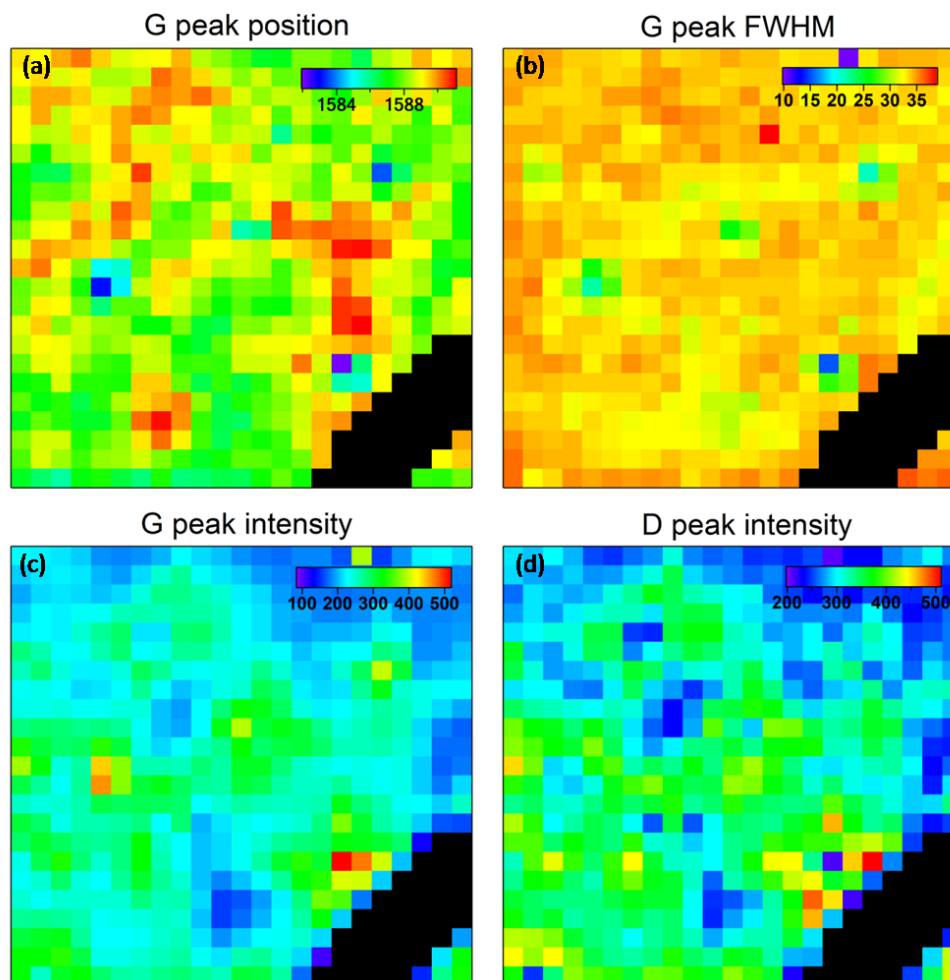


Figure 4.30 Raman maps of CVD grown graphene.

In more detailed Raman maps ($0.5 \mu\text{m}$ step size) of the area around a single non-oxidized region shown in the red rectangle of optical image given in Figure 4.31a, the features of the Raman G and D peaks can be better characterized for oxidized and non-oxidized regions (see Figures 4.31b-e). First, the G peak FWHM values are higher than the non-oxidized regions as expected. In addition, G peak intensity is higher from the oxidized regions when compared to the intensity from the non-oxidized regions. Third, the D peak intensity map also shows the cross shape observed in the AFM inspection of the oxidized flakes, confirming the strong oxide formation in these regions. Finally, the

weak D peak intensity observed from the non-oxidized region is not a result of the oxide in this part but rather is due to the finite resolution power of the Raman microscope (around 1 μm) and the residual D-peak feature due to the defective nature of the CVD graphene.

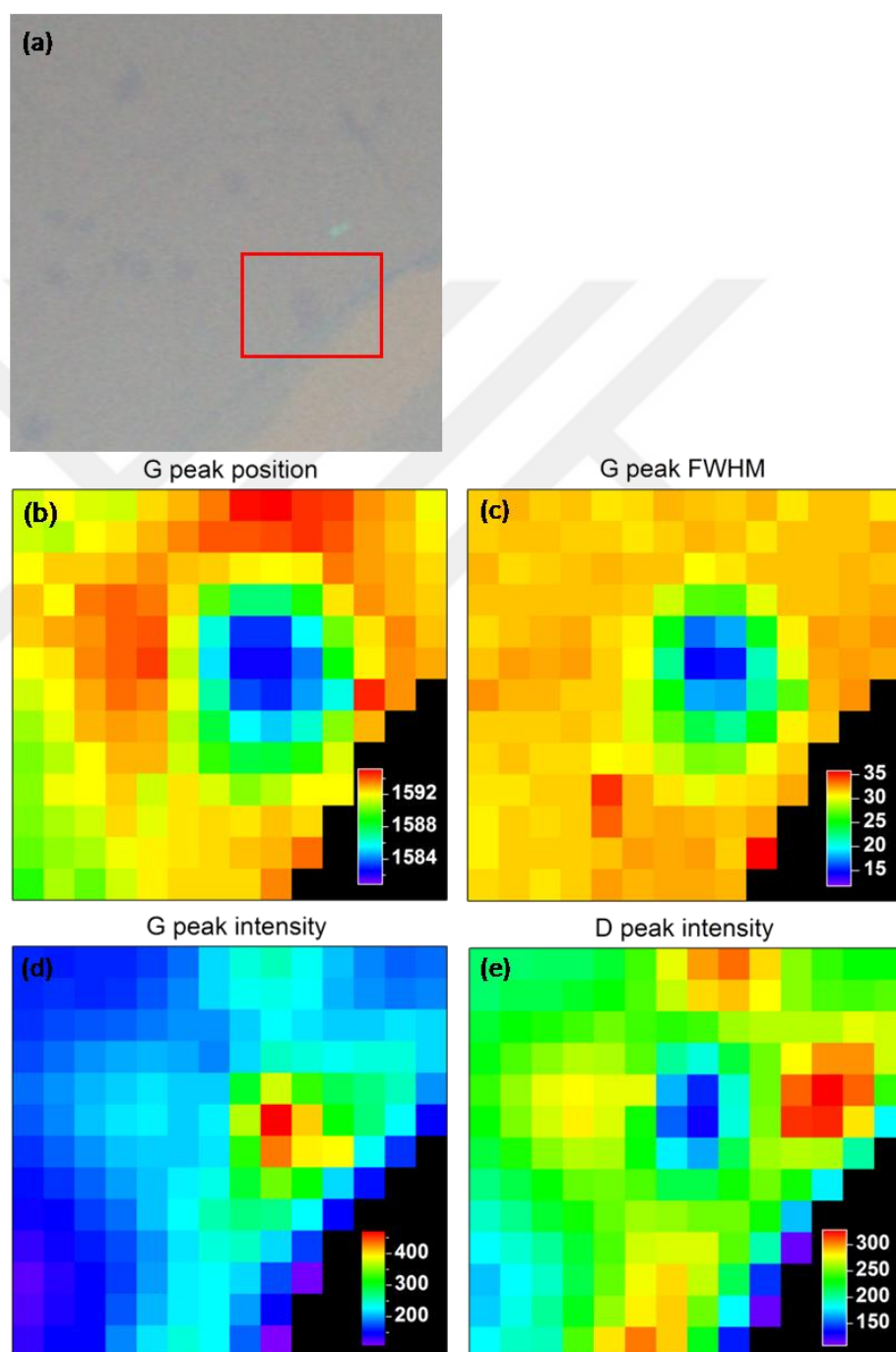


Figure 4.31 a) Optical image and (b-e) Raman maps of non-oxidized region on the CVD grown graphene.

CHAPTER 5

CONCLUSIONS

In this study graphene and graphene oxide obtained by wet chemical oxidation of single layer graphene were investigated. Graphene samples prepared by mechanical exfoliation method onto SiO₂/Si and CVD grown graphene transferred onto SiO₂/Si were used. Thin graphene flakes were identified under optical microscope and number of layers were determined using AFM and Raman spectroscopy. Graphene sample were, then, oxidized by wet chemical method. Two different solutions were used. Raman spectroscopy and AFM were used to investigate sample prior to and after oxidation.

First Graphene and graphite sample were oxidized in a solution formed of 0.4 M KMnO₄ in 50% H₂SO₄ and then were characterized by Raman spectroscopy and AFM. Raman spectroscopy from multilayer graphene and graphite flakes showed a D' peak formation at around 1610 cm⁻¹ which can be attributed to sulfuric acid intercalation between the graphene layers. D' peak for single layer graphene was not observed for first solution. AFM measurements indicated that intercalation causes an increase in the height of the flakes due to the intercalation.

In the second solution using 0.015 M KMnO₄ in 50% H₂SO₄ (1:1 volume ratio), single layer graphene flakes showed D peak at around 1350 cm⁻¹ upon oxidation for more than 5 min in the solution. Multi layer graphene did not show and sign of D peak formation for oxidation durations up to 15 min. This is due to more reactive nature of single layer graphene when compared to multilayer samples. The samples were also investigated as a function of oxidation duration using Raman and AFM. In the earlier parts of the oxidation process a phase where both graphe oxide and non-oxidized graphene features coexisting together in the Raman spectra were observed. AFM images showed that such spectra are due to the formation of graphene oxide nano-

domains (GONDs) within non-oxidized graphene. Further, we observed that during the wet chemical oxidation of graphene flakes, the oxidation initiates at the edges of the sample and progresses inward as the oxidation duration is increased. GONDs are observed at the graphene oxide/graphene interface. If the flakes are narrow (a few micrometers wide), it is possible to prepare completely GOND covered samples. Such samples which provide a long interface between the conducting graphene medium and the nano-domains, may be used as a template material for further functionalization to be used in novel electronic devices. The formation of GONDs and the variations in the reactivity of different SLGs are attributed to the local impurity doping state of the flake. Finally, CVD grown single layer graphene was oxidized and its analysis was done using Raman and AFM measurements. In general, CVD grown graphene was more reactive than exfoliated graphene, however, three very different reactive behaviors were observed. Most of the CVD graphene was covered with GONDs but there were also about 2 μm wide completely non-oxidized regions. These non-oxidized regions were at the center of completely oxidized cross shaped areas. This behavior of CVD graphene is attributed to its growth dynamics.

REFERENCES

- [1] K.S. Novoselov, A.K. Geim, S.V. Morozov, D. Jiang, Y. Zhang, S.V. Dubonos, I.V. Grigorieva, A.A. Firsov, Electric field effect in atomically thin carbon films, *Science*, 306 (2004) 666-669.
- [2] A.K. Geim, K.S. Novoselov, The rise of graphene, *Nature materials*, 6 (2007) 183-191.
- [3] A.K. Geim, Graphene: Status and Prospects, *Science*, 324 (2009) 1530-1534.
- [4] K.I. Bolotin, K.J. Sikes, Z. Jiang, M. Klima, G. Fudenberg, J. Hone, P. Kim, H.L. Stormer, Ultrahigh electron mobility in suspended graphene, *Solid State Communications*, 146 (2008) 351-355.
- [5] L. Liao, H. Peng, Z. Liu, Chemistry makes graphene beyond graphene, *J. Am. Chem. Soc.*, 136 (2014) 12194-12200.
- [6] J.W. Hershey, *The book of diamonds: their curious lore, properties, tests and synthetic manufacture*, Hearthsides Press, 1940.
- [7] B. Bhushan, Chemical, mechanical and tribological characterization of ultra-thin and hard amorphous carbon coatings as thin as 3.5 nm: recent developments, *Diamond and related materials*, 8 (1999) 1985-2015.
- [8] J. Robertson, Diamond-like carbon, *Pure and applied chemistry*, 66 (1994) 1789-1796.
- [9] J. Robertson, Hard amorphous (diamond-like) carbons, *Progress in Solid State Chemistry*, 21 (1991) 199-333.
- [10] H.W. Kroto, J.R. Heath, S.C. O'Brien, R.F. Curl, R.E. Smalley, C₆₀: buckminsterfullerene, *Nature*, 318 (1985) 162-163.

- [11] W. Kratschmer, L.D. Lamb, K. Fostiropoulos, D. Huffman, Solid C₆₀: a new form of carbon, *Nature*, 347 (1990) 27.
- [12] S. Iijima, Helical microtubules of graphitic carbon, *nature*, 354 (1991) 56-58.
- [13] P.M. Ajayan, Capillarity-induced filling of carbon nanotubes, *Nature*, 361 (1993) 333-334.
- [14] Z. Yao, C.L. Kane, C. Dekker, High-field electrical transport in single-wall carbon nanotubes, *Physical Review Letters*, 84 (2000) 2941.
- [15] P.R. Wallace, The band theory of graphite, *Physical Review*, 71 (1947) 622.
- [16] R. Peierls, Quelques propriétés typiques des corps solides, in, pp. 177-222.
- [17] L.D. Landau, Zur Theorie der phasenumwandlungen II, *Phys. Z. Sowjetunion*, 11 (1937) 26-35.
- [18] N.D. Mermin, Crystalline order in two dimensions, *Physical Review*, 176 (1968) 250.
- [19] K.S. Novoselov, D. Jiang, F. Schedin, T.J. Booth, V.V. Khotkevich, S.V. Morozov, A.K. Geim, Two-dimensional atomic crystals, *Proceedings of the National Academy of Sciences of the United States of America*, 102 (2005) 10451-10453.
- [20] K.S. Novoselov, A.K. Geim, S.V. Morozov, D. Jiang, M.I. Katsnelson, I.V. Grigorieva, S.V. Dubonos, A.A. Firsov, Two-dimensional gas of massless Dirac fermions in graphene, *Nature*, 438 (2005) 197-200.
- [21] Y. Zhang, Y.-W. Tan, H.L. Stormer, P. Kim, Experimental observation of the quantum Hall effect and Berry's phase in graphene, *Nature*, 438 (2005) 201-204.
- [22] A.K. Geim, A.H. MacDonald, Graphene: Exploring carbon flatland, *Physics Today*, 60 (2007) 35-41.
- [23] Y. Zhu, S. Murali, W. Cai, X. Li, J.W. Suk, J.R. Potts, R.S. Ruoff, Graphene and graphene oxide: synthesis, properties, and applications, *Advanced materials*, 22 (2010) 3906-3924.

- [24] K. Novoselov, A.K. Geim, S. Morozov, D. Jiang, M. Katsnelson, I. Grigorieva, S. Dubonos, A. Firsov, Two-dimensional gas of massless Dirac fermions in graphene, *nature*, 438 (2005) 197-200.
- [25] C. Soldano, A. Mahmood, E. Dujardin, Production, properties and potential of graphene, *Carbon*, 48 (2010) 2127-2150.
- [26] J.C. Slonczewski, P.R. Weiss, Band Structure of Graphite, *Physical Review*, 109 (1958) 272-279.
- [27] K.S. Novoselov, Z. Jiang, Y. Zhang, S. Morozov, H. Stormer, U. Zeitler, J. Maan, G. Boebinger, P. Kim, A. Geim, Room-temperature quantum Hall effect in graphene, *Science*, 315 (2007) 1379-1379.
- [28] S.V. Morozov, K.S. Novoselov, M.I. Katsnelson, F. Schedin, D.C. Elias, J.A. Jaszczak, A.K. Geim, Giant intrinsic carrier mobilities in graphene and its bilayer, *Phys Rev Lett*, 100 (2008) 016602.
- [29] E. Hwang, S. Adam, S.D. Sarma, Carrier transport in two-dimensional graphene layers, *Physical Review Letters*, 98 (2007) 186806.
- [30] F. Schedin, A.K. Geim, S.V. Morozov, E.W. Hill, P. Blake, M.I. Katsnelson, K.S. Novoselov, Detection of individual gas molecules adsorbed on graphene, *Nat Mater*, 6 (2007) 652-655.
- [31] X. Du, I. Skachko, A. Barker, E.Y. Andrei, Approaching ballistic transport in suspended graphene, *Nature nanotechnology*, 3 (2008) 491-495.
- [32] J. Chen, M. Zhao, Y. Li, J. Liang, S. Fan, S. Chen, Preparation of graphene oxide/multiwalled carbon nanotubes 3D flexible architecture for robust biosensing application, *Ceramics International*, 41 (2015) 15241-15245.
- [33] G. Van Lier, C. Van Alsenoy, V. Van Doren, P. Geerlings, Ab initio study of the elastic properties of single-walled carbon nanotubes and graphene, *Chemical Physics Letters*, 326 (2000) 181-185.
- [34] C.D. Reddy, S. Rajendran, K.M. Liew, Equilibrium configuration and continuum elastic properties of finite sized graphene, *Nanotechnology*, 17 (2006) 864.

- [35] I.W. Frank, D.M. Tanenbaum, A.M. Van der Zande, P.L. McEuen, Mechanical properties of suspended graphene sheets, *J Vac Sci Technol B*, 25 (2007) 2558-2561.
- [36] M. Poot, H.S.J. van der Zant, Nanomechanical properties of few-layer graphene membranes, *Applied Physics Letters*, 92 (2008) 063111.
- [37] C. Lee, X.D. Wei, J.W. Kysar, J. Hone, Measurement of the elastic properties and intrinsic strength of monolayer graphene, *Science*, 321 (2008) 385-388.
- [38] C. Lee, X. Wei, J.W. Kysar, J. Hone, Measurement of the elastic properties and intrinsic strength of monolayer graphene, *Science*, 321 (2008) 385-388.
- [39] D.A. Dikin, S. Stankovich, E.J. Zimney, R.D. Piner, G.H.B. Dommett, G. Evmenenko, S.T. Nguyen, R.S. Ruoff, Preparation and characterization of graphene oxide paper, *Nature*, 448 (2007) 457-460.
- [40] R. Nair, P. Blake, A. Grigorenko, K. Novoselov, T. Booth, T. Stauber, N. Peres, A. Geim, Fine structure constant defines visual transparency of graphene, *Science*, 320 (2008) 1308-1308.
- [41] M.Y. Han, B. Özyilmaz, Y. Zhang, P. Kim, Energy band-gap engineering of graphene nanoribbons, *Phys. Rev. Lett.*, 98 (2007) 206805.
- [42] L. Yang, C.-H. Park, Y.-W. Son, M.L. Cohen, S.G. Louie, Quasiparticle energies and band gaps in graphene nanoribbons, *Phys. Rev. Lett.*, 99 (2007) 186801.
- [43] C. Stampfer, J. Guttinger, S. Hellmüller, F. Molitor, K. Ensslin, T. Ihn, Energy gaps in etched graphene nanoribbons, *Phys. Rev. Lett.*, 102 (2009) 056403.
- [44] D.C. Elias, R.R. Nair, T.M. Mohiuddin, S.V. Morozov, P. Blake, M.P. Halsall, A.C. Ferrari, D.W. Boukhvalov, M.I. Katsnelson, A.K. Geim, K.S. Novoselov, Control of graphene's properties by reversible hydrogenation: evidence for graphane, *Science*, 323 (2009) 610-613.
- [45] I.-S. Byun, D. Yoon, J.S. Choi, I. Hwang, D.H. Lee, M.J. Lee, T. Kawai, Y.-W. Son, Q. Jia, H. Cheong, Nanoscale lithography on monolayer graphene using hydrogenation and oxidation, *ACS nano*, 5 (2011) 6417-6424.

- [46] J.T. Robinson, J.S. Burgess, C.E. Junkermeier, S.C. Badescu, T.L. Reinecke, F.K. Perkins, M.K. Zalalutdniov, J.W. Baldwin, J.C. Culbertson, P.E. Sheehan, Properties of fluorinated graphene films, *Nano Lett.*, 10 (2010) 3001-3005.
- [47] R.R. Nair, W. Ren, R. Jalil, I. Riaz, V.G. Kravets, L. Britnell, P. Blake, F. Schedin, A.S. Mayorov, S. Yuan, Fluorographene: A Two-Dimensional Counterpart of Teflon, *Small*, 6 (2010) 2877-2884.
- [48] S. Gilje, S. Han, M. Wang, K.L. Wang, R.B. Kaner, A chemical route to graphene for device applications, *Nano Lett.*, 7 (2007) 3394-3398.
- [49] C. Gomez-Navarro, R.T. Weitz, A.M. Bittner, M. Scolari, A. Mews, M. Burghard, K. Kern, Electronic transport properties of individual chemically reduced graphene oxide sheets, *Nano Lett.*, 7 (2007) 3499-3503.
- [50] J.R. Lomeda, C.D. Doyle, D.V. Kosynkin, W.-F. Hwang, J.M. Tour, Diazonium functionalization of surfactant-wrapped chemically converted graphene sheets, *J. Am. Chem. Soc.*, 130 (2008) 16201-16206.
- [51] D.B. Farmer, R. Golizadeh-Mojarad, V. Perebeinos, Y.-M. Lin, G.S. Tulevski, J.C. Tsang, P. Avouris, Chemical doping and electron– hole conduction asymmetry in graphene devices, *Nano Lett.*, 9 (2008) 388-392.
- [52] S. Niyogi, E. Bekyarova, M.E. Itkis, H. Zhang, K. Shepperd, J. Hicks, M. Sprinkle, C. Berger, C.N. Lau, W.A. Deheer, Spectroscopy of covalently functionalized graphene, *Nano Lett.*, 10 (2010) 4061-4066.
- [53] A. Sinitskii, A. Dimiev, D.A. Corley, A.A. Fursina, D.V. Kosynkin, J.M. Tour, Kinetics of diazonium functionalization of chemically converted graphene nanoribbons, *ACS Nano*, 4 (2010) 1949-1954.
- [54] J.M. Englert, C. Dotzer, G. Yang, M. Schmid, C. Papp, J.M. Gottfried, H.-P. Steinrück, E. Spiecker, F. Hauke, A. Hirsch, Covalent bulk functionalization of graphene, *Nat. Chem.*, 3 (2011) 279-286.
- [55] W.S. Hummers Jr, R.E. Offeman, Preparation of graphitic oxide, *Journal of the American Chemical Society*, 80 (1958) 1339-1339.

- [56] W. Gao, L.B. Alemany, L. Ci, P.M. Ajayan, New insights into the structure and reduction of graphite oxide, *Nature chemistry*, 1 (2009) 403-408.
- [57] K. Krishnamoorthy, M. Veerapandian, K. Yun, S.J. Kim, The chemical and structural analysis of graphene oxide with different degrees of oxidation, *Carbon*, 53 (2013) 38-49.
- [58] D.R. Dreyer, S. Park, C.W. Bielawski, R.S. Ruoff, The chemistry of graphene oxide, *Chemical Society Reviews*, 39 (2010) 228-240.
- [59] S. Stankovich, D.A. Dikin, G.H. Dommett, K.M. Kohlhaas, E.J. Zimney, E.A. Stach, R.D. Piner, S.T. Nguyen, R.S. Ruoff, Graphene-based composite materials, *Nature*, 442 (2006) 282-286.
- [60] L. Weng, L. Zhang, Y.P. Chen, L.P. Rokhinson, Atomic force microscope local oxidation nanolithography of graphene, *Applied Physics Letters*, 93 (2008) 093107.
- [61] S. Neubeck, F. Freitag, R. Yang, K.S. Novoselov, Scanning probe lithography on graphene, *physica status solidi (b)*, 247 (2010) 2904-2908.
- [62] S. Masubuchi, M. Arai, T. Machida, Atomic force microscopy based tunable local anodic oxidation of graphene, *Nano letters*, 11 (2011) 4542-4546.
- [63] S. Wang, R. Wang, X. Liu, X. Wang, D. Zhang, Y. Guo, X. Qiu, Optical Spectroscopy Investigation of the Structural and Electrical Evolution of Controllably Oxidized Graphene by a Solution Method, *The Journal of Physical Chemistry C*, 116 (2012) 10702-10707.
- [64] S. Park, R.S. Ruoff, Chemical methods for the production of graphenes, *Nature nanotechnology*, 4 (2009) 217-224.
- [65] B.C. Brodie, On the Atomic Weight of Graphite, *Philosophical Transactions of the Royal Society of London*, 149 (1859) 249-259.
- [66] L. Staudenmaier, Verfahren zur darstellung der graphitsäure, *Berichte der deutschen chemischen Gesellschaft*, 31 (1898) 1481-1487.

- [67] O.C. Compton, S.T. Nguyen, Graphene Oxide, Highly Reduced Graphene Oxide, and Graphene: Versatile Building Blocks for Carbon-Based Materials, *small*, 6 (2010) 711-723.
- [68] M.J. McAllister, J.-L. Li, D.H. Adamson, H.C. Schniepp, A.A. Abdala, J. Liu, M. Herrera-Alonso, D.L. Milius, R. Car, R.K. Prud'homme, Single sheet functionalized graphene by oxidation and thermal expansion of graphite, *Chemistry of materials*, 19 (2007) 4396-4404.
- [69] A.B. Bourlinos, D. Gournis, D. Petridis, T. Szabó, A. Szeri, I. Dékány, Graphite oxide: chemical reduction to graphite and surface modification with primary aliphatic amines and amino acids, *Langmuir*, 19 (2003) 6050-6055.
- [70] U. Hofmann, R. Holst, Über die Säurenatur und die Methylierung von Graphitoxyd, *Berichte der deutschen chemischen Gesellschaft (A and B Series)*, 72 (1939) 754-771.
- [71] G. Ruess, Zur Wasserbindung im Halloysit, *Monatshefte für Chemie/Chemical Monthly*, 76 (1946) 168-173.
- [72] W. Scholz, H. Boehm, Untersuchungen am graphitoxid. VI. Betrachtungen zur struktur des graphitoxids, *Zeitschrift für anorganische und allgemeine Chemie*, 369 (1969) 327-340.
- [73] T. Nakajima, A. Mabuchi, R. Hagiwara, A new structure model of graphite oxide, *Carbon*, 26 (1988) 357-361.
- [74] H. He, T. Riedl, A. Lerf, J. Klinowski, Solid-state NMR studies of the structure of graphite oxide, *The Journal of physical chemistry*, 100 (1996) 19954-19958.
- [75] A. Lerf, H. He, M. Forster, J. Klinowski, Structure of graphite oxide revisited, *The Journal of Physical Chemistry B*, 102 (1998) 4477-4482.
- [76] H. He, J. Klinowski, M. Forster, A. Lerf, A new structural model for graphite oxide, *Chemical physics letters*, 287 (1998) 53-56.
- [77] M. Hirata, T. Gotou, S. Horiuchi, M. Fujiwara, M. Ohba, Thin-film particles of graphite oxide 1:: High-yield synthesis and flexibility of the particles, *Carbon*, 42 (2004) 2929-2937.

- [78] A.J. Glover, M. Cai, K.R. Overdeep, D.E. Kranbuehl, H.C. Schniepp, In situ reduction of graphene oxide in polymers, *Macromolecules*, 44 (2011) 9821-9829.
- [79] P. Solís-Fernández, J. Paredes, S. Villar-Rodil, L. Guardia, M. Fernández-Merino, G. Dobrik, L. Biró, A. Martínez-Alonso, J. Tascón, Global and local oxidation behavior of reduced graphene oxide, *The Journal of Physical Chemistry C*, 115 (2011) 7956-7966.
- [80] Y.W. Zhu, S. Murali, W.W. Cai, X.S. Li, J.W. Suk, J.R. Potts, R.S. Ruoff, Graphene and Graphene Oxide: Synthesis, Properties, and Applications, *Advanced materials*, 22 (2010) 3906-3924.
- [81] P. Blake, E.W. Hill, A.H. Castro Neto, K.S. Novoselov, D. Jiang, R. Yang, T.J. Booth, A.K. Geim, Making graphene visible, *Applied Physics Letters*, 91 (2007) 063124.
- [82] C. Berger, Z. Song, T. Li, X. Li, A.Y. Ogbazghi, R. Feng, Z. Dai, A.N. Marchenkov, E.H. Conrad, P.N. First, Ultrathin epitaxial graphite: 2D electron gas properties and a route toward graphene-based nanoelectronics, *The Journal of Physical Chemistry B*, 108 (2004) 19912-19916.
- [83] S. Bae, H. Kim, Y. Lee, X. Xu, J.-S. Park, Y. Zheng, J. Balakrishnan, T. Lei, H.R. Kim, Y.I. Song, Roll-to-roll production of 30-inch graphene films for transparent electrodes, *Nature nanotechnology*, 5 (2010) 574-578.
- [84] L. Ma, W. Ren, Z. Dong, L. Liu, H. Cheng, Progress of graphene growth on copper by chemical vapor deposition: Growth behavior and controlled synthesis, *Chinese Science Bulletin*, 57 (2012) 2995-2999.
- [85] A. Ferrari, J. Meyer, V. Scardaci, C. Casiraghi, M. Lazzeri, F. Mauri, S. Piscanec, D. Jiang, K. Novoselov, S. Roth, Raman spectrum of graphene and graphene layers, *Physical review letters*, 97 (2006) 187401.
- [86] D. Graf, F. Molitor, K. Ensslin, C. Stampfer, A. Jungen, C. Hierold, L. Wirtz, Spatially resolved Raman spectroscopy of single-and few-layer graphene, *Nano letters*, 7 (2007) 238-242.

- [87] A. Gupta, G. Chen, P. Joshi, S. Tadigadapa, Eklund, Raman Scattering from High-Frequency Phonons in Supported n-Graphene Layer Films, *Nano letters*, 6 (2006) 2667-2673.
- [88] S. Pisana, M. Lazzeri, C. Casiraghi, K.S. Novoselov, A.K. Geim, A.C. Ferrari, F. Mauri, Breakdown of the adiabatic Born–Oppenheimer approximation in graphene, *Nature materials*, 6 (2007) 198-201.
- [89] C. Casiraghi, S. Pisana, K. Novoselov, A. Geim, A. Ferrari, Raman fingerprint of charged impurities in graphene, *Applied Physics Letters*, 91 (2007) 233108.
- [90] C. Stampfer, F. Molitor, D. Graf, K. Ensslin, A. Jungen, C. Hierold, L. Wirtz, Raman imaging of doping domains in graphene on SiO₂, *Appl Phys Lett*, 91 (2007) 241907.
- [91] C. Casiraghi, A. Hartschuh, H. Qian, S. Piscanec, C. Georgi, A. Fasoli, K. Novoselov, D. Basko, A. Ferrari, Raman spectroscopy of graphene edges, *Nano letters*, 9 (2009) 1433-1441.
- [92] T. Mohiuddin, A. Lombardo, R. Nair, A. Bonetti, G. Savini, R. Jalil, N. Bonini, D. Basko, C. Galiotis, N. Marzari, Uniaxial strain in graphene by Raman spectroscopy: G peak splitting, Grüneisen parameters, and sample orientation, *Physical Review B*, 79 (2009) 205433.
- [93] M.M. Lucchese, F. Stavale, E.H.M. Ferreira, C. Vilani, M.V.O. Moutinho, R.B. Capaz, C.A. Achete, A. Jorio, Quantifying ion-induced defects and Raman relaxation length in graphene, *Carbon*, 48 (2010) 1592-1597.
- [94] E.M. Ferreira, M.V. Moutinho, F. Stavale, M. Lucchese, R.B. Capaz, C. Achete, A. Jorio, Evolution of the Raman spectra from single-, few-, and many-layer graphene with increasing disorder, *Phys. Rev. B*, 82 (2010) 125429.
- [95] L.G. Cancado, A. Jorio, E.H. Ferreira, F. Stavale, C.A. Achete, R.B. Capaz, M.V. Moutinho, A. Lombardo, T.S. Kulmala, A.C. Ferrari, Quantifying defects in graphene via Raman spectroscopy at different excitation energies, *Nano letters*, 11 (2011) 3190-3196.

- [96] A.C. Ferrari, Raman spectroscopy of graphene and graphite: disorder, electron–phonon coupling, doping and nonadiabatic effects, *Solid state communications*, 143 (2007) 47-57.
- [97] A.M. Dimiev, G. Ceriotti, N. Behabtu, D. Zakhidov, M. Pasquali, R. Saito, J.M. Tour, Direct real-time monitoring of stage transitions in graphite intercalation compounds, *ACS nano*, 7 (2013) 2773-2780.
- [98] L. Liu, S. Ryu, M.R. Tomasik, E. Stolyarova, N. Jung, M.S. Hybertsen, M.L. Steigerwald, L.E. Brus, G.W. Flynn, Graphene oxidation: thickness-dependent etching and strong chemical doping, *Nano letters*, 8 (2008) 1965-1970.
- [99] R. Sharma, J.H. Baik, C.J. Perera, M.S. Strano, Anomalously large reactivity of single graphene layers and edges toward electron transfer chemistries, *Nano letters*, 10 (2010) 398-405.
- [100] M. Lazzeri, F. Mauri, Nonadiabatic Kohn anomaly in a doped graphene monolayer, *Physical review letters*, 97 (2006) 266407.
- [101] A. Das, S. Pisana, B. Chakraborty, S. Piscanec, S. Saha, U. Waghmare, K. Novoselov, H. Krishnamurthy, A. Geim, A. Ferrari, Monitoring dopants by Raman scattering in an electrochemically top-gated graphene transistor, *Nature nanotechnology*, 3 (2008) 210-215.
- [102] X. Fan, R. Nouchi, K. Tanigaki, Effect of Charge Puddles and Ripples on the Chemical Reactivity of Single Layer Graphene Supported by SiO₂/Si Substrate, *The Journal of Physical Chemistry C*, 115 (2011) 12960-12964.
- [103] H. Tao, J. Moser, F. Alzina, Q. Wang, C.M. Sotomayor-Torres, The Morphology of Graphene Sheets Treated in an Ozone Generator, *The Journal of Physical Chemistry C*, 115 (2011) 18257-18260.
- [104] M. Yamamoto, T.L. Einstein, M.S. Fuhrer, W.G. Cullen, Charge inhomogeneity determines oxidative reactivity of graphene on substrates, *ACS Nano*, 6 (2012) 8335-8341.
- [105] Q.H. Wang, Z. Jin, K.K. Kim, A.J. Hilmer, G.L. Paulus, C.J. Shih, M.H. Ham, J.D. Sanchez-Yamagishi, K. Watanabe, T. Taniguchi, J. Kong, P. Jarillo-Herrero, M.S.

Strano, Understanding and controlling the substrate effect on graphene electron-transfer chemistry via reactivity imprint lithography, *Nature chemistry*, 4 (2012) 724-732.

[106] S. Berciaud, S. Ryu, L.E. Brus, T.F. Heinz, Probing the intrinsic properties of exfoliated graphene: Raman spectroscopy of free-standing monolayers, *Nano letters*, 9 (2008) 346-352.

[107] C. Stampfer, F. Molitor, D. Graf, K. Ensslin, A. Jungen, C. Hierold, L. Wirtz, Raman imaging of doping domains in graphene on Si O₂, *Applied Physics Letters*, 91 (2007) 241907.

[108] S. Berciaud, S. Ryu, L.E. Brus, T.F. Heinz, Probing the intrinsic properties of exfoliated graphene: Raman spectroscopy of free-standing monolayers, *Nano Lett.*, 9 (2009) 346-352.

[109] M. Lazzeri, F. Mauri, Nonadiabatic Kohn anomaly in a doped graphene monolayer, *Phys. Rev. Lett.*, 97 (2006) 266407.

[110] C. Casiraghi, Probing disorder and charged impurities in graphene by Raman spectroscopy, *Phys. Status Solidi RRL*, 3 (2009) 175-177.

CURRICULUM VITAE

CONTACT INFORMATION

Esra YAZICI

Fatih Mah. Dilek Sk. Mimoza Park Evleri B-Blok No: 19/7 Büyükçekmece, İstanbul.

Email: esrayazici2905@gmail.com

EDUCATION

- Ph.D., Fatih University - The Graduate School of Sciences and Engineering, Physics, 2011- June, 2015, Istanbul, Turkey.
Thesis: *Raman and AFM Study of Grapheneoxide Prepared by Wet Oxidation of Graphene*
- M.S., Anadolu University - The Graduate School of Sciences, Advance Technology Program / Nanotechnology, 2008-2011, Eskisehir, Turkey.
Thesis: *Capacitance-Voltage Measurements in Nitrate-Based Nano Semiconductors*
- B.S, Anadolu University - The Faculty of Science, Physics, 2003-2008 Eskişehir, Turkey.

PUBLICATIONS

Academic Journals

- Esra Yazici, Serhat Yanik, Mehmet Burak Yilmaz “Grapheneoxide nano-domain formation via wet chemical oxidation of graphene” *Carbon*, Vol.111, pp.822-827, 2017.

Conference Proceedings

- M Burak Yilmaz, Esra Yazici, Serhat Yanik, “*Investigation of the early stages of graphite oxide formation via modified Hummers*”, NonoTr 12, Gebze, Kocaeli Jun, 2016.
- Esra Yazici*, Z. Ruya Develi, Serhat Yanik, Aidyn Kemeldinov, Kurtulus Golcuk and M. Burak Yilmaz, “*Investigation of the early stages of graphite oxide formation via modified Hummers*”, NonoTr 9, Erzurum, Turkey Jun, 2013.

Posters

- Esra Yazıcı, Engin Tıraş, Naci Balkan, Adebawale Olufunso Ajagunna, Eleftherios Iliopoulos and Alexandros Georgakilas, “*Capacitance-voltage and capacitance-frequency measurements in InN*”, E-MRS Spring Meeting, Nice, France, May, 2011.

RESEARCH PROJECTS

- “Formation of Graphene/Grapheneoxide Hybrid structures characterization”, TUBITAK “The Scientific and Technical Research Council of Turkey” under grant number 110T801, 2011-2014, Researcher.

REVIEWING ACTIVITIES**CERTIFICATES**

- Training School on “Theoretical Techniques in Semiconductor”, “Novel Gain Materials and Devices Based On III-V-N Compounds”, COST Action MP 0805, Dokuz Eylül University, 12-14 April 2010, İzmir, Turkey

LANGUAGES

- Turkish (Native)
- English (Advance)

TECHNICAL SKILLS

- Operating systems: Windows,
- Scientific Softwares: LabVIEW, IGOR.
- Experience in laboratory processes and equipments including AFM and Raman spectroscopy techniques.
- Excellent team work abilities and guidance for an interactive academic environment.